Aalto University
School of Chemical
Technology

School of Chemical Technology
Degree Programme of Materials Science and Engineering

Taina Kalliomäki

EFFECT OF COMPOSITION AND TEMPERATURE ON PHYSICO-CHEMICAL PROPERTIES OF COPPER ELECTROLYTE

Master's thesis for the degree of Master of Science in Technology submitted for inspection, Espoo, 23 November, 2015.

Supervisor Professor Olof Forsén

Instructors D.Sc. Jari Aromaa
M.Sc. Iiro Lehtiniemi

Aalto University
School of Chemical
Technology

Aalto University, P.O. BOX 11000, 00076 AALTO
www.aalto.fi

Abstract of master's thesis

Author Taina Kalliomäki

Title of thesis Effect of composition and temperature on physico-chemical properties of copper electrolyte

Department Materials Science and Engineering

Professorship Corrosion and Hydrometallurgy **Code of professorship** MT-85

Thesis supervisor Professor Olof Forsén

Thesis advisor(s) / Thesis examiner(s) D.Sc. Jari Aromaa and M.Sc. Iiro Lehtiniemi

Date 23.11.2015 **Number of pages** 116 + appendices **Language** English

Abstract

The objective was to develop accurate mathematical models, for physico-chemical properties of copper electrorefining electrolytes as a function of temperature and composition. The physico-chemical properties affect significantly the yield and quality of cathode copper in the refining process. Typical physico-chemical properties are conductivity, density, viscosity and the diffusion coefficient of cupric ion (Cu^{2+}).

The design of experiments was the full factorial design of which 305 tests were conducted. Conductivities, viscosities, densities and limiting current densities of synthetic copper electrolytes were measured. The diffusion coefficient of Cu^{2+} was defined from limiting current density results. The electrolyte variables were copper, nickel, arsenic, sulfuric acid, and temperature. The measurements were analyzed using modeling and design tool MODDE.

The results support the previous research, except for viscosity and the accurate effects of arsenic. According to this research arsenic decreases conductivity and increases density more than according to literature. The viscosity values obtained were noticed to contain error due to meter unsuitability for defining viscosities at measured conditions. Thus, the viscosity models were not usable. The other models were both usable and valid.

Keywords copper electrorefining, conductivity, density, viscosity, diffusion coefficient of cupric ion

Aalto-yliopisto
Kemian tekniikan korkeakoulu

Aalto-yliopisto, PL 11000, 00076 AALTO
www.aalto.fi

Diplomityön tiivistelmä

Tekijä Taina Kalliomäki	
Työn nimi Koostumuksen ja lämpötilan vaikutus kuparielektrolyytin fysikaaliskemiallisiin ominaisuuksiin	
Laitos Materiaalitekniikka	
Professuuri Korroosio ja hydrometallurgia	**Professuurikoodi** MT-85
Työn valvoja Professori Olof Forsén	
Työn ohjaaja(t)/Työn tarkastaja(t) TkT Jari Aromaa ja DI Iiro Lehtiniemi	
Päivämäärä 23.11.2015	**Sivumäärä** 116 + liitteet **Kieli** Englanti

Tiivistelmä

Tutkimuksen tavoitteena oli kehittää kuparin raffinointielektrolyysin elektrolyytin fysikaaliskemiallisille ominaisuuksille tarkat matemaattiset mallit, joissa ominaisuudet esitetään lämpötilan ja koostumuksen funktiona. Fysikaaliskemialliset ominaisuudet vaikuttavat merkittävästi katodikuparin saantoon ja pinnoitteen laatuun. Tyypillisiä fysikaaliskemiallisia ominaisuuksia ovat johtokyky, tiheys, viskositeetti ja kupri-ionin (Cu^{2+}) diffuusiokerroin.

Koesuunnitelma luotiin full factorial -mallina, jonka koevaihtoehdoista toteutettiin 305 koetta. Johtokyky-, viskositeetti-, tiheys- ja rajavirrantiheysarvot mitattiin synteettisistä kuparielektrolyyteistä. Cu^{2+}-ionien diffuusiokertoimet määritettiin rajavirrantiheysarvoista. Muuttujina kokeissa olivat kuparin, nikkelin, arseenin ja rikkihapon pitoisuudet sekä lämpötila. Tulosten analysoimisessa käytettiin MODDE-suunnittelu- ja mallinnusohjelmaa.

Tulokset olivat linjassa kirjalisuusarvojen kanssa viskositeettituloksia ja tarkkoja arseenin vaikutuksia lukuun ottamatta. Tämän tutkimuksen mukaan arseeni alentaa johtokykyä ja lisää tiheyttä enemmän, kuin aiempien tutkimusten mukaan. Mitatuissa viskositeettiarvoissa havaittiin virheitä, jotka johtuivat mittarin soveltumattomuudesta viskositeettimittauksiin näissä koeolosuhteissa. Tästä syystä tutkimuksessa määritetyt viskositeettimallit eivät olleet käyttökelpoisia. Muut mallit sitä vastoin olivat sekä käyttökelpoisia että valideja.

Avainsanat kuparin raffinointielektrolyysi, johtokyky, tiheys, viskositeetti, kupri-ionin diffuusiokerroin

Preface

This thesis was performed during January–September 2015 at Aalto University School of Chemical Technology, in the Laboratory of Corrosion and Hydrometallurgy. In addition, the conductivity measurements of the electrolytes without arsenic were carried out during September–December 2014. The research was a part of the SIMP (System Integrated Metal Production) project of FIMECC (Finnish Metals and Engineering Competence Cluster).

I would like to thank all involved in this research and also those not involved but supporting me in one way or another.

This thesis was supervised by Professor Olof Forsén as well as advised by D.Sc. Jari Aromaa and M.Sc. Iiro Lehtiniemi. I express my sincere gratitude to them for help and advice. I would also like to thank all staff members of the research group of Corrosion and Hydrometallurgy for support and for creating pleasant working atmosphere. Furthermore, I would like to thank workshop's staff for producing high-quality custom-made parts for test equipment.

Contents

1 Introduction

Copper is widely used in many applications, including construction and electronics [1]. In the electronics industry, high-purity copper has become increasingly important [1]. Traditionally, copper has been produced from copper ores and copper scrap [1]. These copper ores typically contain copper-iron-sulfide or copper sulfide minerals, such as chalcopyrite ($CuFeS_2$), bornite ($CuSFeS_4$) or chalcocite (Cu_2S) [1]. The production procedure utilizing these ores, which is the most common procedure for producing copper, consists of concentration, smelting and refining [1]. Copper is also produced in large amounts from scrap copper by remelting and refining [1]. In addition, copper is produced hydrometallurgically from oxidized minerals, such as carbonates, oxides, hydroxy-silicates and sulfates, and from chalcocite (Cu_2S) [1].

Copper electrorefining is the most common method for producing high-purity copper [1]. The first refinery (Pembrey Copper Works) was established in 1869 with the first patent of commercial electrorefining process developed by James Elkington in 1865 [2, 3]. Since then, industry and the researchers have developed the process further [2]. In the copper electrorefining process, copper is dissolved from impure copper anodes into the electrolyte and deposited onto cathodes as high-purity copper [4].

Industrial copper refining electrolyte mainly consists of water, copper sulfate and sulfuric acid [4]. In addition, the electrolyte contains impurities as well as leveling and grain refining addition agents [4]. The impurities, most commonly nickel, arsenic and iron, dissolve into the electrolyte from the anode [4]. The other common impurities, in small amounts, are bismuth, antimony and chloride [4, 5]. The electrolytes also contain addition agents for obtaining smoother and denser cathode deposits [4].

The physico-chemical properties of copper electrolyte affect significantly the yield of cathodic copper in the electrorefining process [6, 7]. The four typical physico-chemical properties are conductivity, density, viscosity and the diffusion coefficient of cupric ion (Cu^{2+}) [6–12]. The best yield of copper can be obtained keeping the viscosity low and electrical conductivity [6] as well as the diffusion coefficient high [8]. These properties of the copper electrolyte are influenced by composition and temperature. Temperature rise, for example, lowers density and viscosity [7] as well as accelerates the chemical reactions [4]. Whereas too high temperature causes unnecessary energy expenses and excessive

evaporation [4]. Composition with high concentration of copper, nickel and sulfuric acid, for instance, makes the electrolyte denser and more viscous than with lower concentrations [7]. In addition, increasing viscosity decreases the diffusion coefficient of Cu^{2+} [8]. Nevertheless, an increase in the concentration of sulfuric acid enhances conductivity [6–8]. Thus, in order to optimize the yield of cathode copper, it is important to thoroughly determine the effects of these parameters. The main effects of composition and temperature are presented in table 1. However, as seen in the table 1, the information about the effects of arsenic on the diffusion coefficient has not been found. Arsenic was assumed to decrease the diffusion coefficient like nickel and copper.

Table 1. The main effects of composition and temperature presented as increase or decrease in values of the properties [6–10, 13].

Increase	Conductivity	Density	Viscosity	Diffusion coefficient of Cu^{2+}	Ref.
H_2SO_4	↑	↑	↑	↓	[6, 7]; [6, 7]; [6, 7]; [9, 8]
$Cu/CuSO_4$	↓	↑	↑	↓	[6, 7]; [6, 7]; [6, 7]; [8, 9, 13]
Ni	↓	↑	↑	↓	[7]; [6, 7]; [6, 7]; [10]
As	↓	↑	↑	?	[7]; [7]; [7]
Temperature	↑	↓	↓	↑	[6, 7, 9]; [6, 7]; [6, 7]; [8, 9, 10]

Although much past work has been devoted to determining the physico-chemical properties of the electrolytes used in the copper electrorefining processes [6–12], these studies have not exploited recent equipment for obtaining more accurate measurements of these properties. Moreover, the former studies have not utilized recent modeling and design tools for developing accurate models of complicated data as well as for assessing the probable combined effects of the parameters. Therefore, new research is needed to obtain data for more accurately optimizing the copper refining process.

The objective of this thesis is to develop mathematical models for the four physico-chemical properties of the electrolytes used in the copper electrorefining process and similarly investigate if the variables, composition components and temperature, have combined effects. These models are defined as a function of temperature and composition. To accomplish this, in this thesis conductivity, viscosity, density and the diffusion coefficient of

Cu^{2+} of copper electrolytes with varying amounts of copper, nickel, arsenic and sulfuric acid were measured. These measurements were analyzed using MODDE, a modeling and design tool. All measurements were performed at temperatures within the temperature range employed in copper refineries and using electrolytes similar to those used in the refineries [5]. However, the electrolytes in this thesis included no addition agents, since the tests measure the properties of the electrolytes, not the deposition process. The test electrolytes were chosen to avoid containing too many substances. All the measurement data reported in this thesis will be used for developing mathematical models improving the recovery of cathodic copper. However, this thesis does not assess the larger system-integrated modeling. This thesis is a part of research project System Integrated Metals Processing (SIMP) which is financed by Finnish Metals and Engineering Competence Cluster FIMECC.

2 Copper electrorefining

Copper electrorefining is an electrolytic method in which copper is dissolved from impure copper anodes into the electrolyte and deposited to the cathode with minimal amount of impurities [1]. This method in one of the final phases in the primary copper production [1]. The methods preceding electrorefining in the processing are concentration by froth flotation, smelting the concentrate to matte, converting the matte to impure copper and fire refining [1]. After electrorefining the refined cathodic copper is melted, cast and processed further [1].

This chapter introduces copper electrorefining at a general level. Section 2.1 presents the principles of the process as well as sections 2.2 and 2.3 discuss cell voltage and mass transport.

2.1. Principles

In copper electrorefining anode copper (Cu 98.5–99.5%) [14] is dissolved electrochemically into the electrolyte which mainly consists of copper sulfate ($CuSO_4$), sulfuric acid (H_2SO_4) as well as water and electrodeposited on cathode, practically without impurities [1, 4]. Cathode copper contains over 99.997% copper and 0.018–0.025% oxygen [14]. The insoluble anodic impurities fall to the bottom of the electrorefining cell or adhere to the anode, whereas soluble impurities dissolve into the electrolyte [4]. Impurities are removed from the system thoroughly enough, since many of them are valuable or harmful, and they must be obstructed adhering on the cathode surface [4]. The common impurities in the system are silver, nickel, selenium, lead, iron, tellurium, sulfuric, arsenic, antimony, bismuth, cobalt and gold [4]. The electrorefining process is presented schematically in figure 1.

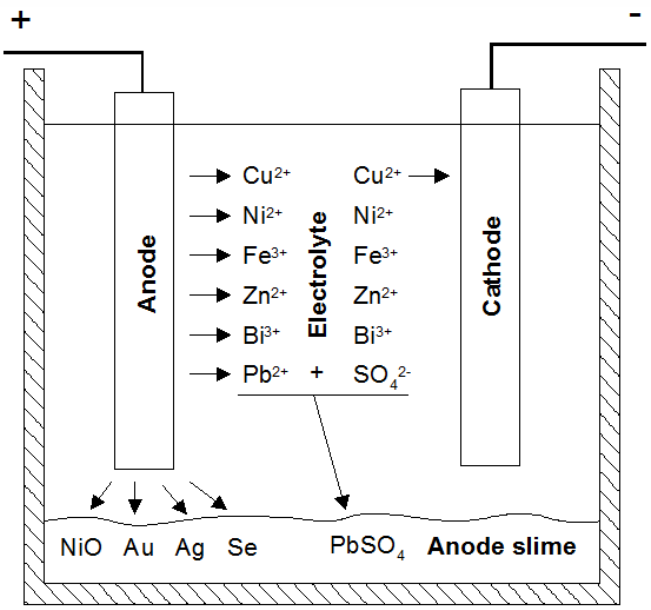

Figure 1. Basic principle of copper electrorefining [15].

In industry, the electrorefining cell consists of 30–60 anode-cathode pairs, their connections and the electrolyte [4]. The anodes are impure copper which has been converted as well as fire refined, and the cathodes are in most cases stainless steel [4, 5]. The cell walls are commonly polymer concrete or concrete with lining of lead or plastic [5]. All the anodes are connected so that they share the same potential as well as all the cathodes are at the lower shared potential [4]. Anodes and cathodes are connected in parallel, and the cells form sections which are connected in series (figure 2) of 20–40 cells [4]. The cell length is commonly 3–6 m, in some refineries even more [5], and the other dimensions of the cell depend on the dimensions of the electrodes [4]. The approximate dimensions of cathodes are usually 1 m x 1 m x 1–3 mm and anodes slightly less except for thickness which is 4–5 cm [4].

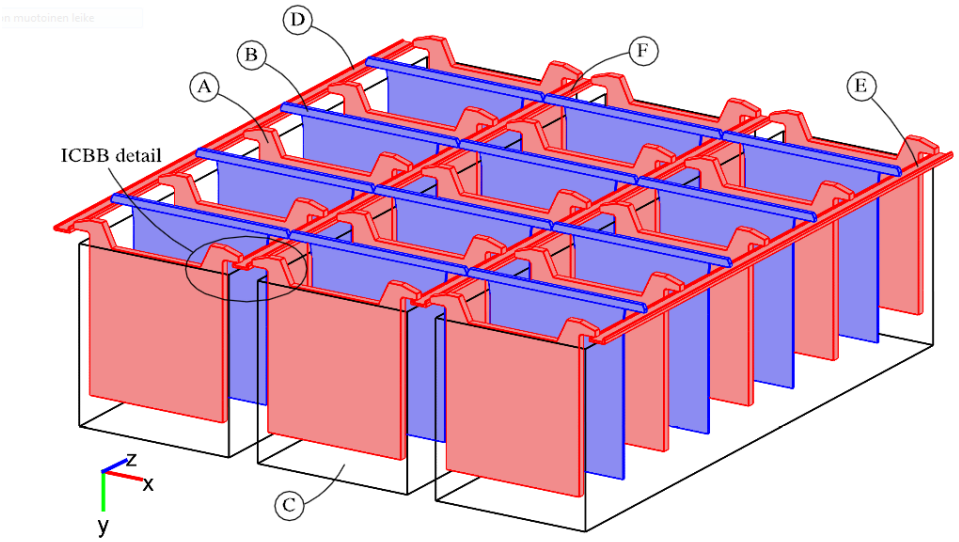

(a) Cell group layout.

Figure 2. Electrorefining cells presented schematically. A = anode, B = cathode, C = electrolyte, D = cathode busbar, E = anode busbar, F = intercell busbar. [16]

Industrial electrorefining process is carried out in cycles of generally 21 days for anodes and 7–10 days for cathodes [4]. The total cycle begins by installing the electrodes in their places and filling the electrolyte into the cell [4]. The electrolyte is then heated to 60–65 °C, and the anodes as well as cathodes are connected to power supply [4]. During the electrorefining process the copper anodes are dissolving into the electrolyte and the cathodes obtain the copper deposit on them [4]. The electrolyte is kept flowing continuously into and out of the cells as long as the anodes are dissolving [4]. The anodes are removed when 80–85% of them have dissolved [4]. At that time, the electrolyte is also replaced and the cell cleaned of anode slimes [4]. The cells can be serviced separately which enables the refining process to continue during the cell maintenance [4].

After their cycles the electrodes and the electrolyte are further processed [4]. The anodes are cleaned of the slime of impurities formed on them, melted and then recast [4]. The cathodes are also cleaned and the deposits are mechanically stripped if the material used is stainless steel [4]. Stripping is made easier by covering the side edges of the cathode with polymer strips to prevent the coating from spreading all over the cathodes [4]. The copper cathodes are ready to be further processed by melting and casting to suitable shapes [4]. In addition, the electrolyte is filtered, and the byproducts are recovered from the slimes [4].

Copper electrorefining process needs good electric contacts and correct distances between the electrodes, steady electrolyte circulation (approximately 0.02 m^3/minute) [4] as well as

active dissolution of anodes [17] to succeed. Electrolyte circulation is important in keeping the electrolyte concentrations of Cu^{2+} and addition agents uniform as well as removing dissolved and floating impurities before they adhere on the cathode [4, 15]. Thus the coatings on the cathodes also become uniform, dense and pure [4].

Dissolution of anodes decreases or stops if the anodes passivate which increases energy consumption. The passivation is due to non-conducting copper sulfate precipitation layer which attaches on the anode surface [17, 18]. Anode slime layer on anodes has also been regarded to enable and enhance this progress [18]. The factors affecting the anode passivation are the composition of anode and electrolyte [17, 18] as well as the rate of electrolyte circulation [17]. Anode impurities, for example, affect the passivation [17]. In addition, other factors regarded to affect that are temperature, parameters affecting the mass transport of copper ions and solubility of $CuSO_4$ [18].

The anode slimes consist of insoluble or soluble but precipitating impurities which adhere on anodes or fall to the bottom of the cell [4]. In addition, the impurities which have precipitated after dissolved, can form floating slimes [19]. The most common insoluble impurities are gold, platinum group metals as well as compounds of selenium, tellurium, lead and tin [4]. The most common soluble impurities are arsenic, antimony, bismuth, cobalt, iron, nickel and sulfur [4]. In addition, silver partly dissolves into the electrolyte [4].

2.2. Cell voltage

In copper electrorefining, the cell voltage is set to dissolve the anode copper as well as deposit copper on the cathodes avoiding depositing other elements [4]. In addition, when setting the cell voltage the surface quality and adhesion are taken into account (figure 3). Copper is oxidized at the anode and reduced on the cathodes [20]. The copper dissolving from the anode generates cupric ions and electrons [4]:

$Cu°_{anode} \rightarrow Cu^{2+} + 2e^-$ $E° = +0.337$ V [15].

These particles move into the electrolyte and there towards the cathode, the electrons by conduction and cupric ions by convection as well as diffusion [4]. Copper anions and electrons combine at the cathode surface and form metallic copper [4]:

$Cu^{2+} + 2e^- \rightarrow Cu°_{cathode}$ $E° = +0.337$ V [15].

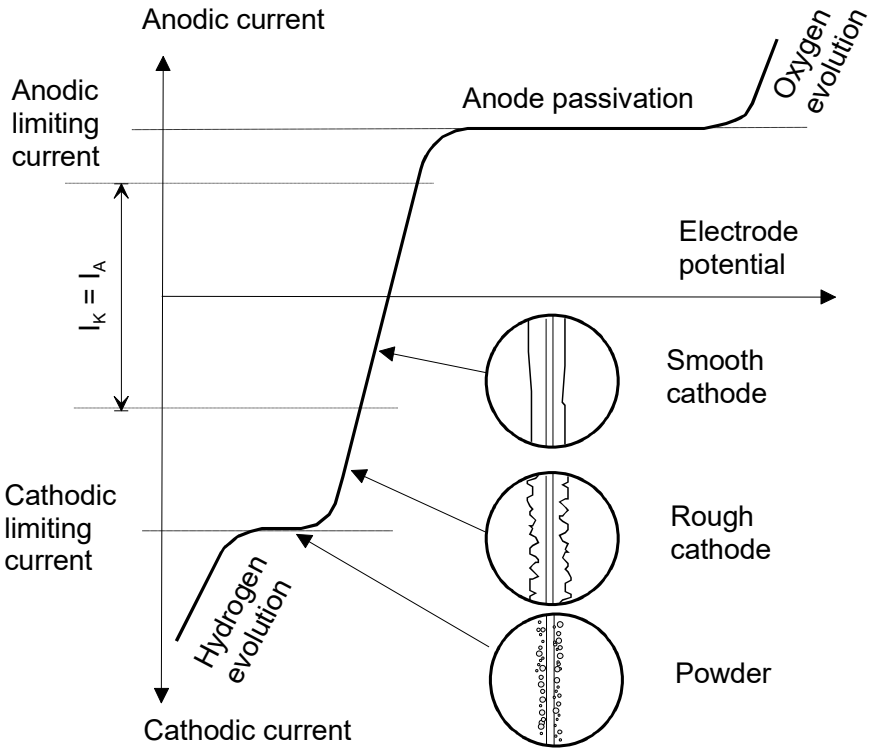

Figure 3. The effects of cell voltage and current in electrorefining of copper [15].

The theoretical cell voltage is 0 V [4]. However, overcoming the resistance to current flow demands applying a potential between anode and cathode, as well as overvoltages are needed for dissolving copper from anode and plating the cathode [4]. Copper dissolving demands 0.1 and cathode deposition 0.05 V overpotential [4].

It is essential to use correct cell voltage for avoiding depositing on cathode other elements soluble to the electrolyte. Nevertheless, most of these other soluble elements, As, Bi, Co, Fe, Ni, S and Sb, plate at lower potential than copper, and the plating of these impurities is easily minimized [4]. In addition, most of them precipitate in the electrolyte [15]. However, according to [3, 15, 21] the standard electrode potentials of reduction for As and Sb are higher than copper's as well as for Bi close to it. Thus there is a risk of these impurities to depositing on cathode [15]. One impurity metal, silver, is an exception to the behavior of impurities, since it dissolves partly in the electrolyte and plates at higher potential than copper and more easily end up to copper deposit [4]. That is, fortunately, not really harmful, because the properties of Ag are not very different from the properties of Cu, and the amounts of Ag are usually 8–10 ppm [4]. Both the soluble and insoluble impurities can, however, also accidently drift to cathode with electrolyte or slime particles and in worst case get entrapped in the deposit [4].

The cell voltage depends on current density, electrolyte composition, temperature, electrode activation polarization, overvoltages caused by concentration polarization and ohmic losses [21].

2.3. Mass transport

Mass transport or mass transfer can take place by migration, diffusion and convection [8, 22]. Generally, diffusion, electrical conduction and viscosity are transport properties of a substance [20]. Diffusion is movement of species and influenced by a concentration gradient. Analogously, migration is movement of charged components and influenced by a gradient of electrical potential. In convection fluid is transported hydrodynamically or by stirring [23]. The fluid flows due to natural or forced convection of which natural convection is caused by density gradients [23].

Mass transport of copper ions is a limiting factor in refining process [10]. In copper electrorefining, diffusion and convection are the main transport types of Cu^{2+} while migration does not affect the process that significantly [22]. The insignificance is due to small transport number (0.02) of Cu^{2+} [22]. Diffusion affects the ion transfer from the anode as well as to the cathode critically [5]. During the process, the ions diffuse through the anode slimes and through diffusion layers [10]. Convection is not significant at the electrode surfaces, thus diffusion is there dominant, but becomes significant further from the surface, on diffusion layers [22]. The diffusion layers are formed due to diffusion, which is influenced by concentration gradients, as well as natural convection is caused by the concentration and consequently density gradients [22]. The concentration of Cu^{2+} in electrolyte is highest at anode as well as lowest at cathode [15, 22] (figure 4). As a result of convective flow the hydrodynamic boundary layers are formed on diffusion layers [22]. These hydrodynamic layers limit the thickness of diffusion layers during the electrorefining process [22] and thus increase the mass transport rate [15].

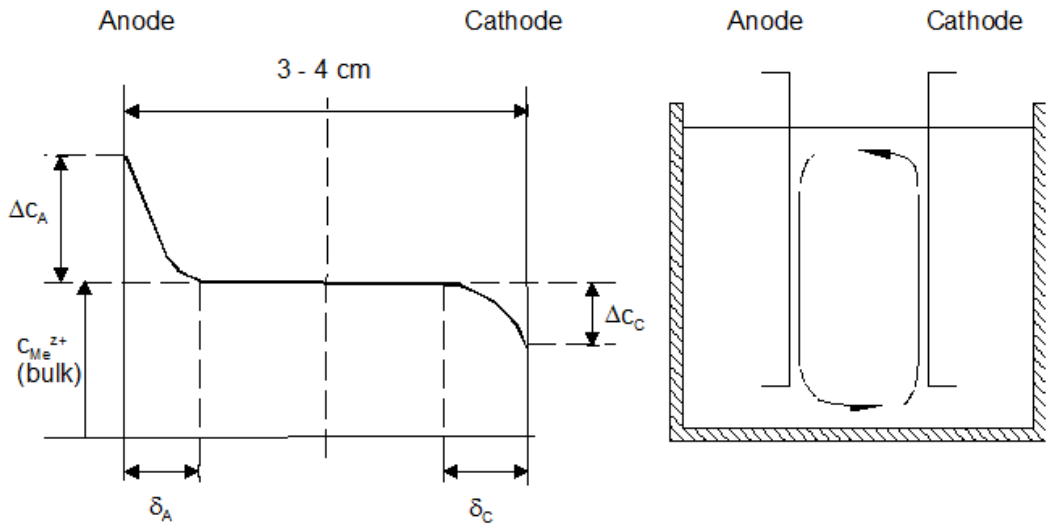

Figure 4. Metal ion concentration profile of a cell (left) and consequent natural convection (right) [15].

In addition to natural convection, there occurs also forced convection in the refining cell due to continuous flow into and out of the cells [22]. However, that flow is not that significant than natural convection [15].

3 Copper electrodeposition

Electrodeposition is used in various engineering and decorative applications, including electroforming, electrorefining and electroplating [24]. In copper electrodeposition process the copper is deposited on a conductive surface from copper salt containing electrolyte using direct current [25]. The deposition takes place when the object to be coated is polarized sufficiently to cathodic direction [25]. The process and its parameters are essential to be understood to obtain good deposit quality.

This chapter discusses electrodeposition in general and copper electrodeposition. Section 3.1 defines the principles of the process. Section 3.2 introduces the nucleation and growth mechanisms of the deposit as well as section 3.3 defines the structure and shape of the deposit.

3.1. Principles

Copper electrodeposition is an electrolytic process which is based on electrochemical reduction reaction on cathode, like all electrodeposition processes [15, 25]. The reduction takes place, when the absolute value of cathodic current is higher than that of anodic current, due to polarization [25]. The reducing copper is deposited on cathode [25]. In copper electrodeposition the reducing takes place in two steps, of which the first (1) is slow and the second (2) fast [26]. The slow step determines the reaction rate [26].

$$Cu^{2+} + e \rightarrow Cu^{+} \quad (1)$$

$$Cu^{+} + e \rightarrow Cu \quad (2)$$

Electrolytes used commercially in copper electrodeposition are commonly acidic sulfate or fluoborate based solutions. The acid solutions are used, since the required voltages for depositing copper are lower than when using alkaline solutions [24]. Copper sulfate solutions are commonly used in electrorefining plants because of the lower price, easier controllability and less susceptibility to impurities than with fluoborate solutions [24].

Faraday's law expresses the relationship between the amount of substance and quantity of electricity [15]. Thus, the law can be used as form (3) calculating the mass of depositing metal, and it is more precise when multiplying that by current efficiency [15, 25].

$$\Delta m = \frac{I \cdot \Delta t \cdot M}{z \cdot F}, \tag{3}$$

where

m = mass, g

I = current, A

t = time, s

M = atomic mass, M_{Cu} = 63.55 g/mol

z = valency of the metal (number of electrons), z_{Cu} = 2

F = Faraday's constant = 96485 C/mol.

Electrodeposition process consists of several stages [15]. Basically the stages are transfer of reactive species from electrolyte to cathode surface, adsorption of the species, charge transfer at the surface, surface diffusion and deposition of the metal, first nucleation and then growing into crystal structure [15]. The slowest stage of these determines the rate of the total reaction [15]. These stages are also connected to the factors of overpotential [15, 25]. Overpotential η can be determined subtracting equilibrium potential from polarized potential, and the cathodic overpotential is negative [25]. The most important overpotential factors are activation, concentration and resistance [15]. Slow charge transfer stage causes activation overpotential, slow mass transfer causes concentration overpotential and ohmic resistances of solution cause resistance overpotential [15]. The resistance overpotential decreases charge transfer between the electrodes, and the activation overpotential can be regarded as a threshold voltage which has to be overcome to start the reactions [15]. However, chemical reactions can take place preceding or following the charge transfer stage [15].

Concentration overpotential, which is also called mass transfer overpotential and is a result of slow mass transfer from electrolyte to electrode, causes limiting current density [15, 25]. Limiting current density is a limit, where the absolute values of current increasing stops, though overpotential increases [25] until the hydrogen evolution begins [15] (figure 3). The limiting current, I_{lim}, can be calculated with equation (4), if the diffusion coefficient, D, the thickness of diffusion layer, δ, and concentration of diffusing species, c, are known [15, 25].

$$I_{lim} = \frac{D}{\delta} \cdot z \cdot F \cdot A \cdot c\,, \qquad (4)$$

where

z = valency of the metal, $z_{Cu} = 2$

F = Faraday's constant = 96485 C/mol.

A = area

c = concentration

The electrochemical reactions take place on the interface between the electrode and the electrolyte [15, 25]. The process on cathode and the surface layers are presented in figure 5 [15]. The deposition process stages can also be seen in the figure.

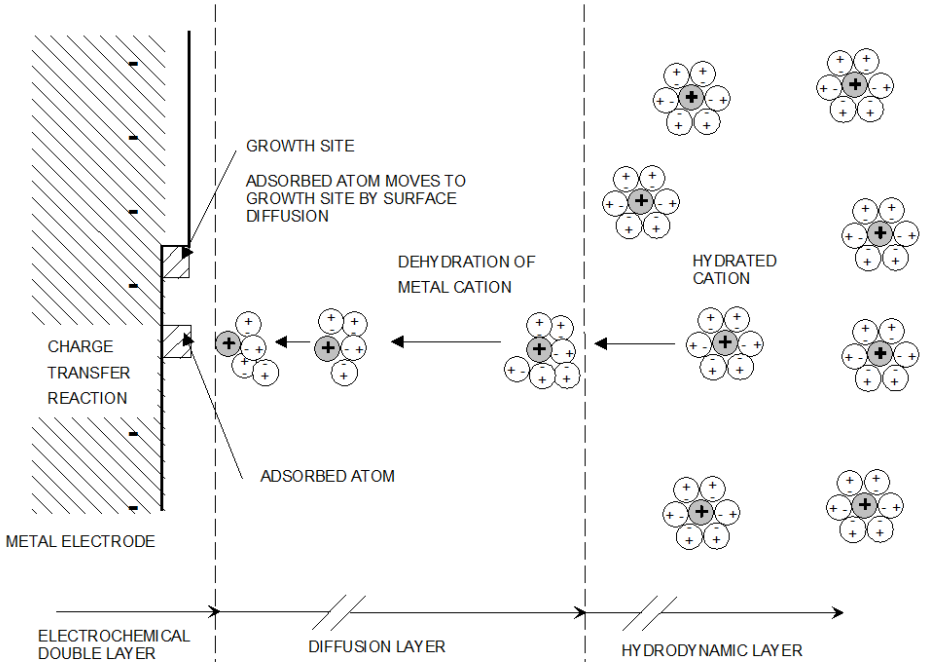

Figure 5. Layers on cathode surface during electrodeposition [15].

3.2. Nucleation and growth of copper

Nucleation is the first and necessary phase in deposition process since the growth cannot begin before it [27]. The small nuclei are not stable and can dissolve, while nuclei larger than the critical size grow on the substrate [27]. The nuclei are commonly formed on phase boundaries, dislocations, impurities and other kind of distortions on surfaces [27]. Thus, the texture of the substrate surface strongly affect the nucleation [28]. The texture have noticed to have even stronger effect on the nucleation than grain faces [29]. Nucleation can also be affected by overpotential [29]. Increasing overpotential increases nucleation [29]. Nucleation affects significantly the structure of the deposit [15], as the increase in nucleation decreases the size of the crystals [25].

In electrorefining copper is electrodeposited on stainless steel blanks, on which are typically grooves and corrosion pits [29]. Those inhomogeneities increase nucleation [29]. Conversely, the passive film on the steel surface lowers nucleation [29]. The surface morphology affects the number of the active sites which react at the overpotential used, as the nucleation takes place on protrusions at lower overpotential than on surface recesses [29]. The overpotential is affected by additives, the surface film resistance, and the surface morphology [29]. Surface film resistance due to passivation limits the sites for copper nucleation [29]. In addition, nucleation process is limited by charge transfer and diffusion [26].

The average volumetric growth rate, r_{gr}, of nuclei is proportional to current density, i, and can be calculated using equation (5) [27].

$$r_{gr} = \frac{M}{zF\rho}|i|F_n, \tag{5}$$

where

M = atomic mass, M_{Cu} = 63.55 g/mol

z = charge of metal ion, z_{Cu} = 2

F = Faraday's constant = 96485 C/mol

ρ = specific density of the deposited metal

F_n = maximum statistical area of the active grain.

The thickness of the deposit depends on current density [15]. Current density locally on the cathode is determined by current distribution [15]. Current distribution is determined by the geometry of the cathode and the cell, the mass transfer, and the polarization at the surface [15].

The deposit is considered to consist of three zones of which the first is the narrow interface between the substrate and the deposit. In that zone takes place the nucleation and the first stages of growth, which are affected by substrate surface and its interactions with the particles of deposit metal [28]. The second zone is transition zone between these interior and outer zones. In the second zone the shape and the number of crystal gradually change from the first to those of the third zone [28]. The third zone is the external zone, in which the substrate structure does not affect the deposit structure [28].

3.3. Structure and shape of the deposit layer

Metal deposits can grow in various shapes. The shape and structure of the deposit are influenced by the current density and inhibition of the electrolyte as well as the mass transfer and concentration of metal ions in the electrolyte [25, 30]. Fischer [31] has developed classification for the metal deposit types, and Winand [30] has further constructed a diagram of those presenting the deposit types as a function of inhibition and the ratio of current density to diffusion-limiting current density. According to Fischer's classification, the metal deposits are divided into five types, FI, BR, Z, FT and UD, the four of which are presented in figure 6 [25, 31]. In types FI, field oriented isolated crystal type, and FT, field oriented texture type, the crystals are oriented parallel to electric field [15, 25]. BR, base oriented reproduction type, is a deposition type, in which the crystals are oriented after the base metal structure [15]. UD is unoriented dispersion type of deposition [15]. Type Z is a twinning intermediate type between types BR and FT [15]. All these types except UD are two dimensional; UD is three dimensional [15].

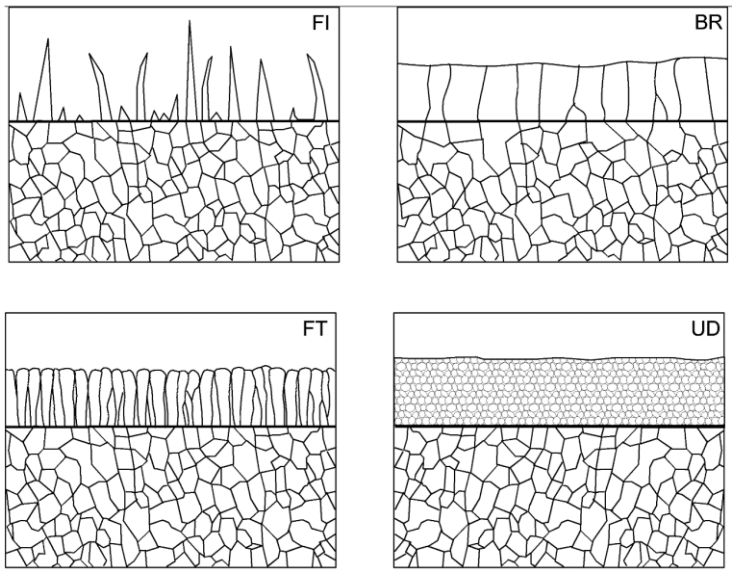

Figure 6. Main morphologies of metal deposits [31].

In addition to these basic metal deposit types there are two types, N and RL, formed when the growth has been disrupted and inhibitors covered the base respectively [25, 32]. N, the nodular deposit takes place, when small solid conductive or semiconductive particles adsorb to the surface and form nodules, as they are covered with metal deposition [15, 25]. RL, rythmic lamellar deposit forms, when the inhibitors has been reacted with the surface or covered the whole surface [25].

Inhibition is used in electrodeposition, since it inhibits growth of crystals and thus increases nucleation [25]. The effects of inhibition, current density and density of metal ion on metal deposit are presented in the diagram (figure 7) [30, 32], which was established in 1960 by Winand [28]. In the diagram the deposit morphologies are presented schematically as a function of inhibition intensity and the ratio of the current density to the concentration of the metal ion deposited [25, 30, 32]. The ratio can also be presented as the current density to diffusion-limiting current density (mass transfer), since the effect of limiting current density increase or decrease is analogous to equivalent metal ion concentration changes [32].

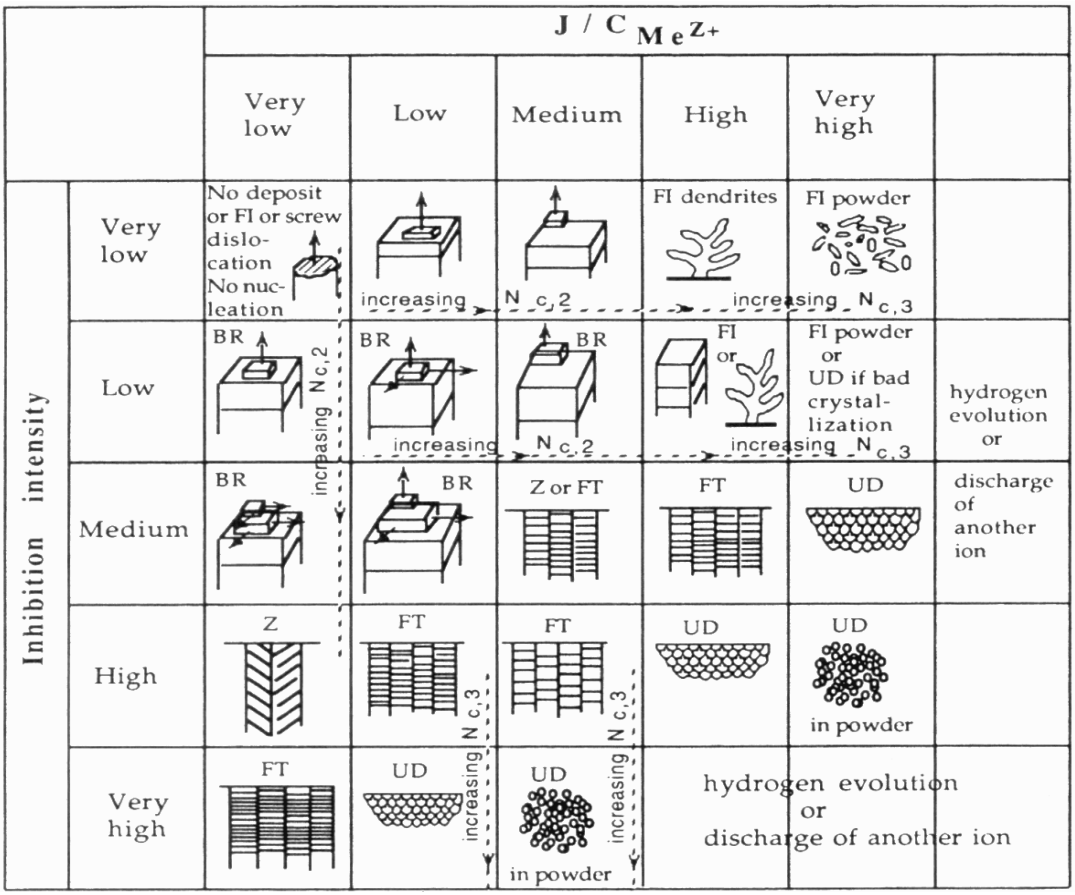

Figure 7. Winand diagram of deposit morphologies [30].

According to Winand diagram FI type forms when using low inhibition and UD type when inhibition intensity is at least medium [30]. The FI type deposit formation becomes with increasing current density first whiskers, then prismatic crystals, dendritic, and eventually powder [15, 30]. FI forms also when BR type deposit is degraded due to long deposition time [32]. The other deposit types are smoother than FI type, except when using high current densities as they form as powder [30].

Winand's research [32] of depositing copper from solutions containing no inhibits indicates that the sulfuric acid in copper electrolyte acts as weak inhibitor. The copper deposits obtained in that research were BR (Z) and FT as well as, with increasing current density, UD deposits types. In Winand's later research [33] using sufficient amount of additive thiourea the copper deposit type obtained was FT-UD, and with insufficient amount of the additive the deposit consisted of types FT-UD, BR and FI [28].

The best morphologies for the deposits are types BR, Z, FT and particularly combination type FT mixed with UD [15]. For good quality of deposit the surface roughness is also

moderate, since the electrolyte could be entrapped in the deposit if the crystals are too large [32]. Too protruding parts of the deposit can cause short circuits in the electrolysis system and thus reduce current efficiency. The good quality deposit can be obtained according to Winand diagram [30] using optimal amount of inhibits as well as choosing the electrolyte concentration and current density correctly.

4 Copper electrolytes

Copper electrorefining electrolytes have widely been investigated in order to optimize the recovery of cathodic copper. The commonly investigated sectors of the electrolytes are physico-chemical properties and composition. The physico-chemical properties, conductivity, density, viscosity and mass transfer, have significant effect on the yield of cathodic copper in electrorefining process.

This chapter describes the composition and physico-chemical properties of the copper electrorefining electrolytes. Section 4.1 presents the common industrial electrolytes and the effects of their compositions. Section 4.2 describes the common temperatures used in industry as well as the effect of temperature changes on the physico-chemical properties conductivity, density, viscosity, and the diffusion coefficient of Cu^{2+}. Sections 4.3–4.5 discuss these properties and the equations to define their values. In addition, section 4.5 presents not only the diffusion coefficient but also mass transfer.

4.1. Composition

Composition of copper electrorefining electrolytes has been designed to enable effective and optimal refining process, and it depends, during the process, on the composition of corroding anodes as well as circulation of the electrolyte regenerating the solution [4]. Composition of electrolytes along with temperature significantly affects the properties of electrolytes [4] as well as anode slime formation and anode passivation [18].

In copper refineries, copper electrolytes usually contain 40–50 [4] or 40–60 g/l [5] copper, 0–25 g/l nickel, 0–20 g/l [4] (in some refineries over 20 g/l) [5] arsenic and approximately 150–200 g/l sulfuric acid [4, 5]. In addition to nickel and arsenic, the electrolyte invariably contains small amounts of other contaminants, such as iron, bismuth, antimony and chlorine, as well as leveling and grain refining addition agents [4, 5]. The usual contents of the electrolytes in five example refineries (in 2007) are shown in table 2.

Table 2. Composition of copper electrolyte in five example copper refineries in 2007. [5]

Electrolyte analysis g/l	Cu	H_2SO_4	As	Sb	Bi	Ni	Fe	Cl
Boliden Harjavalta Oy Pori, Finland	59	145	15.0	0.2	0.1	17	0.2	0.06
Boliden Mineral AB Skelleftehamn, Sweden	49	171	1.6	0.29	0.03	20		0.05
Huttenverke Kayser Lunen, Germany	45	165	7.0	0.4		20	0.2	0.06
Phelps Dodge El Paso, TX, USA	40–50	170–200	13–23	0.07–0.25	0.03–0.1	15–24	1.1	0.037
Codelco Las Ventanas, Chile	50–60	170–180	10–12	0.5–0.6	0.02	2–3	0.8–1	0.04–0.05

The electrolyte should contain enough sulfuric acid and suitable amount of copper (approximately 40 g/l of Cu and 200 g/l H_2SO_4) in order to inhibit dissolution of arsenic, antimony and bismuth, thus enhancing moving of those impurities to the bottom of the cell into the anode slime [21]. However, arsenic is confirmed to be not only contaminant but also essential in forming co-precipitations with antimony and bismuth in form which does not generate floating anode slime but sinks to the bottom of the cell. For that the sufficient amount of arsenic is over 7 g/l [19]. Sulfuric acid is also used in the electrolyte because it enhances conductance, inhibits the hydrolysis of copper(I) sulfate, can be used in high amounts and at high temperatures, as well as because it is not expensive, and possible lead in cell structure withstands it [21]. That conductance enhancing is due to mobile H^+ cations in contrast to less mobile metal cations [7].

A number of the investigations have been devoted to measuring the properties of synthetic copper electrolytes containing compounds similar to those in industrial electrolytes [6–12]. Such studies were carried out by Price and Davenport [6, 7], Jarjoura et al. [10], Moats et al. [8] as well as Subbaiah and Das [9]. The results of such studies have widely been utilized optimizing the refining process. In contrast, research has also been carried out with much lower concentrations, for example in Hinatsu and Foulkes' [13] research. They defined the diffusion coefficients of cupric ion (Cu^{2+}) and used the concentration of copper as variable.

Various approaches have been used by the research groups in their work to determine the effects of composition on the properties of electrolytes. Likewise, the properties focused on and the variables changed in the tests vary. The effects of composition and temperature on conductivity were investigated by Kern et al. [11] and on resistivity by Skowronski and Reinoso [12]. In addition, the effects on conductivity, viscosity and density were investigated by Price and Davenport [6, 7] as well as Subbaiah and Das [9]. They changed copper and sulfuric acid concentration and temperature in their experiments. In addition, Price and Davenport investigated the effects of nickel, arsenic and iron in [7]. Similarly, Subbaiah and Das [9] inspected the effects of composition and temperature on conductivity, viscosity and density on electrolytes, also with cobalt, manganese, nickel and iron impurities. Furthermore, Subbaiah and Das [9], as well as Moats et al. [8], investigated the effects of concentration and temperature on the diffusion coefficient of Cu^{2+}. In addition, viscosity, density and the diffusion coefficient of Cu^{2+} were determined by Jarjoura et al. [10] changing the concentration of nickel and the temperature.

The results of the studies [6–11, 13] showed a clear correlation between the composition and the physico-chemical properties of copper electrolytes. Investigations [6, 7, 9, 10] indicated, that increasing Cu, Ni or As concentration increases density and viscosity, though it mainly decreases conductivity and the diffusion coefficient of Cu^{2+}. Likewise, H_2SO_4 increases density and viscosity and reduces the diffusion coefficient of Cu^{2+}, although it enhances conductivity [6–8]. Exceptions of these effects have noted to be that in low H_2SO_4 concentrations (< appr. 20 g/l) the conductivity increases with increasing Cu concentration [6, 7], and at 25 °C with Cu concentrations between 4.64–60 g/l, according to [13], the increase in the Cu concentration leads to a rise in the diffusion coefficient. The effects of the composition are compiled and roughly presented in table 3.

Table 3. The effects of composition presented as increase or decrease in values of the properties [6–10, 13].

Increase	Conductivity	Density	Viscosity	Diffusion coefficient of Cu^{2+}	Ref.
$Cu/CuSO_4$	↓ [a] /↑ [b]	↑	↑	↓ [c f d] /↑ [e]	[6, 7]/[6, 7]; [6, 7]; [6, 7]; [8, 9, 13]/[13]
H_2SO_4	↑	↑	↑	↓ [c g]	[6, 7]; [6, 7]; [6, 7]; [9, 8]
Ni	↓	↑	↑	↓	[7]; [6, 7]; [6, 7]; [10]
As	↓	↑	↑	?	[7]; [7]; [7]

	a	b	c	d	e	f	g
Cu^{2+}, g/l	0–55	0–55	1.04–43.5	0.127–4.64	4.64–60	35–60	40
H_2SO_4, g/l	> appr. 40	< appr. 20	46.8–450	50	50	160	160–250
Temperature, °C	20–70	20–70	20–60	25	25	65	65

4.2. Temperature

The electrolytes are heated because temperature affects the physico-chemical properties of electrolyte solution increasing the solubility of copper sulfate and speeding up the electrochemical reactions [4] by increasing the mobility of ions [7]. Sufficient solubility of copper sulfate prevents the precipitation of it on anodes [4]. The temperatures in the industrial copper electrorefining processes of different refineries commonly vary between 50–70 °C, and is on average approximately 63 °C [5].

Much research [6–10] described in section 4.1 have been devoted to defining the effects of temperature on the physico-chemical properties of copper electrorefining electrolytes with variable compositions and temperatures. Most of these studies which deal with the effects of temperature also deal with the effects of composition. The investigations show that raising the temperature lowers viscosity and density while it simultaneously increases the conductivity and the diffusion coefficient of Cu^{2+} (table 4).

Table 4. The effects of temperature changes on properties as increase or decrease in values [6–10].

	Conductivity	Density	Viscosity	Diffusion coefficient of Cu^{2+}	Ref.
Temperature rise	↑	↓	↓	↑	[6, 7, 9]; [6, 7]; [6, 7]; [8, 9, 10]

The process conditions in electrorefining can be optimized, when the effects of temperature and composition as well as the process demands are known. Thus, the best yield can be obtained by keeping the electrical conductivity high and viscosity low, which can be achieved using low-copper concentration and high temperature [6].

4.3. Conductivity

Conductivity is important transport property of solution [34] and it affects the electrical energy consumption of electrorefining process [6, 7]. Therefore, when optimizing the refining process, by altering the temperature or composition the conductivity value is an easy quantity to be controlled by measuring it or defining it with an applicable equation.

The accurate effects of separate constituents on conductivity have been systemically investigated to define equations of physico-chemical properties. The effects of Ni, As and Fe on conductivity compared to each other by Kern et al. are presented in figure 8 [11].

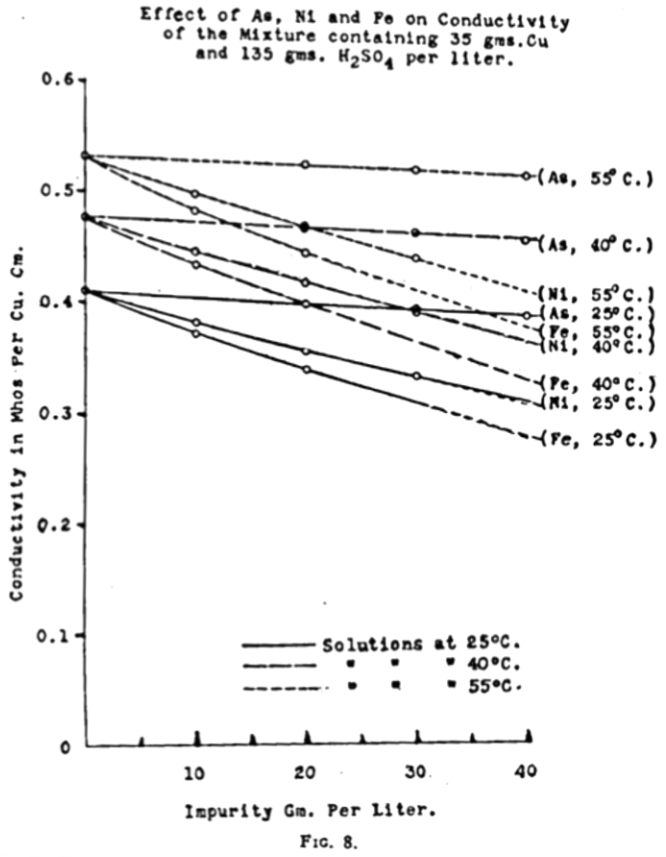

Figure 8. Effect of As, Ni and Fe on copper electrolyte (Mho = S) [11].

Equations for quantifying conductivity as a function of concentration and temperature have been defined by Price and Davenport [6], [7] as well as Subbaiah and Das [9]. These studies are described more in details in section 4.1. Price and Davenport [6] defined an equation (6) on conductivity using concentrations of Cu and H_2SO_4 and temperature as the variables. Furthermore, they [7] defined an equation (7) which also takes into account the usual impurities in copper electrolyte nickel, arsenic and iron as well as a combined equation (8) based on their own results and Kern and Chang's [11] as well as Skowronski and Reinoso's results [12]. A similar equation (9) was adapted by Subbaiah and Das [9] in their research.

$$\kappa = 0.134 - 0.00356\,[\mathrm{Cu}] + 0.00249\,[\mathrm{H_2SO_4}] + 0.00426\,\mathrm{T}, \quad (6)$$

$$1/\kappa = 3.2 + 10^{-3} \cdot (1.3\,[\mathrm{As}] + 7.3\,[\mathrm{Cu}] + 4.5\,[\mathrm{Fe}] - 5.6\,[\mathrm{H_2SO_4}] + 9.5\,[\mathrm{Ni}] - 14.6\,\mathrm{T}), \quad (7)$$

$$1/\kappa = 3.2 + 10^{-3} \cdot (1\,[\mathrm{Co}] + 2\,[\mathrm{As} + \mathrm{Mg}] + 3\,[\mathrm{Al}] + 9\,[\mathrm{Cu}] + 11\,[\mathrm{Ni}] + 12\,[\mathrm{Fe}] - 6\,[\mathrm{H_2SO_4}] - 15\,\mathrm{T}), \quad (8)$$

$$^{1}/_{\kappa} = 3.2 + 10^{-3} \cdot (1\,[\mathrm{Co}] + 1\,[\mathrm{Mn}] + 9\,[\mathrm{Ni}] + 12\,[\mathrm{Fe}] - 6\,[\mathrm{H_2SO_4}] - 15\,\mathrm{T}),$$ (9)

where [Cu], [H_2SO_4] and other concentrations are in g/dm^3 and T is in °C, while κ is in S/cm.

An equation (10) for quantifying conductivity of ternary mixed solutions using the conductivity values of their binary subsystem solutions was established by Hu et al. [35] as a part of their semi-ideal solution theory studies. They also utilized the generalized Young's rule (11) analogously for predicting conductivity values of solutions using the values of the binary subsystems. The usefulness of the semi-ideal solution theory [35] and the generalized Young's rule predicting conductivity was verified by Zhang et al. [34].

$$\ln\kappa = z_1 \ln\kappa_1 + z_2 \ln\kappa_2, \quad (10)$$

where z_i = mole fraction ratio of i·$H_2O_{(Li)}$

$$\kappa = y_1\kappa_1 + y_2\kappa_2, \quad (11)$$

where

$y_i = \frac{I_i}{I_1 + I_2}$ and I = ionic strength, i = 1 or 2.

4.4. Density and viscosity

Both viscosity and density raising lowers the diffusion coefficient of cupric ion [8] as well as decreases the rate in which the anode slime falls to the bottom of the cell [4]. Decreasing falling rate of anode slime increases the movement of the slime to other directions than downward [4]. If the anode slime ends up on cathode, the impurities could entrap into the coating [4]. Thus, viscosity and density affect the purity of the cathode copper [7]. Due to that viscosity and density are tried to keep sufficiently low [4].

Equations to evaluate densities and viscosities have been determined by Price and Davenport [6, 7], as well as Subbaiah and Das [9]. Price and Davenport compiled one equation of density [6] using Cu and H_2SO_4 concentrations (12) and two other (13) and (14) with impurities [7]. In defining (14) they used Claessens' [36] results in addition to their

own. Subbaiah and Das [9] used almost identical equation (15) assessing their results. The difference is mainly due to partly different contaminants in the electrolytes they investigated. The dependence of nickel concentration on density was also rated by Jarjoura et al. [10] and the positive linear correlation was verified.

$$\rho \pm 0.005\ \mathrm{g/cm^3} = 1.01856 + 0.00238\ [\mathrm{Cu}] + 0.00054\ [\mathrm{H_2SO_4}] - 0.00059\ \mathrm{T} \quad (12)$$

$$\rho \pm 0.01\ \mathrm{g/cm^3} = 1.022 + 10^{-3}\ (1.04\ [\mathrm{As}] + 2.24\ [\mathrm{Cu}] + 2.37\ [\mathrm{Fe}] + 0.55\ [\mathrm{H_2SO_4}] + 2.24\ [\mathrm{Ni}] - 0.58\ \mathrm{T}) \quad (13)$$

$$\rho \pm 0.02\ \mathrm{g/cm^3} = 1.02 + 10^{-3}\ (1\ [\mathrm{As}] + 2\ [\mathrm{Cu} + \mathrm{Co} + \mathrm{Fe} + \mathrm{Na} + \mathrm{Ni}] + 0.5\ [\mathrm{H_2SO_4}] + 3\ [\mathrm{Mg}] + 6\ [\mathrm{Al}] - 0.6\ \mathrm{T}) \quad (14)$$

$$\rho = 1.02 + 10^{-3}\ (2\ [\mathrm{Cu} + \mathrm{Co} + \mathrm{Fe} + \mathrm{Mn} + \mathrm{Ni}] + 0.5\ [\mathrm{H_2SO_4}] - 0.6\ \mathrm{T}), \quad (15)$$

where the densities are in g/cm^3, concentrations in g/dm^3 and T in °C.

For absolute viscosity, Price and Davenport have defined equations (16) [6] and (17) [7] when impurities are involved. According to these equations, all the reagents increased viscosity. The effect of nickel concentration on viscosity was also rated by Jarjoura et al. [10] and the positive correlation was verified.

$$\mu \pm 0.1\ \mathrm{cp} = 10^{-6}\left(1592 + 0.0108\ [\mathrm{H_2SO_4}]^2 + 2.373\ [\mathrm{H_2SO_4}] + 29.93\ [\mathrm{Cu}] + 76.48\ [\mathrm{Cu}]^{1/2}\right) e^{1890/\mathrm{T}}, \quad (16)$$

where concentrations are in g/dm^3, T in K and μ in cp (= mPa·s).

$$1/\mu \pm 0.1\ \mathrm{cp} = 0.7 - 10^{-3}\ (4.6\ [\mathrm{As}] + 8.3\ [\mathrm{Cu}] + 8.8\ [\mathrm{Fe}] + 1.6\ [\mathrm{H_2SO_4}] + 10.0\ [\mathrm{Ni}] - 18\ \mathrm{T}), \quad (17)$$

where concentrations are in g/dm^3, T is in °C and μ in cp (= mPa·s).

The viscosities of complex ionic solution can also be defined in ionic concentration (18) [6], [7]. It can be calculated for copper sulfate-sulfuric acid solution using equation (19) [6], and when impurities are involved using (20) [7] or (21) [9].

$$\Gamma = \sum C_i Z_i^2, \tag{18}$$

where

C_i = concentration of ion i, g/dm^3

Z_i = valence of ion i.

$$\Gamma = 2 \cdot \frac{[H_2SO_4]}{98.08} \cdot 1^2 + 2 \cdot \frac{[Cu]}{63.54} \cdot 2^2 \tag{19}$$

$$\Gamma = 2\, M_{H_2SO_4} + 8\, (M_{Cu} + M_{Fe} + M_{Ni} + M_{Co} + M_{Mn}) \tag{20}$$

$$\Gamma = 2\, M_{H_2SO_4} + 2\, M_{As} + 8\, (M_{Cu} + M_{Fe} + M_{Ni}) \tag{21}$$

Ion concentration correlates with viscosity (μ) according to [6, 7, 9]. Thus, viscosity can be presented as a function of ionic concentration (22) [6] and (23) [9].

$$\mu = 10^{-6}\, (1834 + 2.609\, \Gamma^{\frac{1}{2}} + 256.9\, \Gamma - 44.56\, \Gamma^2) \cdot e^{1890/T}\ , \tag{22}$$

where T is in K.

$$\mu = m\Gamma + C, \tag{23}$$

where constants m = 0.114 and C = 0.86 [9].

4.5. Mass transfer of copper

Mass transfer of copper to cathode is highly important, and it can be presented as flux of species generally as equation (24), which is a version of Nernst-Planck equation [23, 37].

$$J_j(x) = -D_j \frac{\partial C_j(x)}{\partial x} - \frac{z_j F}{RT} D_j C_j \frac{\partial \phi(x)}{\partial x} + C_j v(x), \tag{24}$$

where the three terms are linked to diffusion, migration, and convection respectively and

$J_j(x)$ = flux of species j (mol/cm^{2}s)
x = distance from surface
D = diffusion coefficient (cm^2/s)
$\partial Cj(x)/\partial x$ = concentration gradient
$\partial \phi(x)/\partial x$ = potential gradient
z_j = charge
C_j = concentration (mol/cm^3)
v(x) = velocity (cm/s).

As described in section 2.3, diffusion and convection are the main modes of mass transport in electrorefining [22]. Diffusion determines the rate of copper transferring across the Nernst boundary layer (diffusion layer) which affect the dissolution of the anode and deposition on the cathode [8, 15].

There are various methods determining diffusion coefficients, for example rotating disc electrode, chronoamperometry, polarography and diaphragm cell methods [38, 39]. However, other methods than rotating disc electrode method are not focused on in this work. Rotating disc electrode technique is a convective electrode system hydrodynamic method, in which convection is generated by rotation of the electrode [23]. In the technique, the work electrode is rotated, the potential is changed to cathodic direction, and the limiting current density is defined [23]. Diffusion coefficient can be determined from limiting current density with Levich equation (25) or Koutecký-Levich equation (26) [37]. Limiting current density is the highest rate of reaction in the mass transfer controlled system, while mass transfer still controls reaction [15]. The limiting current is increased, if flow rate, temperature, concentration or diffusion rate of reacting species increase [15]. Increasing the flow rate increases the limiting current since the flow controls the thickness of the diffusion layer [25]. Lowering the thickness of the diffusion layer, the rate of reactions increases [25].

$$I_{l,c} = 0.62 \cdot nFA \cdot D^{2/3} \cdot \omega^{1/2} \cdot \nu^{-1/6} \cdot c_0 \quad , \tag{25}$$

where
$I_{l,c}$ = diffusion-limited cathodic current, A

n = number of transferred electrons in the reaction

F = Faraday's constant

A = area of the disc work electrode, cm^2

ω = angular velocity, $1/s$

ν = kinematic viscosity, cm^2/s

c_0 = concentration of metal ion, mol/cm^3 [8]

$$\frac{1}{I} = \frac{1}{I_K} + \frac{1}{0.620 \cdot nFA \cdot D^{2/3} \cdot \omega^{1/2} \cdot \nu^{-1/6} \cdot c_0}, \quad (26)$$

where

I = current

I_K = activation-limited current.

Many of the diffusion coefficient measurements of cupric ion (Cu^{2+}) have been conducted in circumstances that have been different from those in industrial electrorefining [13, 38–40]. Diffusion coefficients have been measured of electrolytes with lower concentrations of Cu and H_2SO_4 as well as at lower temperatures compared to the process parameters in the refineries by Hinatsu and Foulkes [13], Quickenden and Jiang [38] as well as Quickenden and Xu [39]. Hinatsu and Foulkes compiled an equation (27) for the diffusion coefficients of Cu^{2+}. In addition, Claessens et al. [40] have carried out experiments at 25 °C with electrolytes containing less copper than in industrial processes, but they measured also electrolytes which contained similar amounts of sulfuric acid as in electrorefining electrolytes.

$$10^6 \cdot D_{Cu} = 6.33 + 2.69 \log [CuSO_4]_0 + 1.62 \log^2 [CuSO_4]_0 + 0.256 \log^3 [CuSO_4]_0, \quad (27)$$

where concentrations are in mol/l.

The measurements of diffusion coefficient of Cu^{2+} of $CuSO_4$-H_2SO_4 electrolytes have been implemented in refining conditions by Moats et al. [5], Jarjoura et al. [10] as well as Subbaiah and Das [9]. In addition to effects of Cu and H_2SO_4 concentration, Jarjoura et al. research the effects of Ni concentration on diffusion coefficients. Subbaiah and Das defined equation (28) for the diffusion coefficients of Cu^{2+}. However the most of their measurements were conducted in lower concentrations of Cu and H_2SO_4 as well as lower temperature than used in the industrial refining processes.

$$10^5 \cdot D_{Cu} = -0.570 - 0.00164\, C_{H_2SO_4} - 0.00175\, C_{Cu} + 0.0607\, T, \qquad (28)$$

where T is in °C and concentrations are in g/dm^3.

The diffusion coefficients of Cu^{2+} have been measured by many researchers [5, 9, 10, 13, 38–40]. However, the results of the measurements have varied significantly even if the conditions and compositions are set similar as seen in figure 9 [9, 13, 40]. It though should be noted that the results from Subbaiah and Das [9] in that figure are plotted using the equation (28) which has been defined of results mainly measured at 30 °C. Only some of these measurements were carried out in other temperatures, only one of those at 20 °C and none at 25 °C. The results from Subbaiah and Das [9] are presented more detailed in figures 10 and 11.

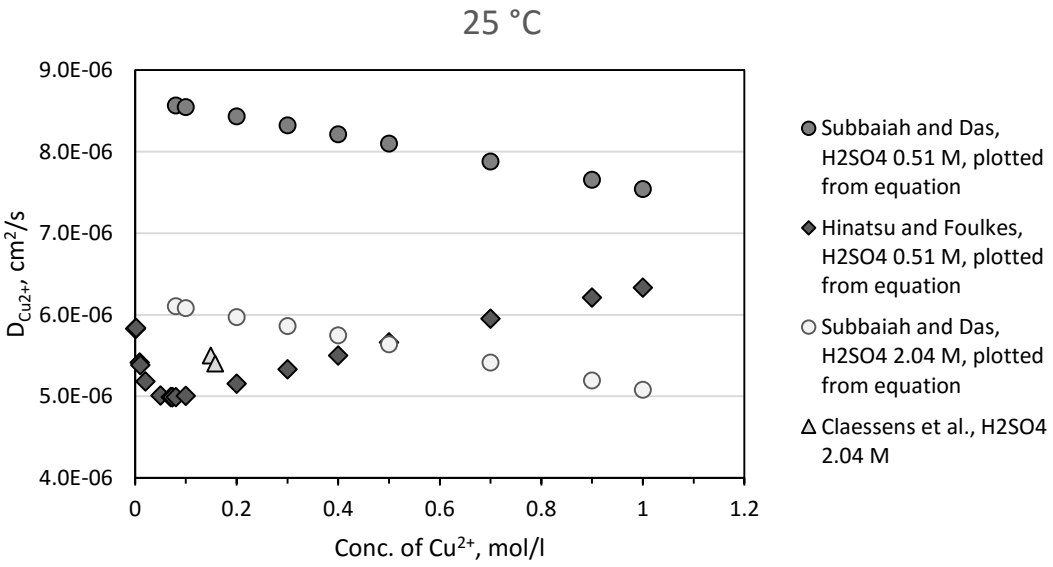

Figure 9. Comparison of literature values of D_{Cu2+} at 25 °C using equations from [9] and [13] as well as measured values from [40].

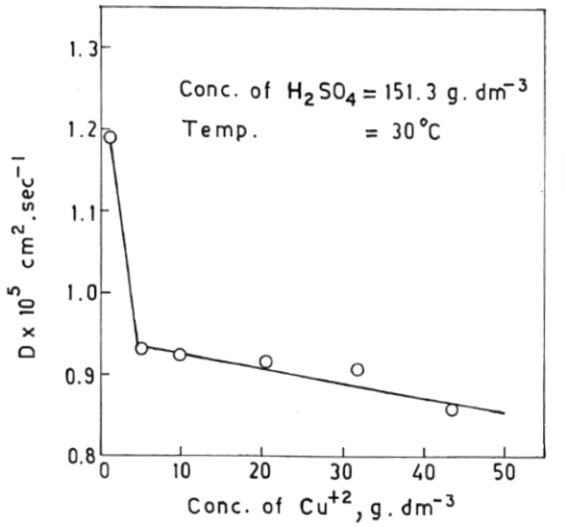

Fig. 1—Effect of copper concentration on diffusion coefficient (*D*).

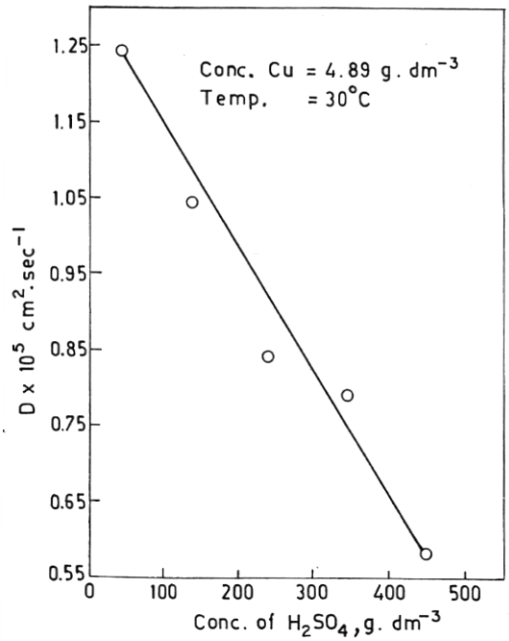

Fig. 2—Effect of H_2SO_4 concentration on diffusion coefficient (*D*).

Figure 10. Effect of Cu and H_2SO_4 concentration on D_{Cu2+} [9].

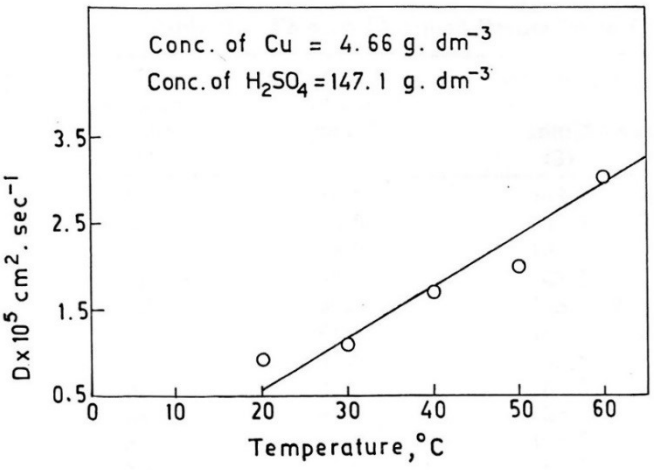

Fig. 3—Effect of temperature on diffusion coefficient (*D*).

Figure 11. Effect of temperature on D_{Cu2+} [9].

The accuracy of determining the diffusion coefficients of Cu^{2+} was criticized by Quickenden and Jiang [38] as well as by Quickenden and Xu [39]. Quickenden and Jiang also criticized the using of simple Levich equation determining the diffusion coefficient of rotating disc electrode measurements. They suggested to use a more precise Koutecký-Levich equation, in which the charge-modified diffusion is considered if there is also charge control in the system in addition to basic diffusion. Furthermore, Quickenden and Xu [39] introduced three precise equations for measuring D_{Cu2+}: Gregory and Riddiford equation (29), Newman

equation (30) as well as mixed-control Newman equation (31). These equations are modified from Levich and Koutecký-Levich equations inserting additional coefficients [39]. Quickenden and Xu recommended to use mixed-control equation (31) of these equations [39], since they had noticed the values obtained ignoring the activation polarization to be too low.

$$I_d = 0.620 \left(1 + 0.3539 \left(\frac{D}{\nu}\right)^{0.36}\right)^{-1} nFAcD^{2/3}\nu^{-1/6}\omega^{1/2} \quad (29)$$

$$I_d = 0.620 \left(1 + 0.2980 \left(\frac{D}{\nu}\right)^{1/3} + 0.14514 \left(\frac{D}{\nu}\right)^{2/3}\right)^{-1} nFAcD^{2/3}\nu^{-1/6}\omega^{1/2} \quad (30)$$

$$\frac{1}{I_L} = \frac{1}{I_K} + \frac{1+0.2980 \left(\frac{D}{\nu}\right)^{1/3} +0.14514 \left(\frac{D}{\nu}\right)^{2/3}}{0.620nFcAD^{2/3}\nu^{-1/6}\omega^{1/2}} \quad (31)$$

5 Materials and methods

This chapter presents the materials and methods used in this thesis. Section 5.1 describes the chemicals used in the synthetic electrolytes, sections 5.2–5.4 present test equipment and the procedures as well as section 5.5 describes the data analysis method.

5.1. Electrolytes

The copper electrolytes used in this thesis contained varying amounts of copper, nickel, arsenic and sulfuric acid. These amounts were chosen to be alike the industrially used electrolytes [5] apart from additives, which were not used in this work. The electrolytes were prepared from copper sulfate ($CuSO_4 \cdot 5\ H_2O$, min. 98%, VWR Chemicals), nickel sulfate ($NiSO_4 \cdot 6\ H_2O$, min. 98%, VWR Chemicals), sulfuric acid (H_2SO_4, 95–98%, Sigma-Aldrich), arsenic acid solution (from Boliden) and distilled water. $CuSO_4 \cdot 5H_2O$, $NiSO_4$ and H_2SO_4 were measured the adequate amounts to achieve the concentrations shown in table 5. Thus, the electrolytes contained at least the target amount of copper, nickel and sulfuric acid. The concentration of arsenic which was 0, 15 or 30 g/l, was very accurate, since the composition of the arsenic acid solution was analyzed (table 6) at Labtium Oy. Cu and nickel contents in arsenic acid were also taken into account when preparing the electrolytes.

Table 5. Concentrations of copper, nickel and sulfuric acid in the electrolytes.

	Cu, g/l			Ni, g/l			H_2SO_4, g/l			
	40	50	60	0	10	20	160	180	200	220
min.	40	50	60	0	10	20	160	180	200	220
max.	40.816	51.02	61.225	appr. 0	10.204	20.408	165.04	185.69	206.33	226.93

Table 6. Analyzed composition of arsenic acid solution.

	mg/l									
	Bi	**Se**	**Te**	**Ag**	**As**	**Ba**	**Cu**	**Ni**	**Pb**	**Sb**
Arsenic acid	6.2	0.07	18.6	0.16	151700	0.01	4794	1688	28.62	3954

5.2. Conductivity measurements

Conductivity measurements were carried out using Knick Portamess® 913 Cond conductivity meter produced by Knick Elektronische Messgeräte GmbH & Co. KG. The meter was used with 4-electrode sensor ZU 6985 which has glass/platinum measuring system and glass casing tube. The meter and the sensor are shown in figure 12.

Figure 12. Conductivity meter with ZU 6985 sensor.

The electrolytes were heated before the measurements in jacketed cell using MGW Lauda MT/M3 circulating water bath (figure 13). During the heating or between the measurements, the cell was covered thoroughly and all the holes of the cover were plugged to prevent evaporation and consequently water loss. The hole for measuring was opened only for measurements. During both heating and measurement periods the electrolyte was stirred using WWR's magnetic stirrer. The stirring rate was 400 RPM during the heating and slightly less during the measurements.

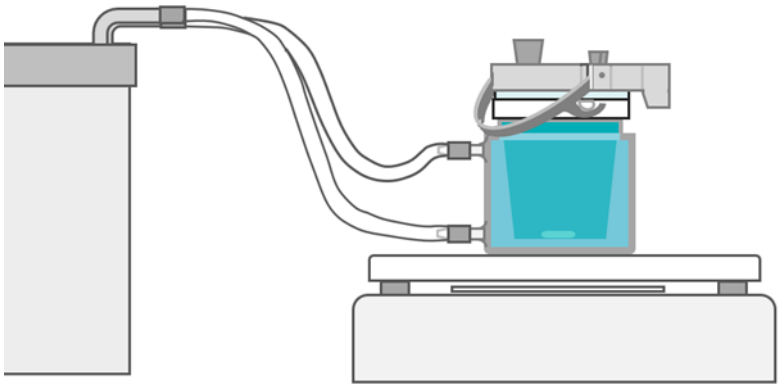

Figure 13. Experimental arrangement for conductivity measurements.

The temperature during the measurements was measured with the conductivity meter, since the sensor contained a temperature detector. During the measurements, the temperatures were within tolerances of ±0.2 °C.

5.3. Density and viscosity measurements

Density and viscosity measurements were carried out using portable viscosity and density meter VDM 250 produced by LEMIS Process (figure 14, right). The measured electrolytes were heated with MGW Lauda MT/M3 circulating water bath in a beaker as shown in figure 14 (left). The beaker was here chosen for a tank of the electrolytes on account of its size since the probe of the viscosity and density meter did not fit into the jacketed cell used in other measurements of this work. The beaker was covered with Parafilm M® around the probe of the meter and mainly kept in place during all measurements of one electrolyte to minimize water loss by evaporation. During the measurement, the probe had to occasionally be removed from the beaker and cleaned its surfaces for preventing getting too high viscosity and density values. Typically, the surfaces of the probe were kept as free as possible from precipitates of the electrolytes by regularly shaking the beaker over the probe. After the shaking, the electrolyte was let to settle down before the value reading.

The temperature during the measurements was measured with the viscosity and density meter, since the probe contained a temperature detector, and the beaker was too narrow to be able to insert there the thermometer. During the measurements, the temperatures were within tolerances of ±0.1 °C.

Figure 14. Experimental arrangement for density-viscosity measurements and the meter.

The portable meter used in these measurements was chosen since it gives viscosity and density values of liquids at the same measurement as well as since it could later be used in field surveying. In addition, the meter has a temperature sensor in the probe. The meter's operating principle was based on resonant oscillation, of which the frequency was measured. However, the meter was actually designed for measuring petroleum products, not such liquids as used in copper refining and it was uncertain if the probe of the meter was suitable for these measurements. The probe was modified to withstand the temperatures and acidity by changing the material to Hastelloy. However, the meter was calibrated to work below 59 °C, and the recalibration was impossible without the manufacturer. The meter was tested before the actual experiments by measuring electrolytes with known densities and dynamic viscosities, compared the obtained values with the literature values. Because the measured values were reasonably close to those of literature at that point, the meter was put into operation, and the suitability of the probe as well as the meter was investigated further.

For obtaining more accurate density results, the measured values of the electrolytes were normalized with respect to the difference between the measured and theoretical values of distilled water. This additional procedure was executed due to the uncertainties of stability of the meter. These water measurements were carried out before the measurements of each electrolyte. However, the accuracy of kinematic viscosity results was not directly able to be improved with normalization. The kinematic viscosity values were used for modelling both without normalization and normalized as quotients of dynamic viscosity values and normalized density values.

5.4. Rotating disc electrode measurements

The limiting current density was measured using linear sweep voltammetry with rotating disc electrode (RDE) apparatus (figure 15). The equipment used was Autolab 30 potentiostat produced by Ecochemie, GPES software and Model 616 RDE (rotating disc electrode) produced by Princeton Applied Research. The limiting current densities measured were used defining diffusion coefficients (D) of Cu^{2+} utilizing Levich equation (25) and Koutecký-Levich equation (26).

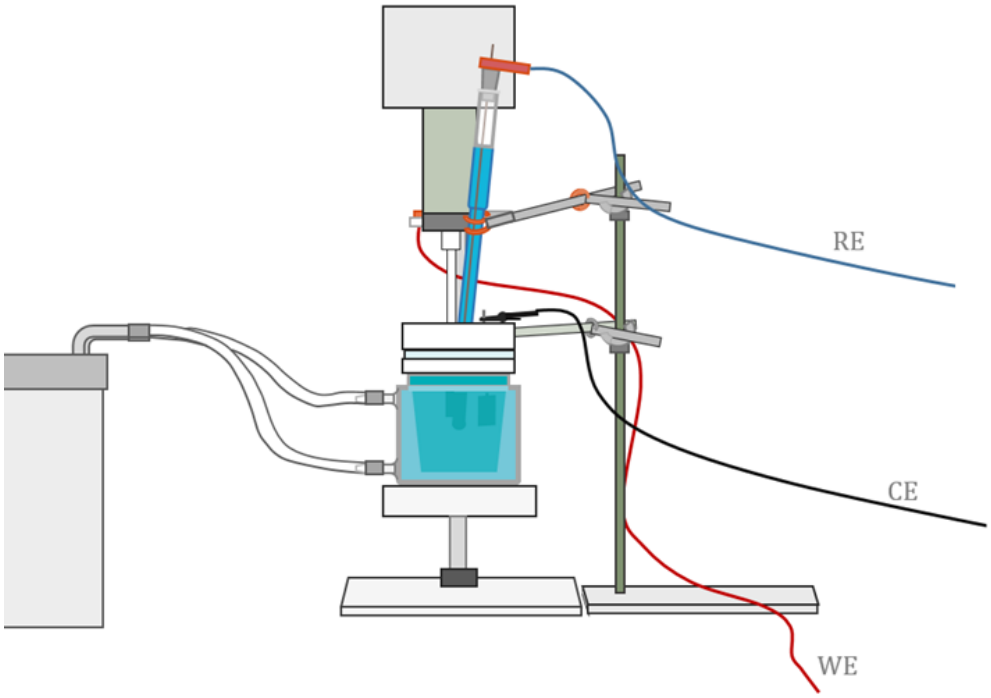

Figure 15. Experimental arrangement for rotating disc electrode measurements.

The same jacketed cell and the circulating water bath MGW Lauda MT/M3A was used in heating the electrolytes as used in conductivity measurements, yet the cell cover was different. The special modified cover was needed because of the electrode arrangement (figure 16). As the figure 16 shows these measurements were conducted with a three-electrode system. That consisted of $CuSO_4$ reference electrode, platinum counter electrode and copper plated platinum rotating disc working electrode. In addition to the electrodes, the cell arrangement included gas dispersion tube for deoxidation with nitrogen prior to each measurement.

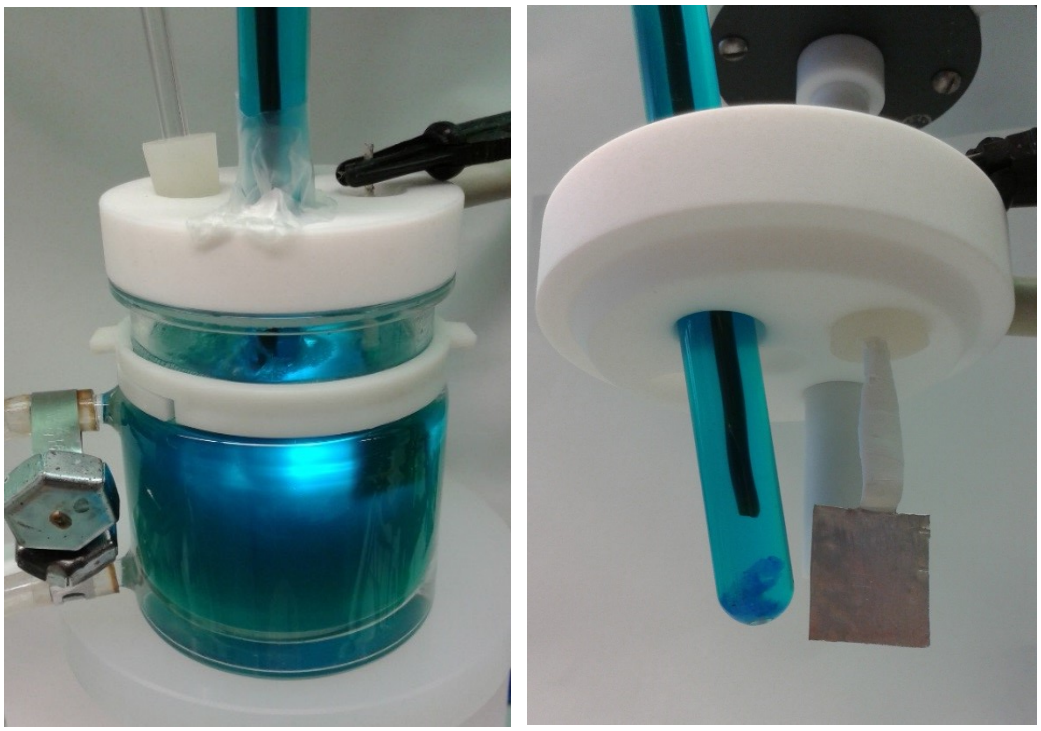

Figure 16. Jacketed cell used in rotating disc electrode measurements and the electrode arrangement.

Before each experiment the quality of the rotating working electrode surface was visually controlled and the impurities formed on metal surface removed. The electrode end was ground manually using clean P1200 emery paper (silicon carbide, made by Struers). The surface was not polished because the time used in the tests wanted to be kept reasonable. The surface of the working electrode was ground each time similarly to keep the surface quality uniform in all measurements. After grinding, the surface was coated with copper if the copper coating on base metal platinum was worn off and the platinum was visible. The variation of surface quality is shown in figure 17.

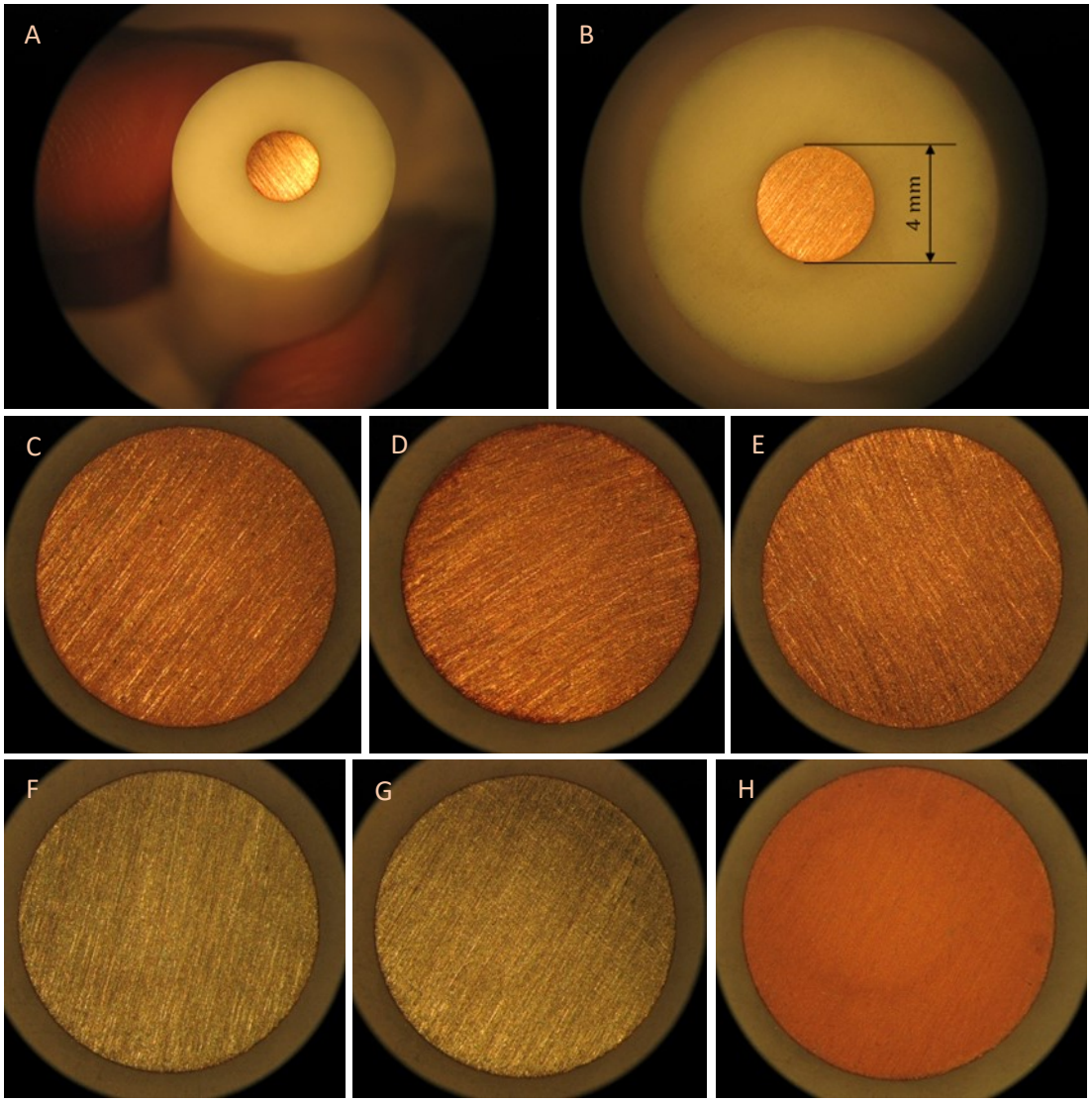

Figure 17. Surface quality of the working electrode with ground copper coating on the platinum surface (A–E) and ground platinum surface before coating (F–G) as well as after coating (H).

The temperature was measured using a thermometer before the first and after the last RDE measurement in each temperature. The RDE measurements were not conducted until the temperature was sufficiently close to the target, in these measurements within tolerances of ±0.5 °C.

The heated electrolytes were visually inspected and deaerated prior to the experiments. In inspection dissolution of sulfate crystals as well as uniform mixing was confirmed. In deaeration the quantity of dissolved oxygen in electrolyte was minimized with nitrogen

sparging. This process was performed in two phases. In the first phase, the sparging was carried out in an arrangement separate from the electrodes using a tighter cover on the cell for avoiding excess evaporation. In this deaeration procedure nitrogen was sparged near the bottom of the cell to both mix and deoxidize the electrolyte. The first phase lasted while the electrode was prepared. The second phase of sparging started when the rotating working electrode was screwed on the RDE apparatus, and the cell was also set to its place. The nitrogen was sparged near the surface to avoid bubbles to adhere on the anode. This phase lasted at least 15 minutes to make sure that the oxygen level in the electrolyte was sufficiently low. The time was set based on experimental potential measurements during sparging. The same sparging time was also used by Hinatsu and Foulkes [41] prior to their measurements of approximately same volume of electrolyte.

The measuring procedure was carefully pretested with electrolytes which contained no nickel or arsenic and less copper than the actual electrolytes as well as with electrolytes with the same amounts of copper, and the suitability of the method was verified. Furthermore, the pretest electrolytes were measured using various rotation rates and scan rates to choose the most applicable rates. The chosen scan rate was 0.01 V/s, the step potential 4.88 mV and rotation rates 10, 30, 50 as well as 100 RPM. The rotation rate 10 RPM was, though, abandoned as a result of lack of linearity at limiting current density area in curves as well as due to recommendations by [37]. According to that specification, the lower limit of angular velocity ω can be calculated with (32):

$$r_1 > 3\,(\nu/\omega)^{½}, \qquad (32)$$
$$\omega > 9\,\nu / r_1^2.$$

Thus, in these measurements ω was measured to be optimal when it was higher than 1.44–3.67 1/s, which is converted to rotations per minutes 13.54–34.16. In two measurements, the rotation rate 30 RPM was according to that too low. Nevertheless, the rate was kept unchanged since the curves and the further results with them seemed correct.

The upper limit of angular velocity can be calculated using equation (33) [37]. That was, however, not necessary here since the surface of the working electrode was not sufficiently smooth to enable using the maximum rotation rate. The ground surface causes more turbulent flow than perfectly polished surface [37].

$$\omega < 2 \cdot 10^5\,\nu / r_1^2 \qquad (33)$$

The limiting current densities (i_{lim}) were measured and the values for calculating diffusion coefficient were determined as average grades of several points as shown in figure 18. As seen in figure 18 the cathodic current cannot be increased unlimitedly. At the limiting current density point the cathodic voltage inserted into a system does not increase the current until the hydrogen evolution begins [15].

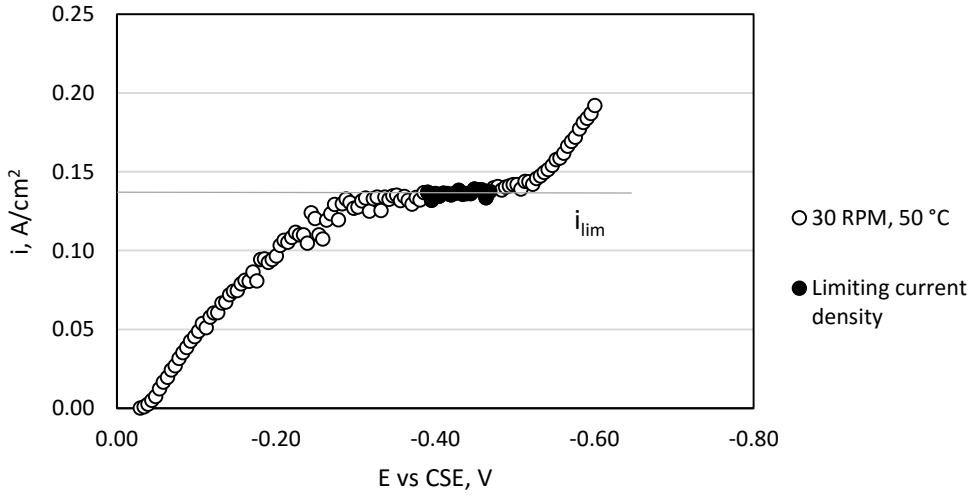

Figure 18. Defining limiting current density of the measured curve.

5.5. Data analysis

Data analysis and experiment designing were carried out using Modeling and design tool MODDE 8 which is the software of Umetrics AB for design of experiments (DOE) and multivariate data analysis. The experiments were designed defining factors, responses and levels of the factors. Those terms were inserted in the program. The factors with levels and the responses used in this work are shown in table 7. The levels of temperature were different in viscosity and density measurements since the meter was calibrated to be able to measure only below 59 °C. In addition, the temperature levels for limiting current density were chosen only 50, 60 and 70 °C. That was due to avoiding unnecessary measurements.

Table 7. Factors, levels and responses of the tests.

Factor	Levels		Responses	
Cu	40; 50; 60	g/l	Conductivity	mS/cm
H_2SO_4	160; 180; 200; 220	g/l	Density	g/cm^3
Ni	0; 10; 20	g/l	Viscosity	mm^2/s
As	0; 15; 30	g/l	Diffusion coefficient of Cu^{2+}	cm^2/s
T	50; 55; 60; 65; 70 or 50; 55; 59	°C		

The objective of investigation chosen for the models in this work was screening in which the fit method was partial least squares (PLS) [42], and the design chosen was full factorial design. That design gave at first phase (without arsenic, for conductivity) 180 combinations of the factors and their levels and at second phase all the 540 combinations. The full factorial design was chosen because of its simplicity and the possibility to select tests of those combinations one by one and reselect easily more tests to carry out of all combinations. The experiments carried out are presented in appendix A (tables A1–A3).

The data obtained from the measurements was put into MODDE software and evaluated with diagnostic tools. The recommended [42] tools scatter plot, histogram of response, descriptive statistics of response and condition numbers were used for evaluating the raw data. According to these evaluations, the data was transformed or processed further taking the properties into account in other ways. The histogram of the response data should be normally or nearly normally distributed to obtain valid models. In case of too skew histogram or descriptive statistics, the response was logarithmically transformed. However, some skewness of the histogram was ignored in order to obtain sufficiently simple models. The condition numbers were observed of the raw data and refined data, and because of slightly high condition numbers in part of the response data after the refining, PLS was confirmed to be suitable for the method [42]. The condition number under 3 indicates a good design, 3–6 a questionable design and over 6 a bad design, when the objective is screening [42]. PLS is in this case more suitable than multiple linear regression (MLR) since it can handle the data with high condition numbers and also the missing response values more reliably than MLR [42].

The models were constructed according to data, evaluated and refined. For evaluating the models was used regression analysis tools summary of fit (figure 19), analysis of variance (ANOVA) and normal probability plot of residuals [42]. The models were refined based on the evaluations in order to attain valid and usable models [42].

Summary of fit (figure 19) is a diagnostic tool which shows two to four bars, at least the regression parameters R^2 and Q^2. The other two bars, model validity and reproducibility, are shown if some of the experiments were replicated. R^2 describes the measure of fit of the data can be explained by obtained model. Analogously, Q^2 describes the measure of fit of the data can be predicted by the model [43]. Both R^2 and Q^2 are percent values. The reproducibility bar represents inversely the variation of the response of measurements with equal factors, and model validity represents the validity of the model [43]. The highest value 1 of reproducibility means that the pure error is 0. Conversely, the reproducibility value 0 means that pure error is equal to the total variation of the response [43]. The model validity value over 0.25 implies that the model does not contain lack of fit and the model error is approximately equal to the pure error [43]. All these four parameter values are perfect if they are one and good if they are over the values presented in figure 19. The values of Q^2, model validity and reproducibility are in good model over 0.5, 0.25 and 0.5 respectively [42]. In addition, in good model the difference between R^2 and Q^2 is less than 0.2–0.3 [42].

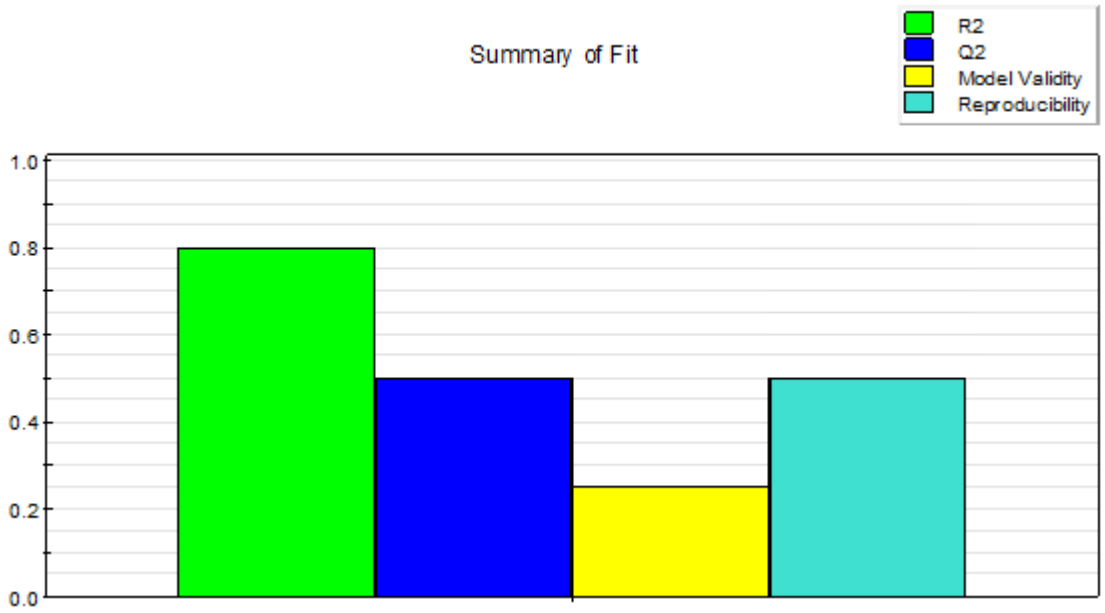

Figure 19. Maximum difference between R^2 and Q^2 as well as minimum values of Q^2, model validity and reproducibility for suitable model [42, 44].

ANOVA is a diagnostic tool for evaluating regression models [42]. It divides the total variation of response into part due to the regression model and due to residuals as well as, in case of replicated tests, residual sum further into pure error and lack of fit [42].

Normal probability plot (N-plot) of residuals is a tool for evaluating response deviation [42]. The response values deviating too much, the outliers, can be detected and eliminated using N-plot [42] (figure 20). The response which is shown in N-plot as outliers can be excluded, or to maintain the number of experiments, reproduced [42]. In the example, N-plot in figure 20 there are a group of outliers which are not on the same line with the other response and should be excluded and the experiments reproduced. Nevertheless, in this plot there are no such outliers which are outside of the standard deviations (-4 –+4) of the data [42].

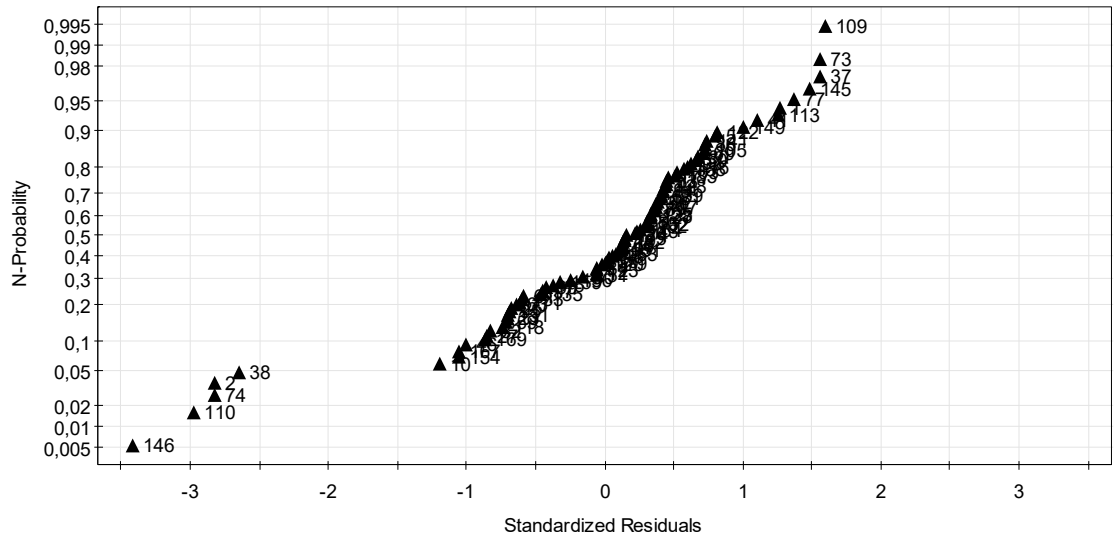

Figure 20. Normal probability plot with outliers (146, 110, 74, 2 and 38).

The accuracy of the models was optimized taken the minimum and maximum possible concentrations of Cu, Ni and H_2SO_4 into account in calculations. The exact concentrations of the electrolytes were not known because of the tolerances in the concentrations of the chemicals used. The models were defined using the highest and the lowest possible concentrations (table 5) as well as the average of them as the levels of the factors. However, the average grade model was used as the official model.

6 Results and discussion

This chapter presents the results of the measurements and data analysis. The results are evaluated as well as the model equations compared to the equivalent literature values and equations presented in chapter 4.

The models for conductivity were determined with and without arsenic. However, due to the usefulness of arsenic in the refining process, all the viscosity, density and diffusion coefficient models were carried out with arsenic. Various models were obtained from the data depending on how the data was selected and the models were refined. The first model evaluation of conductivity model 1 is discussed more profoundly as an example. Thus, the other model evaluations have the same phases but they are not discussed to the same extent.

The models for conductivity, density, viscosity, and diffusion coefficient of cupric ion were constructed separately. The interactions between these properties were not taken into account, since the differences in temperatures would have made the design too complicated to manage. In addition, the coefficients of each property wanted to be determined separately for obtaining accurate models.

6.1. Conductivity

The conductivity models of the measured values with evaluations are presented in tables 11–14 and figures 32–43, as well as the measured values are presented in appendix A (table A1). The coefficients of the models are shown in tables and the evaluations in summary of fit as well as ANOVA plots in figures. The figures and tables have terms of concentrations and temperature which are in g/dm^3 and °C respectively. The conductivity is in mS/cm. Prior to these phases, the evaluation and refining phases are introduced more detailed of one conductivity model.

6.1.1. Conductivity model 1

The histogram and descriptive statistics plot of the conductivity data are slightly skew (figures 21 and 22). In the histograms, in the best case, the highest values should be in the

middle and the values toward the sides decrease smoothly. Correspondingly, in the descriptive statistics plot the bar is then in the middle of the vertical line. However, since the skewness in this data is not too strong, the first model was constructed from this data and the second model from logarithmic conductivities.

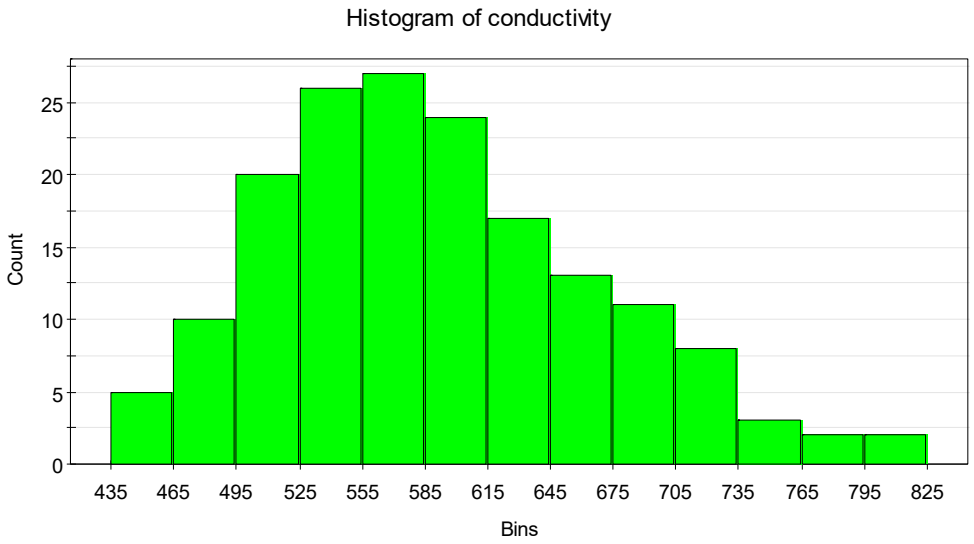

Figure 21. Histogram of conductivity values.

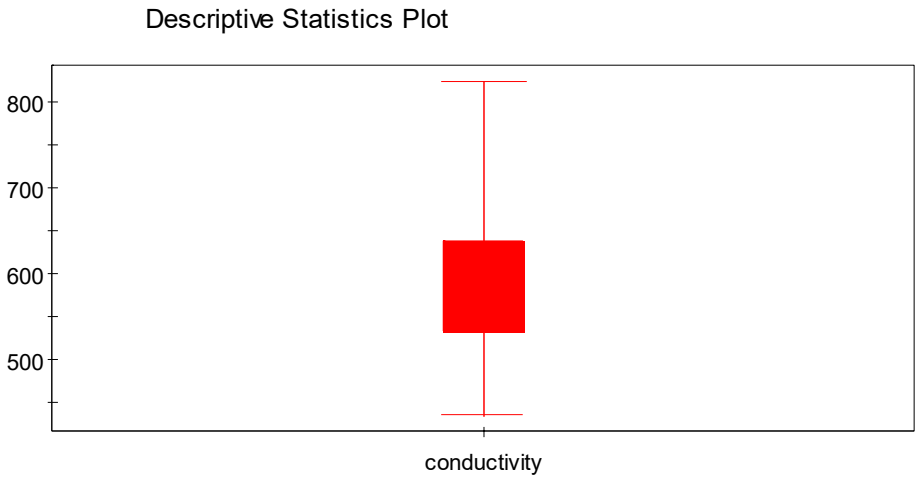

conductivity Min: 435,2 Max: 824 Median: 578,5 Mean: 590,681

Figure 22. Descriptive statistics plot of conductivity values.

Scatter plots of the raw data show rough directions how the factors affect conductivity. Three of the plots are shown in figures 23 and 24. According to these plots, copper, nickel and arsenic lower the conductivity while temperature and H_2SO_4 rise it, which is in line with literature [6, 7]. However, these plots indicate that the relationship between some factors

and the response might be curved, as well as there might be interactions between the factors, since there seems to be non-linearity in some relationships.

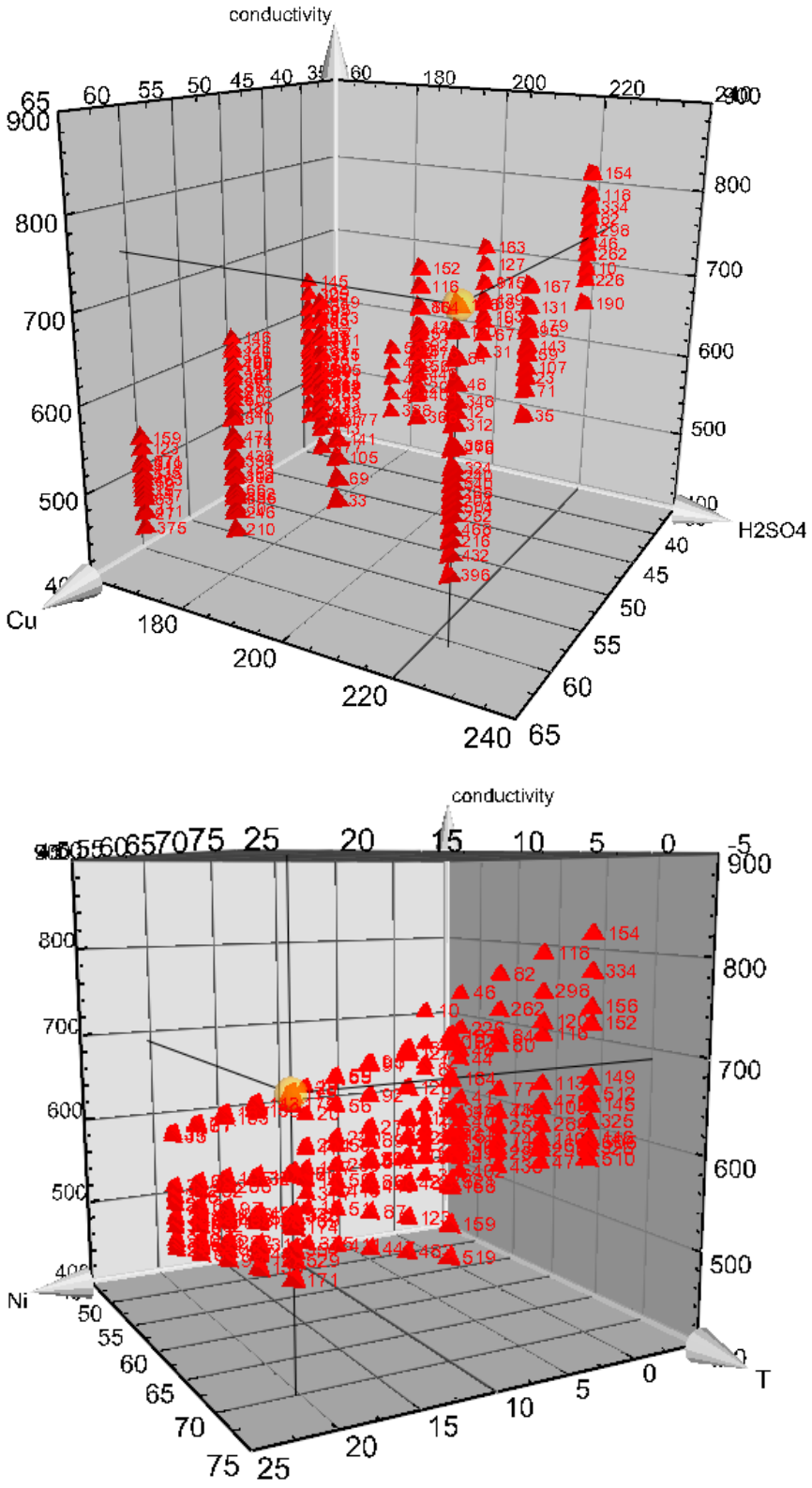

Figure 23. Scatter plots of factors copper and H_2SO_4 concentration as well as Ni concentration and temperature for conductivity model.

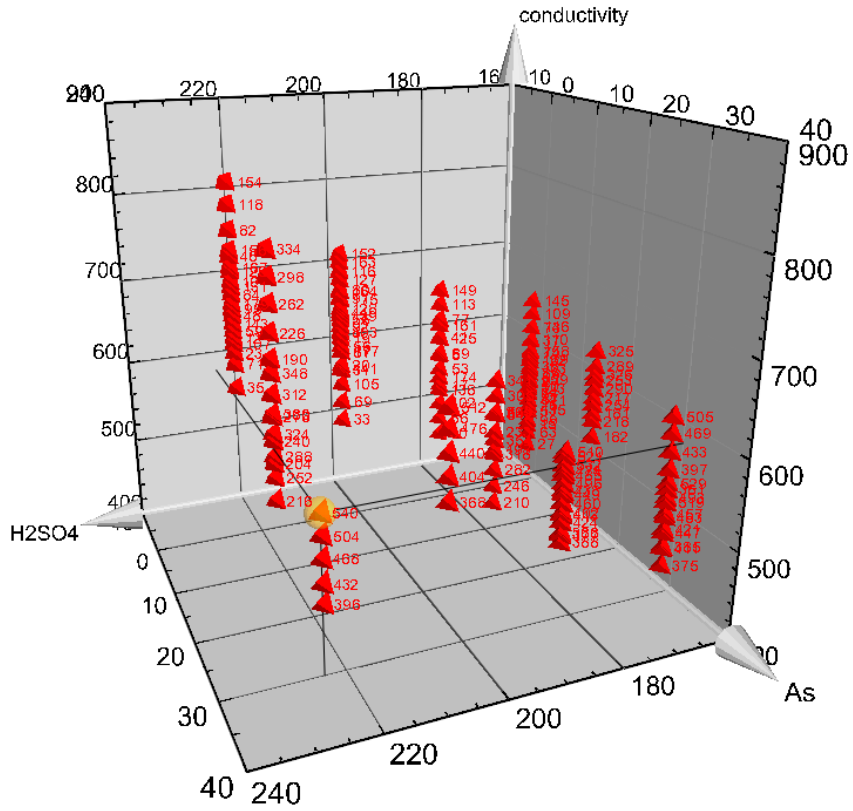

Figure 24. Scatter plot of the factors H_2SO_4 and arsenic concentration for conductivity model.

Coefficients of the unrefined model are shown in figure 25 and in table 8 as scaled form, as well as summary of fit is presented in figure 26. The scaled and centered factors are scaled to values -1 and 1 as well as values between them [42]. Scaling makes all the factors equal and simplifies separating the insignificant terms from the models. The terms with high P value, in which the error bar extends over the zero line, are not significant, and thus they can be excluded from further analysis. The high P values are presented in red font in table 8.

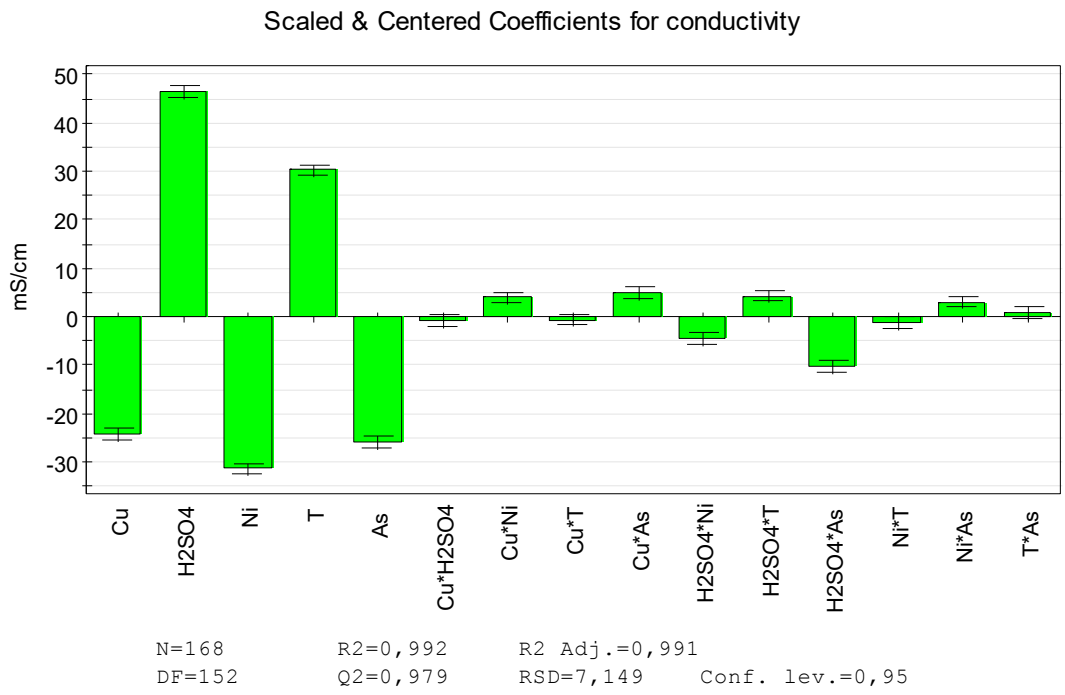

Figure 25. Coefficients for unrefined conductivity model.

Table 8. Coefficients for unrefined conductivity model.

conductivity	Scaled and centered coefficients	Std. Err.	P	Conf. int(±)
Constant	589.027	0.588498	0	1.16268
Cu	-24.2582	0.601925	0	1.18921
H_2SO_4	46.5994	0.603544	0	1.19241
Ni	-31.3596	0.583883	0	1.15356
T	30.3268	0.553204	0	1.09295
As	-25.9261	0.581872	0	1.14959
Cu*H_2SO_4	-0.85884	0.631848	0.176078	1.24833
Cu*Ni	4.0036	0.590811	2.54E-10	1.16725
Cu*T	-0.5917	0.570754	0.301516	1.12763
Cu*As	4.99996	0.62164	2.30E-13	1.22816
H_2SO_4*Ni	-4.47486	0.657278	2.15E-10	1.29857
H_2SO_4*T	4.29895	0.560922	1.98E-12	1.1082
H_2SO_4*As	-10.1664	0.675586	6.48E-32	1.33474
Ni*T	-1.19157	0.565386	0.036712	1.11702
Ni*As	3.08123	0.569005	2.34E-07	1.12417
T*As	0.857762	0.55442	0.123906	1.09536

N = 168	Q^2 = 0.979	Cond. no. = 2.427	
DF = 152	R^2 = 0.992	Y-miss = 0	
Comp. = 2	R^2 Adj. = 0.991	RSD = 7.149	
		Conf. lev. =	0.95

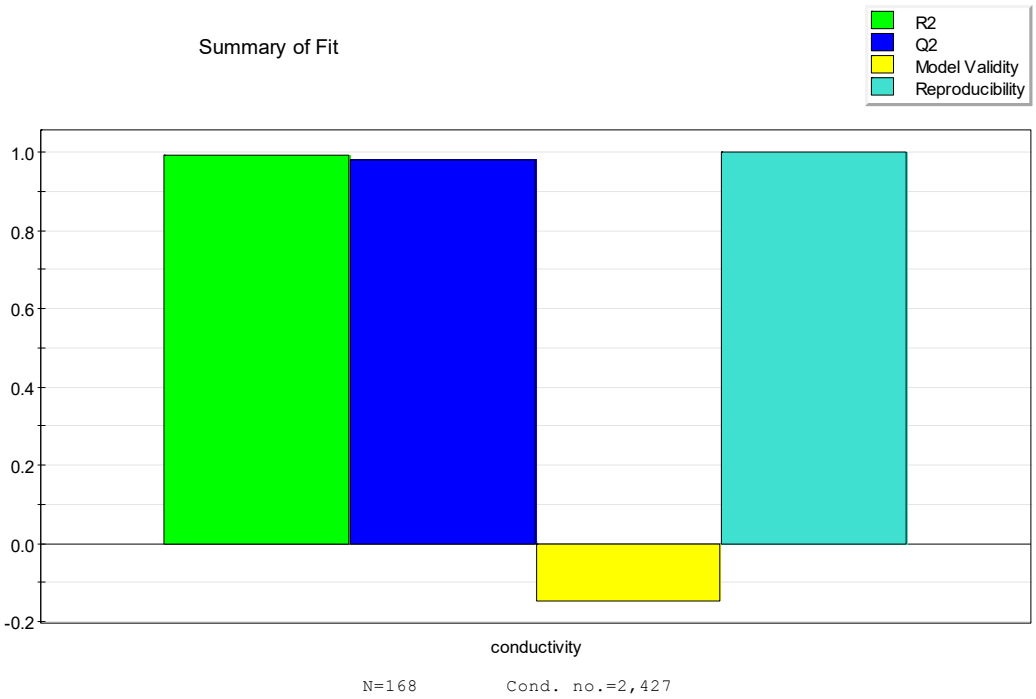

Figure 26. Summary of fit for unrefined conductivity model.

Terms which have high P value were removed from the model, and the obtained remaining coefficients are shown in table 9. There is still one term (Ni*As) with high P value in that model. The term was also removed, and, consequently, obtained coefficients shown in table 10.

Table 9. Coefficients for conductivity model from which terms Cu*H_2SO_4, Cu*T and T*As are removed.

conductivity	Scaled and centered coefficients	Std. Err.	P	Conf. int(±)
Constant	588.938	0.596449	0	1.17828
Cu	-23.6054	0.622958	0	1.23065
H_2SO_4	46.1542	0.618309	0	1.22147
Ni	-31.3557	0.604564	0	1.19431
T	30.1904	0.574325	0	1.13458
As	-26.8762	0.59207	0	1.16963
Cu*Ni	4.74062	0.593077	2.90E-13	1.17162
Cu*As	5.46445	0.614448	1.50E-15	1.21384
H_2SO_4*Ni	-6.17737	0.604408	4.84E-19	1.194
H_2SO_4*T	4.24017	0.570876	7.09E-12	1.12776
H_2SO_4*As	-9.91717	0.686998	2.04E-30	1.35716
Ni*T	-1.23539	0.571368	0.03215	1.12873
Ni*As	0.946042	0.575698	0.102354	1.13729

N = 167	Q^2 = 0.971	Cond. no. =	2.051
DF = 154	R^2 = 0.992	Y-miss =	0
Comp. = 2	R^2 Adj. = 0.991	RSD =	7.399
		Conf. lev. =	0.95

Table 10. Coefficients for conductivity model from which terms Cu*H_2SO_4, Cu*T, T*As and Ni*As are removed.

conductivity	Scaled and centered coefficients	Std. Err.	P	Conf. int(±)
Constant	589.01	0.575391	0	1.13661
Cu	-23.8142	0.59754	0	1.18036
H_2SO_4	46.5109	0.591528	0	1.16849
Ni	-31.1707	0.583047	0	1.15173
T	30.2557	0.554215	0	1.09478
As	-26.7041	0.569936	0	1.12584
Cu*Ni	4.56402	0.570223	2.65E-13	1.1264
Cu*As	5.31934	0.592134	8.44E-16	1.16968
H_2SO_4*Ni	-6.24033	0.582629	2.20E-20	1.15091
H_2SO_4*T	4.24123	0.550887	1.51E-12	1.08821
H_2SO_4*As	-9.56669	0.657528	8.73E-31	1.29886
Ni*T	-1.25069	0.551361	0.0246873	1.08914

N = 167	Q^2 = 0.973	Cond. no. =	2.015
DF = 155	R^2 = 0.992	Y-miss =	0
Comp. = 2	R^2 Adj. = 0.992	RSD =	7.14
		Conf. lev. =	0.95

The summary of fit for that model (Figure 27) shows that R^2, Q^2 and reproducibility are in good level, but the model validity of the model is still poor. That was verified by lack of fit tool which illustrated that there is lack of fit seen in figure 28 as the first bar is higher than the third bar unlike it should be in a good model. In a good model there is no lack of fit, and the lack of fit tool's first bar is lower than or equal to the third bar.

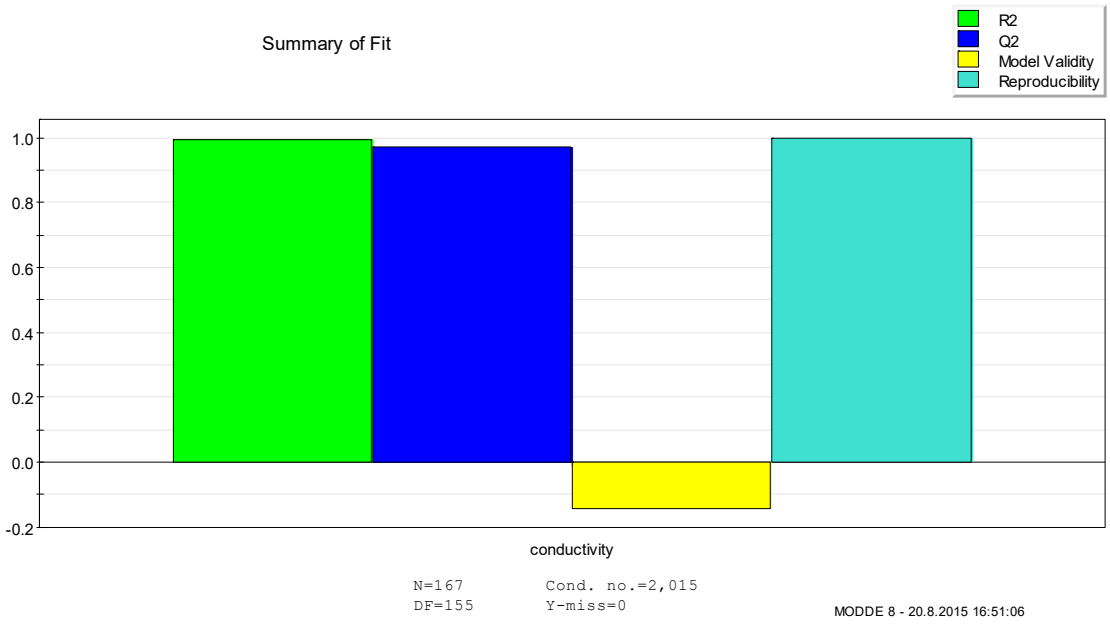

Figure 27. Summary of fit for conductivity model from which terms Cu*H_2SO_4, Cu*T, T*As and Ni*As are removed.

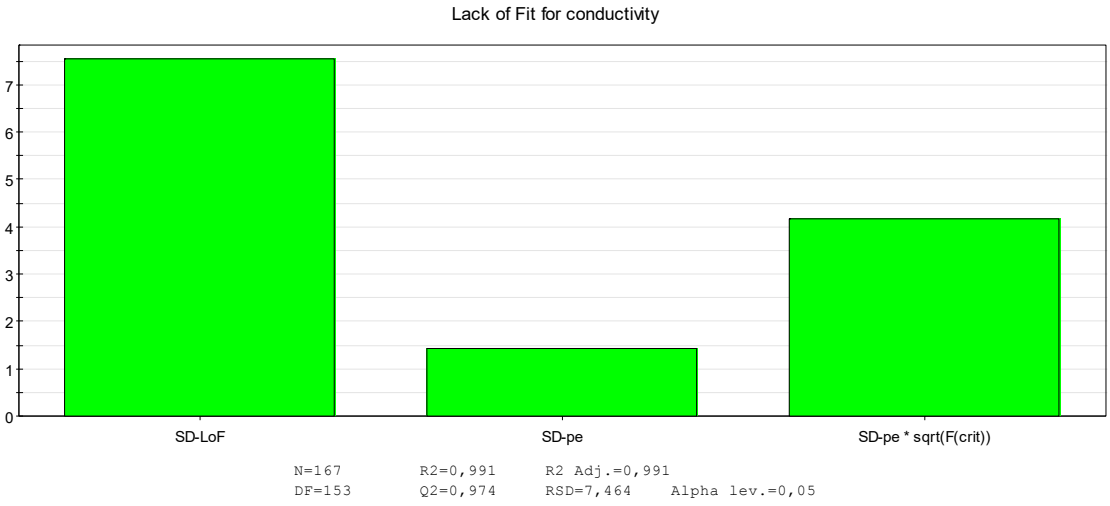

Figure 28. Lack of fit for conductivity model from which terms Cu*H_2SO_4, Cu*T, T*As and Ni*As are removed.

The model validity was tried to be improved adding the squares of the terms to the model, since removing terms neither made the model validity better nor normal probability plot's curve straighter. By adding squares $(H_2SO_4)^2$ and T^2 the irregularities of the normal probability plot were diminished (figure 29), since the curvature of the graph indicates that the model has nonlinearity [42]. However the adding of terms did not improve the model validity. Nevertheless, excluding the results of electrolytes N72 and N108 from the model improved the model validity (figure 30) as the data was refitted, model terms reset as well

as the terms with too high P value removed. These electrolytes contained the maximum amount of copper and nickel, as well as maximum or average amount of arsenic as seen in appendix A (table A1). The excluding of data was due to suspect that the electrolytes were supersaturated and thus skewing the results.

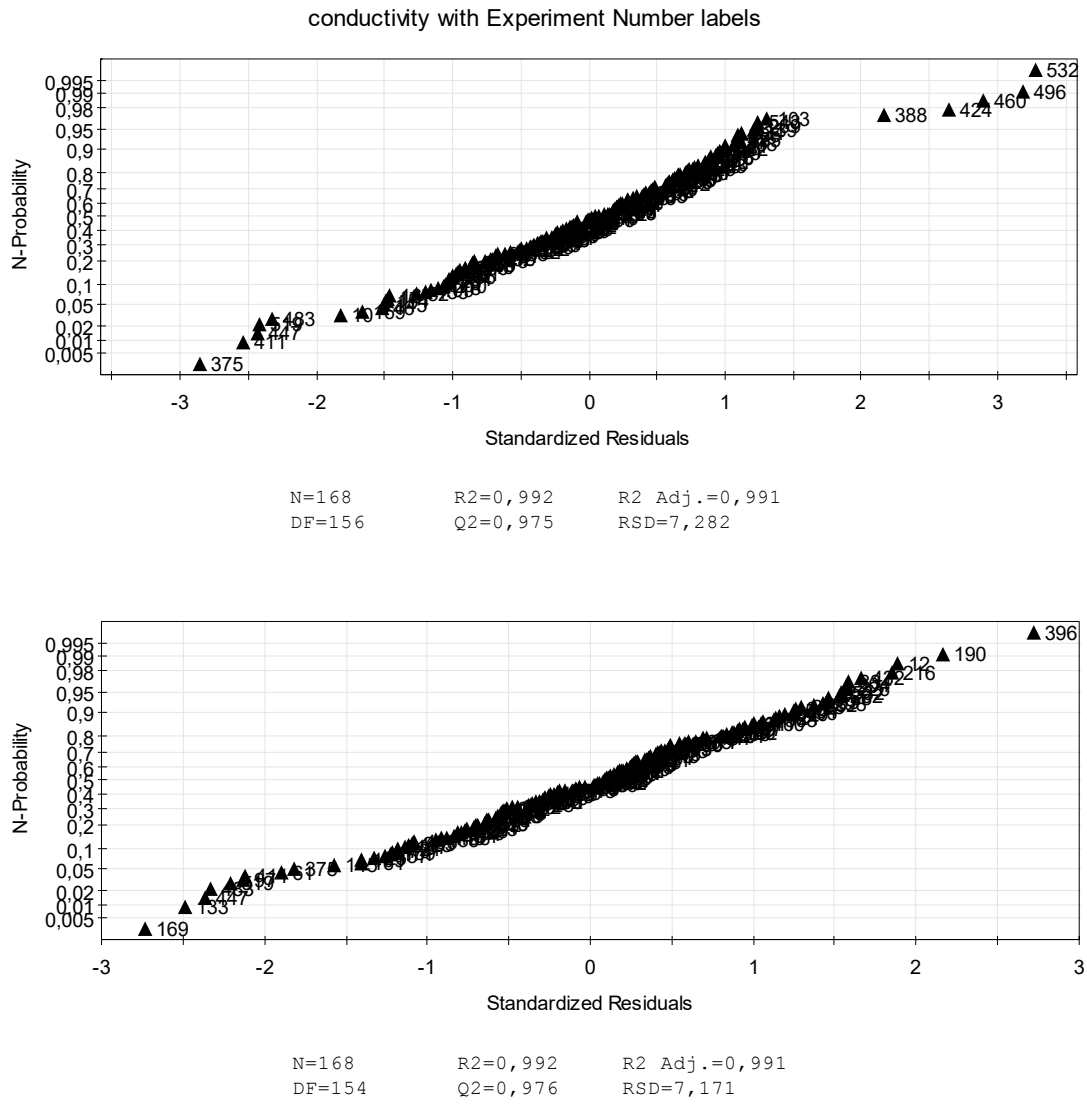

Figure 29. Normal probability plots of conductivity models from which terms Cu*H_2SO_4, Cu*T, T*As and Ni*As are removed. The lower plot is of the model with terms $(H_2SO_4)^2$ and T^2.

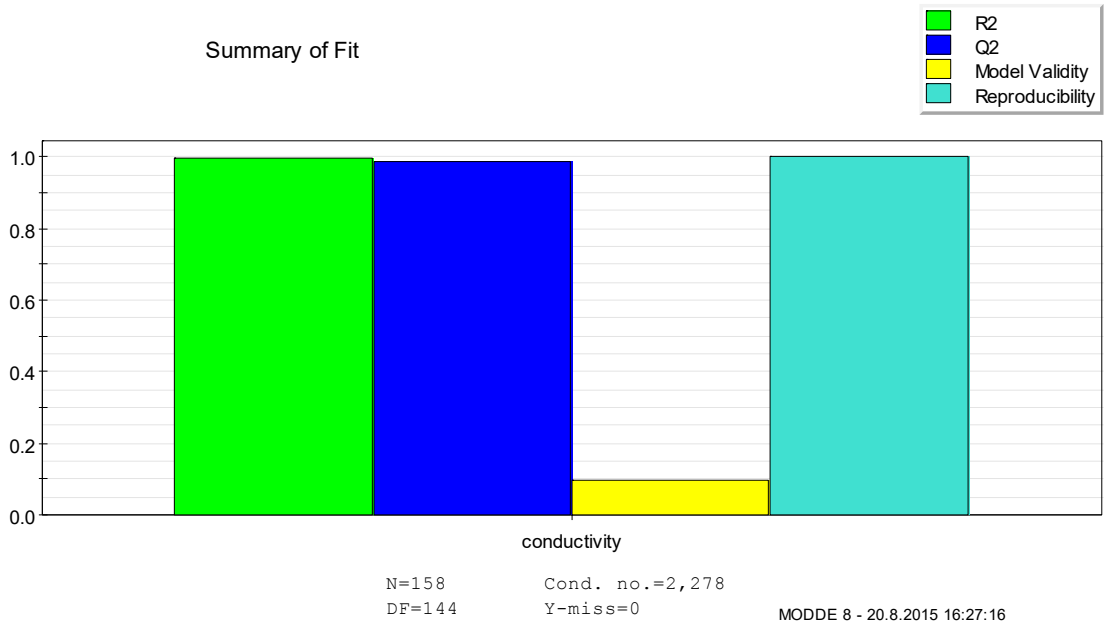

Figure 30. Summary of fit for conductivity model of which some results have been excluded.

The model validity of this model was above zero but lower than 0.25 (figure 30) and the lack of fit was detected (figure 31). Otherwise the model seemed to be good according to ANOVA plot (figure 31). In ANOVA plot of a good model, the first bar standard deviation is significantly higher than the residual standard deviation bars [43].

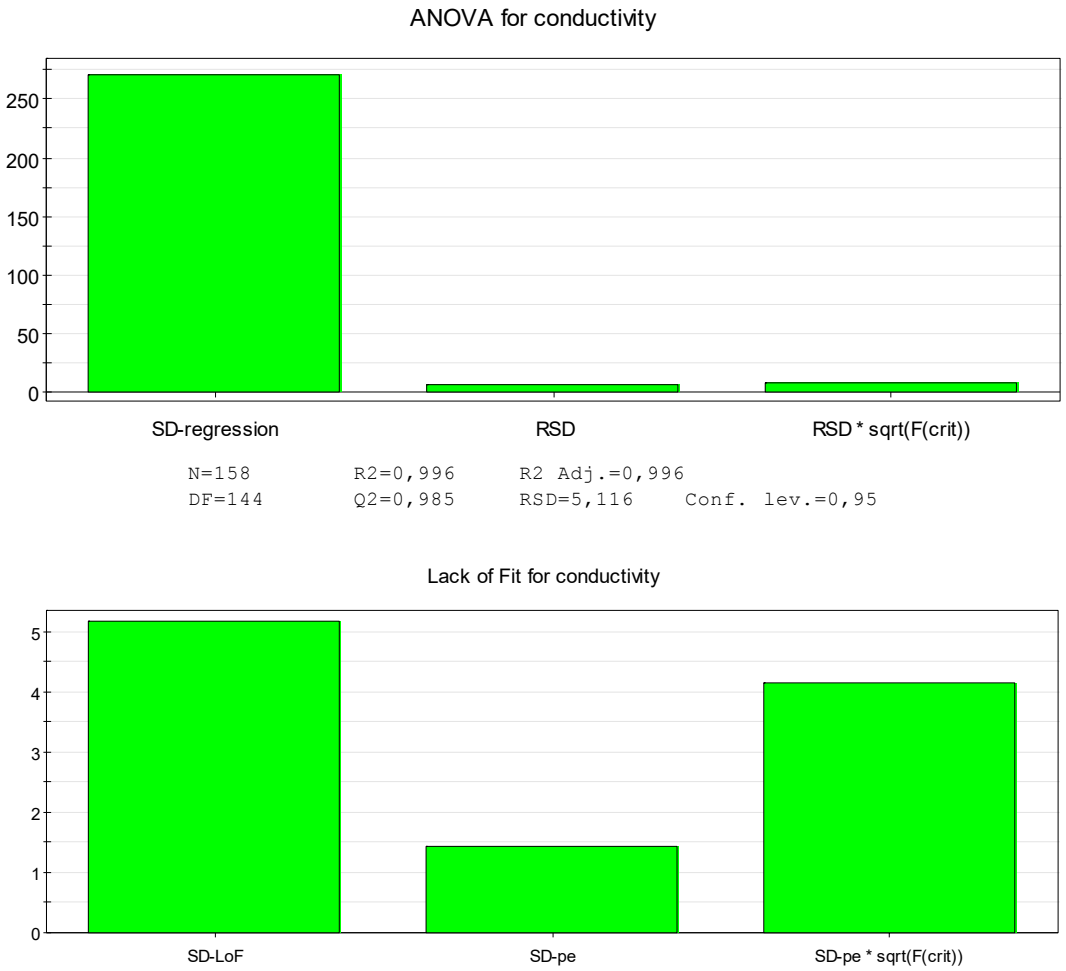

Figure 31. ANOVA and lack of fit plots for conductivity model of which some results have been excluded.

By inserting new terms t^2 and $(H_2SO_4)^2$ to the model was obtained reasonable model validity as well as slightly higher R^2 and Q^2. The coefficients of the model, also as unscaled form, are shown in table 11 and the model validity as well as other properties in figures 32 and 33.The model had no lack of fit in this phase, and the summary of fit indicates that the model is valid.

Table 11. Coefficients for conductivity model.

Scaled and centered coefficients		Std. Err.	P	Conf. int(±)	Coefficients	
Constant	596.005	0.613	0	1.212	**Constant**	97.7242
Cu	-25.8802	0.325	0	0.642	**Cu**	-3.58079
H_2SO_4	49.3204	0.364	0	0.719	**H_2SO_4**	2.94489
Ni	-29.9236	0.335	0	0.662	**Ni**	0.473562
T	30.6798	0.306	0	0.604	**T**	2.74291
As	-24.0575	0.353	0	0.698	**As**	0.596048
H_2SO_4*H_2SO_4	-2.78209	0.417	5.09E-10	0.824	**H_2SO_4*H_2SO_4**	-0.00536
T*T	-1.4544	0.358	8.05E-05	0.708	**T*T**	-0.02946
Cu*Ni	1.54354	0.309	1.75E-06	0.612	**Cu*Ni**	0.023959
Cu*As	0.649205	0.321	0.0449	0.634	**Cu*As**	0.006713
H_2SO_4*Ni	-4.2916	0.340	6.20E-25	0.673	**H_2SO_4*Ni**	-0.02297
H_2SO_4*T	4.40707	0.313	8.75E-29	0.618	**H_2SO_4*T**	0.027544
H_2SO_4*As	-6.07666	0.411	1.73E-30	0.813	**H_2SO_4*As**	-0.02166
Ni*T	-1.09481	0.306	0.000472	0.605	**Ni*T**	-0.01899
Ni*As	1.23169	0.339	0.000391	0.670	**Ni*As**	0.012188
T*As	1.5302	0.314	2.93E-06	0.621	**T*As**	0.017683

N = 158	Q^2 = 0.988	Cond. no. =	4.517
DF = 142	R^2 = 0.998	Y-miss =	0
Comp. = 3	R^2 Adj. = 0.998	RSD =	3.828
		Conf. lev. =	0.95

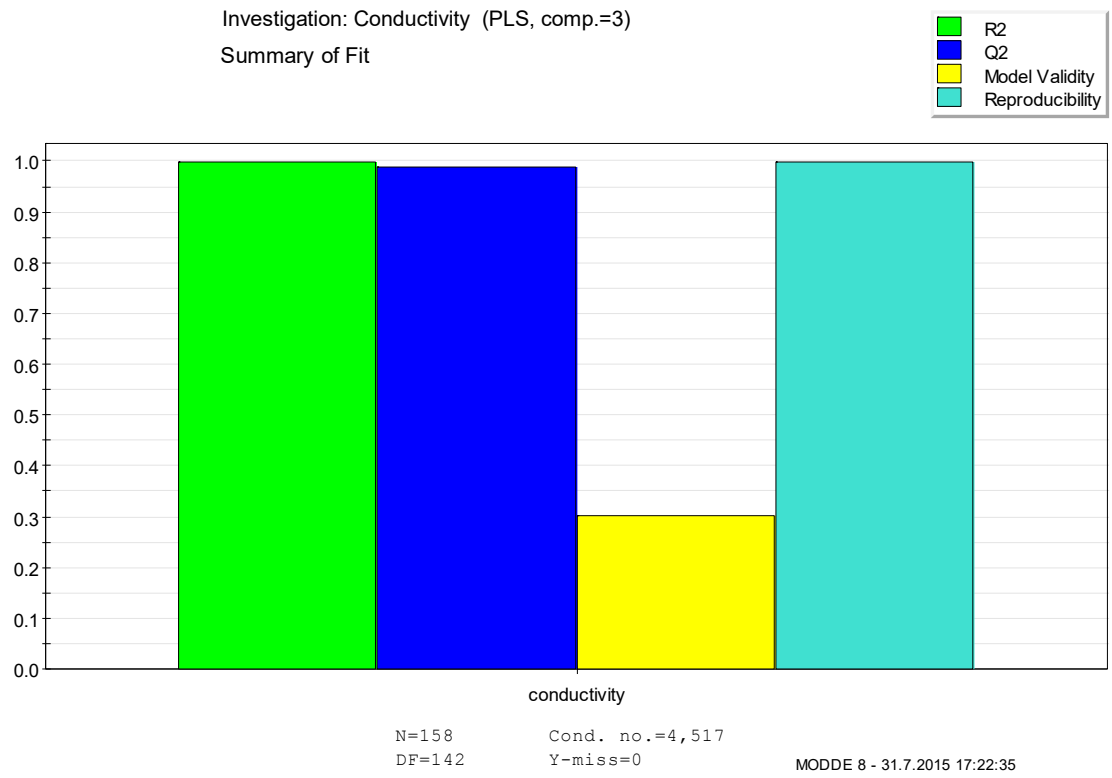

Figure 32. Summary of fit for conductivity model.

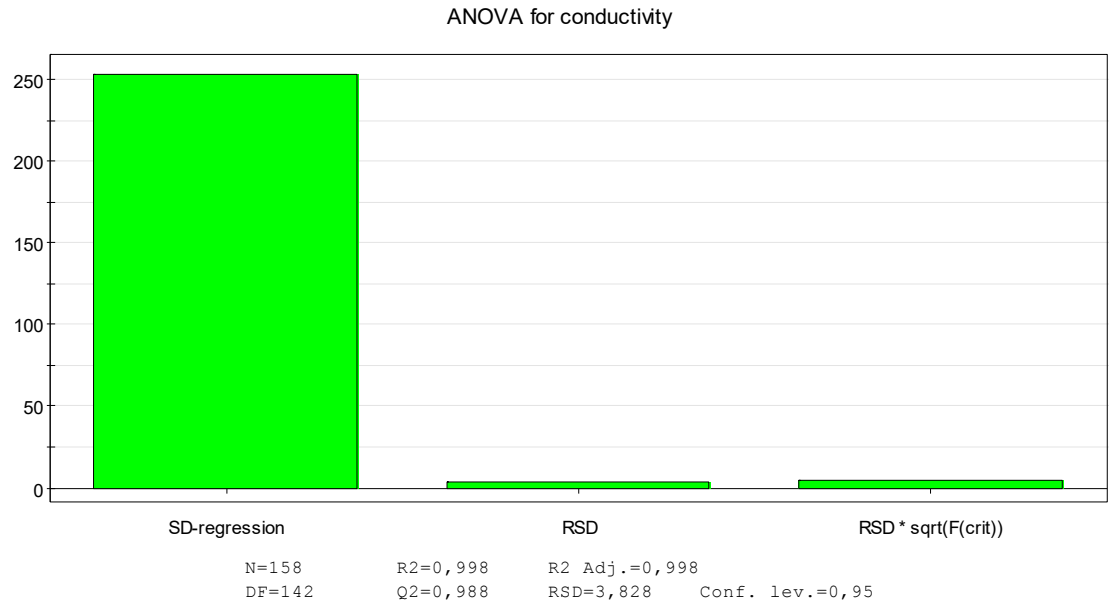

Figure 33. ANOVA plot for conductivity model.

The equation (34) for conductivity is compiled according to unscaled coefficients (table 11). The quantity of the decimals of coefficients was determined according to accuracy of the readings measured. The quantity of the decimals in coefficients was reduced gradually until

the reducing affected the numbers calculated with the equations in the same accuracy as the actual measured readings.

$$\kappa = 97.72 - 3.581\,[\mathrm{Cu}] + 0.4736\,[\mathrm{Ni}] + 0.596\,[\mathrm{As}] + 2.945\,[\mathrm{H_2SO_4}] + 0.02396\,[\mathrm{Cu}][\mathrm{Ni}] + 0.006713\,[\mathrm{Cu}][\mathrm{As}] + 0.01219\,[\mathrm{Ni}][\mathrm{As}] - 0.02297\,[\mathrm{H_2SO_4}][\mathrm{Ni}] - 0.02166\,[\mathrm{H_2SO_4}][\mathrm{As}] - 0.01899\,[\mathrm{Ni}]\,T + 0.01768\,T\,[\mathrm{As}] + 0.02754\,[\mathrm{H_2SO_4}]\,T + 2.743\,T - 0.005364\,[\mathrm{H_2SO_4}]^2 - 0.02946\,T^2\,, \quad (34)$$

where the concentrations are in g/dm^3 and T is in °C, while κ is in mS/cm.

The equation has many terms, and all the effects of the factors are not fully seen in equation coefficients. Some of the terms do not represent the actual effects but are only in the equation to make the results more precise. However, according to low P values, at least H_2SO_4 seems to have combined effect with Ni, temperature and As.

Most of the values shown in the table 11 and the figures 32 and 33 indicate that the model is good. However the condition number 4,517 is slightly high since according to [42] the condition number 3–6 indicates a questionable design. The model can be regarded as a fairly good model in spite of that.

6.1.2. Conductivity model 2

The second model of conductivity was constructed from logarithmic conductivity values. The values of electrolytes N72 and N108 were excluded from this model like in the model 1. Due to logarithmic data, the histogram is quite normally distributed (figure 34).

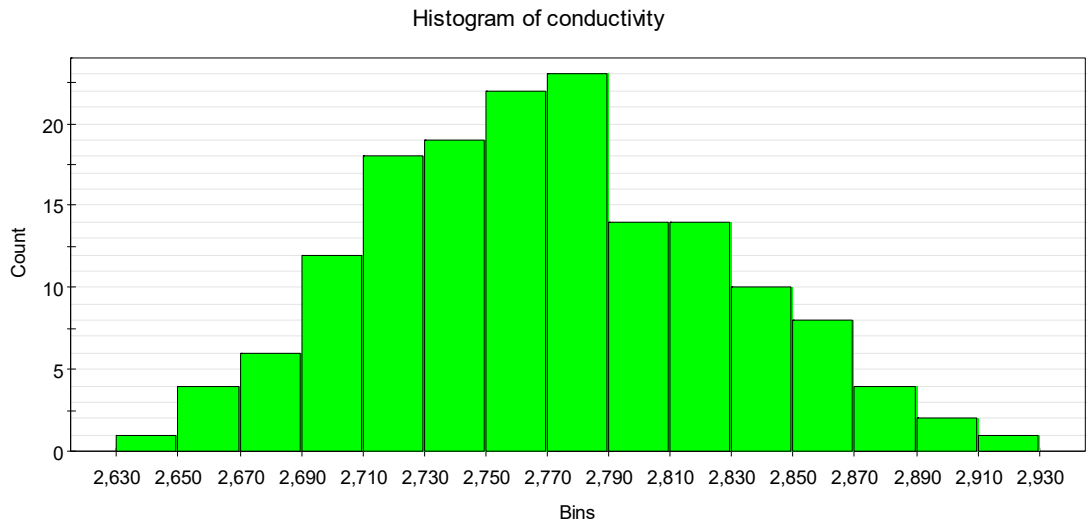

Figure 34. Histogram of logarithmic conductivity values.

This model was refined like Model 1: terms which have high P value were removed from the model as well as terms t^2 and $(H_2SO_4)^2$ were added. Thus, the coefficients obtained are presented in table 12 and the evaluations in figures 35 and 36.

Table 12. Coefficients for logarithmic conductivity model.

Scaled and centered coefficients		**Std. Err.**	**P**	**Conf. int(±)**	**Coefficients**	
Constant	2.77417	3.65E-04	0	0.000721	**Constant**	2.17388
Cu	-0.01844	1.87E-04	0	0.00037	**Cu**	-0.00234789
H_2SO_4	0.036591	2.10E-04	0	0.000414	**H_2SO_4**	0.00377637
Ni	-0.02276	1.92E-04	0	0.000379	**Ni**	-0.00277329
T	0.022092	1.82E-04	0	0.00036	**T**	0.00518459
As	-0.01767	2.03E-04	0	0.000401	**As**	-0.00073729
H_2SO_4*H_2SO	-0.00359	2.44E-04	1.08E-30	0.000482	**H_2SO_4*H_2SO_4**	-6.9222E-06
T*T	-0.0016	2.14E-04	5.42E-12	0.000423	**T*T**	-3.25055E-05
H_2SO_4*T	0.001408	1.86E-04	3.84E-12	0.000368	**H_2SO_4*T**	8.8019E-06
H_2SO_4*As	-0.00299	2.34E-04	1.39E-25	0.000462	**H_2SO_4*As**	-1.06487E-05
T*As	0.001871	1.86E-04	2.15E-18	0.000368	**T*As**	2.16267E-05

N = 158	Q^2 = 0.996	Cond. no. = 4.456
DF = 147	R^2 = 0.998	Y-miss = 0
Comp. = 3	R^2 Adj. = 0.998	RSD = 0.002285
		Conf. lev. = 0.95

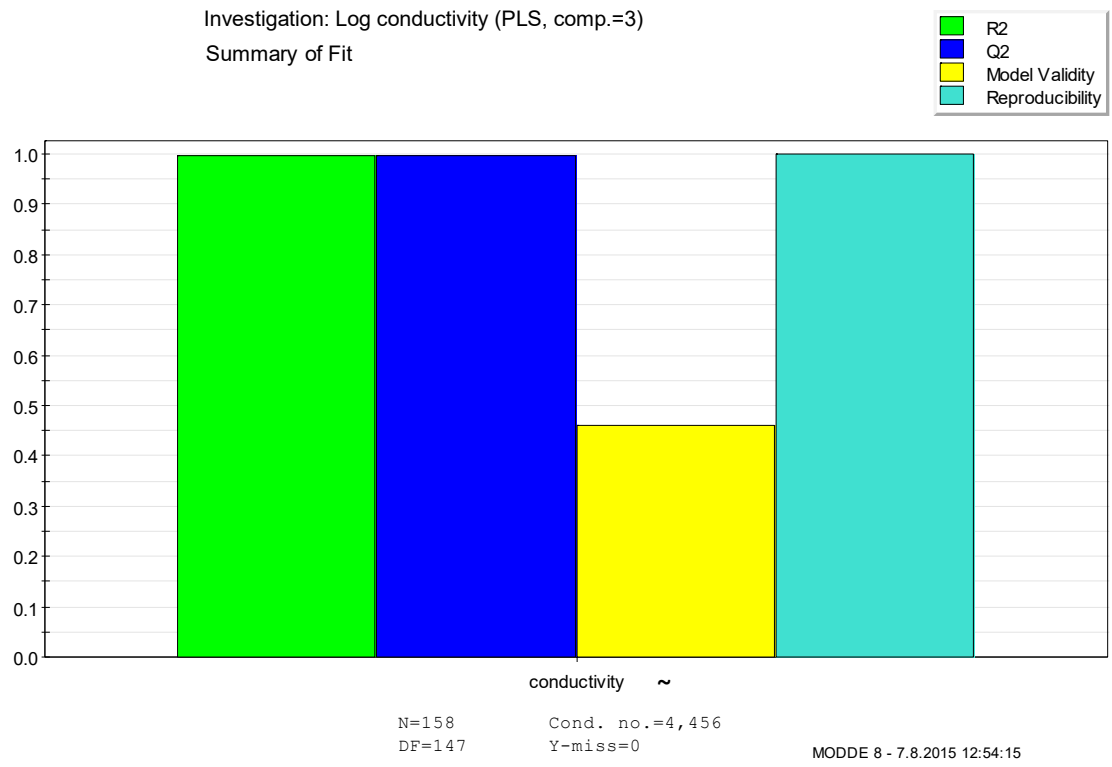

Figure 35. Summary of fit for logarithmic conductivity model.

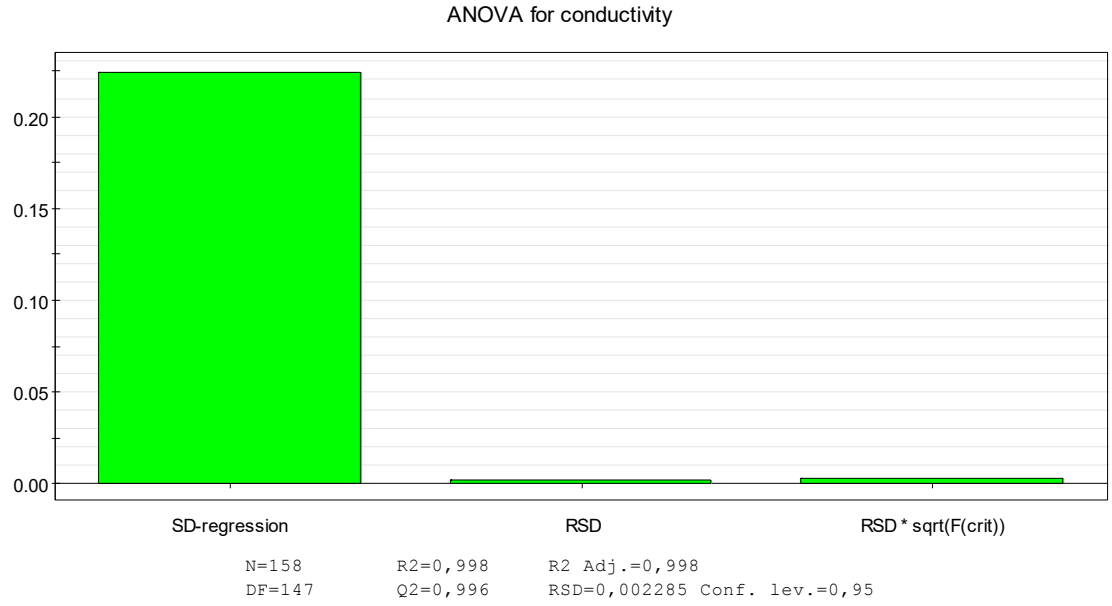

Figure 36. ANOVA plot for logarithmic conductivity model.

The equation (35) for the logarithm of conductivity is compiled according to unscaled coefficients (table 12). The quantity of decimals in coefficients was set as in model 1. As seen in table 12, the strongest combined effects according to low P values are with H_2SO_4 and

temperature, H_2SO_4 and As as well as with temperature and As. However, like in model 1, the combined effects are minor compared to the single effects.

$$\log_{10}(\kappa) = 2.17388 - 0.0023479\,[\mathrm{Cu}] - 0.0027733\,[\mathrm{Ni}] - 0.00073729\,[\mathrm{As}] + 0.0037764\,[\mathrm{H_2SO_4}] - 1.0649 \cdot 10^{-5}\,[\mathrm{H_2SO_4}][\mathrm{As}] + 2.1627 \cdot 10^{-5}\,\mathrm{T}\,[\mathrm{As}] + 8.8019 \cdot 10^{-6}\,[\mathrm{H_2SO_4}]\,\mathrm{T} + 0.0051846\,\mathrm{T} - 6.9222 \cdot 10^{-6}\,[\mathrm{H_2SO_4}]^2 - 3.2506 \cdot 10^{-5}\,\mathrm{T}^2, \quad (35)$$

where the concentrations are in g/dm^3 and T is in °C, while κ is in mS/cm.

The values shown in the table 12 and the figures 35 and 36 indicate that the model is good. However, the condition number 4.456 is slightly high, over 3, like the condition number of model 1. The condition number of this model is, though, slightly lower than in model 1. In addition, model 2 has better model validity and Q^2 value, as well as Q^2 is almost equal to R^2. Thus, the model can be regarded as fairly good and better than model 1.

6.1.3. Conductivity models 3 and 4

Conductivity models 3 and 4 were constructed from data without arsenic. Model 3 was refined to simple form and model 4 to form with the same extra terms, $(H_2SO_4)^2$ and T^2, as in models 1 and 2.

The data is quite normally distributed (figure 37).

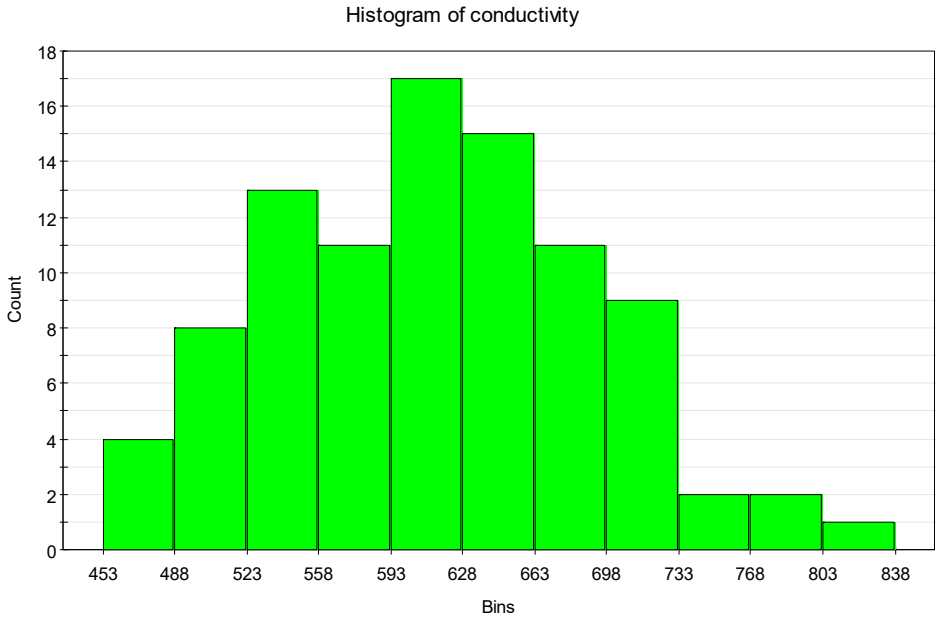

Figure 37. Histogram of conductivity values of models without arsenic.

Scatter plots of the raw data are shown in figures 38 and 39. These plots do not differ much from the equivalent plots of values with arsenic. Analogously, according to these plots, copper and nickel lower the conductivity while temperature and H_2SO_4 rise it, as described in literature [6, 7]. This model, however, seems to have more linearity in the relationships between the factors and the response than the model with arsenic. Thus, arsenic seems to affect the conductivity in more complicated ways than expected on grounds of literature [6, 7, 11].

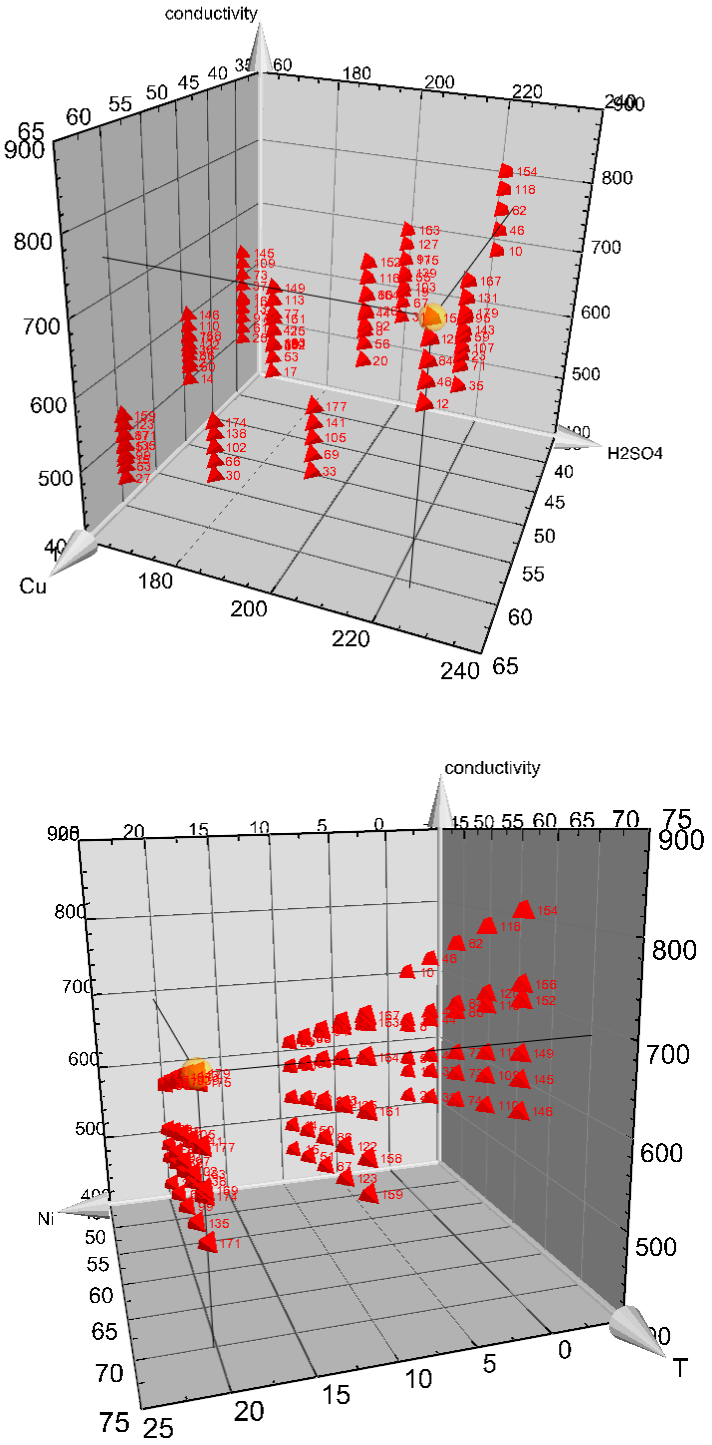

Figure 38. Scatter plots of the factors Cu and H_2SO_4 concentration as well as Ni and temperature for conductivity model without As.

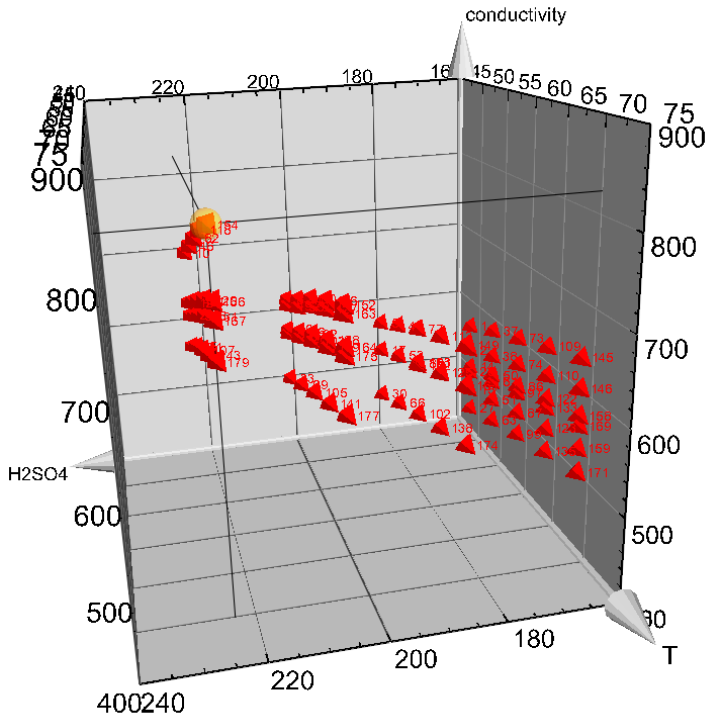

Figure 39. Scatter plot of the factors H_2SO_4 concentration and temperature for conductivity model without As.

The model was refined like model 1. In addition, this model had outliers, visible in the normal probability plot, which were also excluded, and those experiments reproduced. The refined model 3 is presented in table 13 as coefficients and evaluated in figures 40 and 41.

Table 13. Coefficients for simple conductivity model without As.

Scaled and centered coefficients		Std. Err.	P	Conf. int(±)	Coefficients	
Constant	613.233	0.448	0	0.891	**Constant**	307.851
Cu	-24.2367	0.463	0	0.920	**Cu**	-1.58297
H_2SO_4	54.0723	0.454	0	0.902	**H_2SO_4**	1.28502
Ni	-31.0417	0.462	0	0.919	**Ni**	2.73662
T	29.2308	0.449	0	0.893	**T**	-1.17006
Cu*H_2SO_4	-1.52781	0.443	0.000884	0.881	**Cu*H_2SO_4**	-0.008774
H_2SO_4*Ni	-5.2966	0.447	1.32E-19	0.889	**H_2SO_4*Ni**	-0.027769
H_2SO_4*T	4.77313	0.446	2.2E-17	0.886	**H_2SO_4*T**	0.029191
Ni*T	-1.1906	0.445	0.008928	0.884	**Ni*T**	-0.020867

N = 93	Q^2 = 0.966	Cond. no. =	1.375
DF = 84	R^2 = 0.997	Y-miss =	0
Comp. = 2	R^2 Adj. = 0.997	RSD =	4.305
		Conf. lev. =	0.95

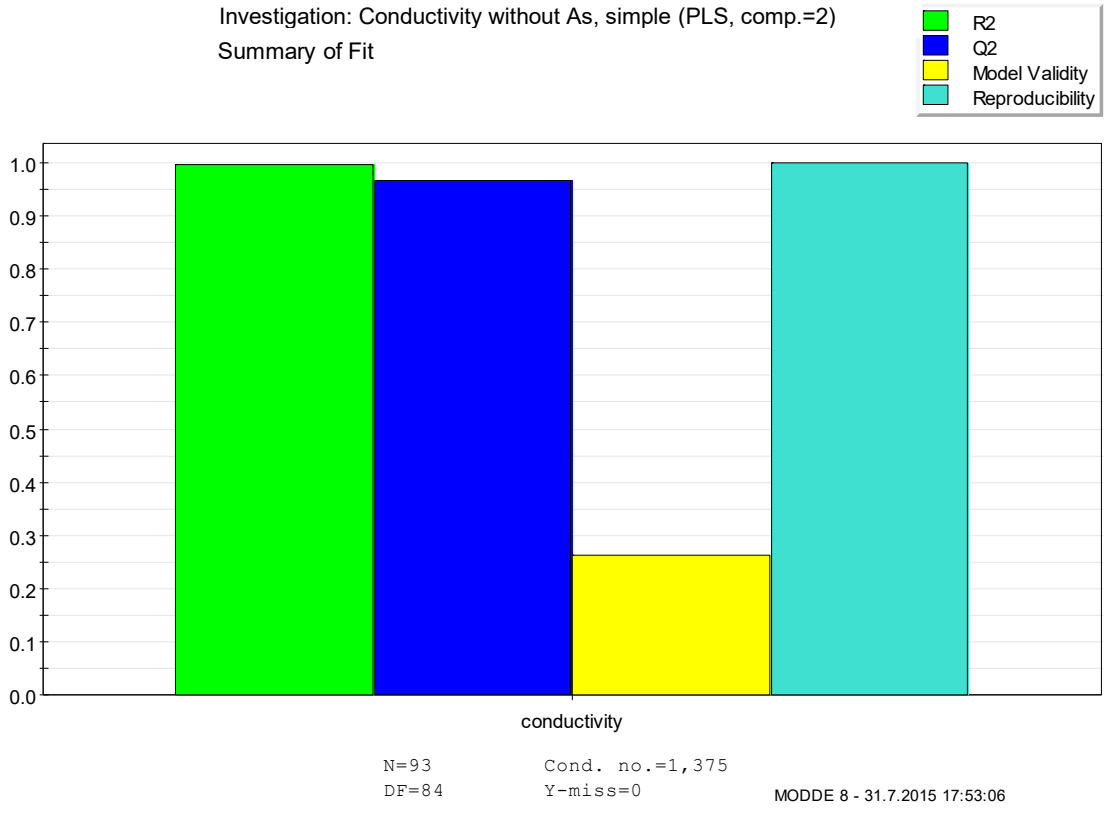

Figure 40. Summary of fit for simple conductivity model without As.

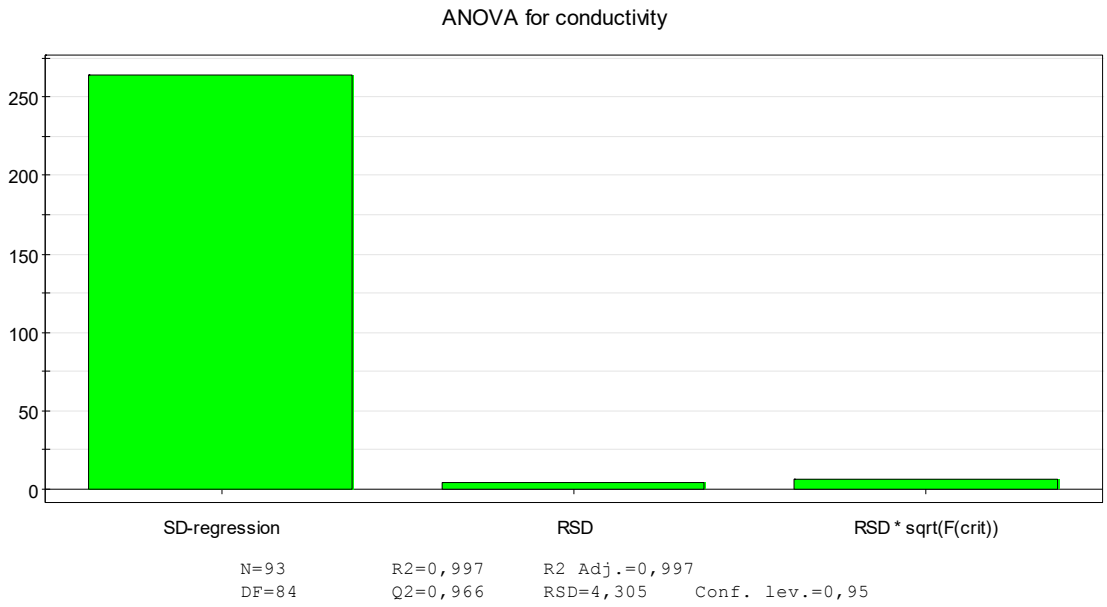

Figure 41. ANOVA plot for simple conductivity model without As.

The refined model 4 is presented in table 14 as coefficients and evaluated in figures 42 and 43.

Table 14. Coefficients for conductivity model without As.

Scaled and centered coefficients		**Std. Err.**	**P**	**Conf. int(±)**	**Coefficients**	
Constant	617.257	0.712	0	1.416	**Constant**	31.8626
Cu	-24.8822	0.367	0	0.730	**Cu**	-1.35943
H_2SO_4	54.2239	0.361	0	0.719	**H_2SO_4**	2.97892
Ni	-30.7548	0.370	0	0.735	**Ni**	1.83503
T	29.695	0.356	0	0.708	**T**	2.72965
H_2SO_4*H_2SO_4	-2.42505	0.489	3.73E-06	0.972	**H_2SO_4*H_2SO_4**	-0.00444
T*T	-1.60372	0.412	0.000201	0.820	**T*T**	-0.03279
Cu*H_2SO_4	-1.81137	0.352	1.82E-06	0.701	**Cu*H_2SO_4**	-0.0104
H_2SO_4*Ni	-4.32611	0.359	7.41E-20	0.713	**H_2SO_4*Ni**	-0.02268
H_2SO_4*T	4.86462	0.353	5.08E-23	0.703	**H_2SO_4*T**	0.02975
Ni*T	-1.22146	0.353	0.000854	0.702	**Ni*T**	-0.02141

N = 93	Q^2 = 0.974	Cond. no. =	4.322
DF = 82	R^2 = 0.998	Y-miss =	0
Comp. = 2	R^2 Adj. = 0.998	RSD =	3.416
		Conf. lev. =	0.95

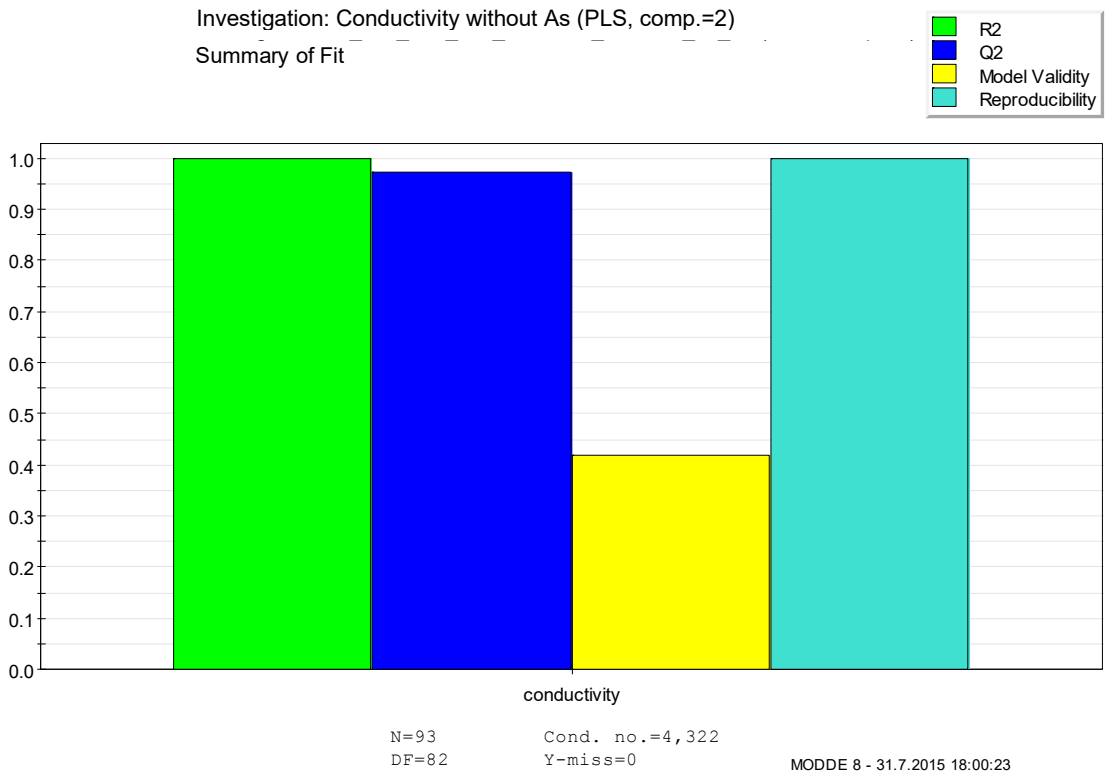

Figure 42. Summary of fit for conductivity model without As.

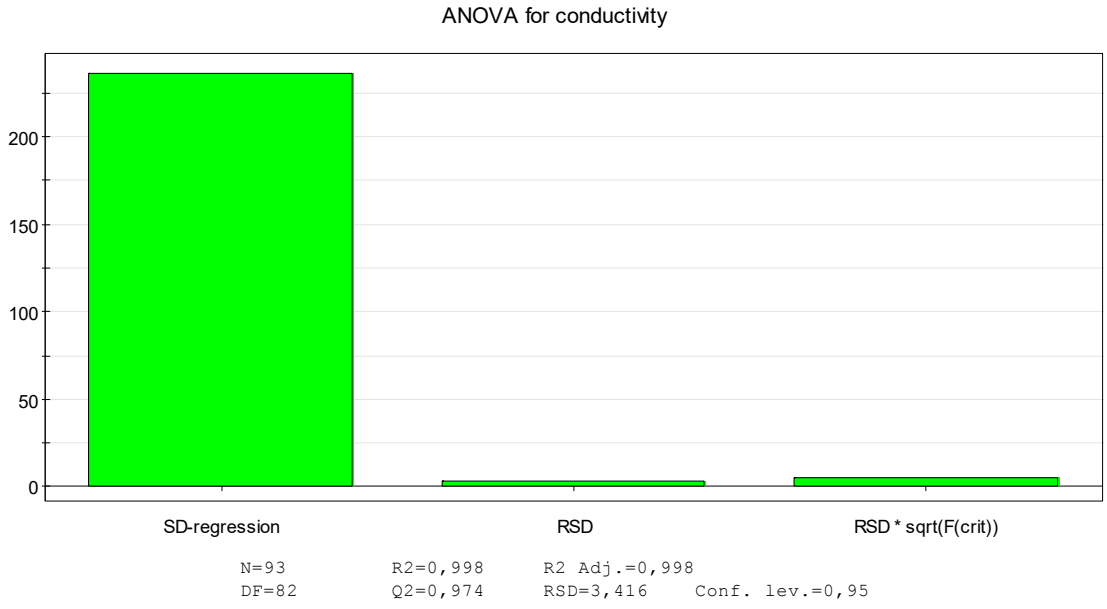

Figure 43. ANOVA plot for conductivity model without As.

The equations (36) and (37) for conductivity from models without As were compiled according to unscaled coefficients (tables 13 and 14). As seen in tables 13 and 14, the strongest combined effects according to low P values are with H_2SO_4 and Ni as well as H_2SO_4

and temperature. However, like in models 1 and 2, the combined effects are minor compared to the single effects.

$$\kappa = 307.9 - 1.583\,[\mathrm{Cu}] + 2.737\,[\mathrm{Ni}] + 1.285\,[\mathrm{H_2SO_4}] - 0.02776\,[\mathrm{H_2SO_4}][\mathrm{Ni}] - 0.008774\,[\mathrm{Cu}][\mathrm{H_2SO_4}] - 0.02087\,[\mathrm{Ni}]\,\mathrm{T} + 0.02919\,[\mathrm{H_2SO_4}]\,\mathrm{T} - 1.17\,\mathrm{T}\,, \quad (36)$$

$$\kappa = 31.863 - 1.3594\,[\mathrm{Cu}] + 1.835\,[\mathrm{Ni}] + 2.9789\,[\mathrm{H_2SO_4}] - 0.022681\,[\mathrm{H_2SO_4}][\mathrm{Ni}] - 0.010403\,[\mathrm{Cu}][\mathrm{H_2SO_4}] - 0.021408\,[\mathrm{Ni}]\,\mathrm{T} + 0.02975\,[\mathrm{H_2SO_4}]\,\mathrm{T} + 2.7297\;\mathrm{T} - 0.0044364\,[\mathrm{H_2SO_4}]^2 - 0.032787\,\mathrm{T}^2\,, \quad (37)$$

where the concentrations are in g/dm^3 and T is in °C, while κ is in mS/cm.

Both model 3 and model 4 are valid models according to summary of fit and ANOVA. The model validity is better in model 4. Conversely, the condition number, 1.375, is better in model 3. The condition number in model 4 was 4.322 which is over 3.

6.1.4. Comparisons

The equations defined are quite complicated due to the interactions of the factors, thus the effects of the factors are impossible to be directly seen in the equations. The effects of Cu and H_2SO_4 on electrolytes containing mean amount of As and Ni at mean temperature defined with model 1 are visualized in figure 44.

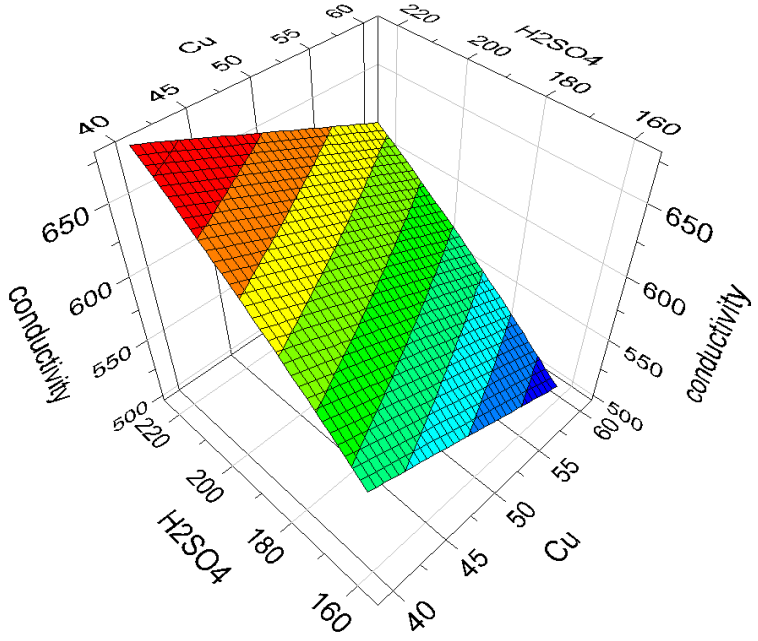

Figure 44. Effects of copper and sulfuric acid defined using model 1, while the temperature is 60 °C as well as the concentrations of Ni and As are 10.102 g/l and 15 g/l respectively.

The effects of temperature, Cu, As and Ni on conductivity are presented in figures 45–47. In addition, these figures present comparisons between the values defined with equations from this work and literature values. Conductivity results obtained in this work are in good agreement with previous research work [7, 11], though according to this work As seems to affect the conductivity slightly more and temperature less than according to [7, 11]. The equation defined by Subbaiah and Das [9] was not used in these comparisons, since it did not work even with their own values, except with low copper concentrations. That error was possibly due to lack of Cu term in the equation.

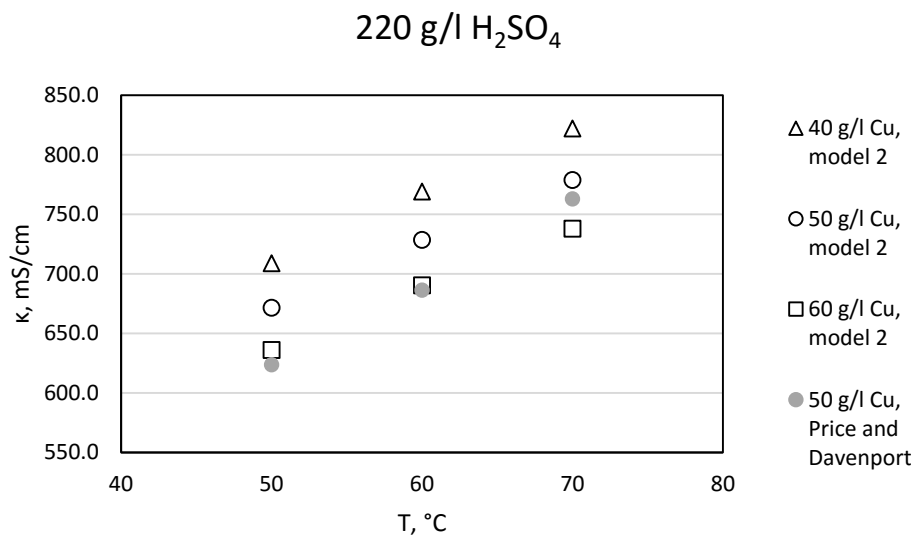

Figure 45. Effects of Cu and temperature according to models from this work and [7].

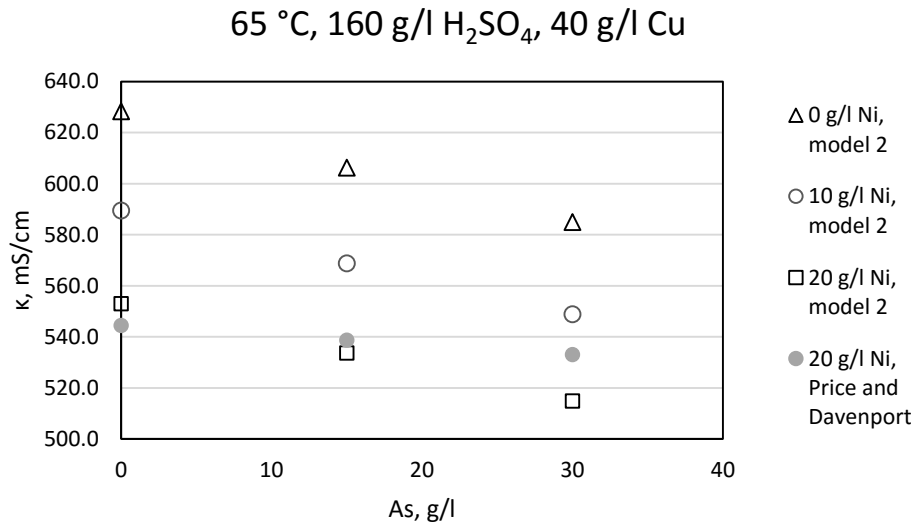

Figure 46. Effects of Ni and As according to models from this work and [7].

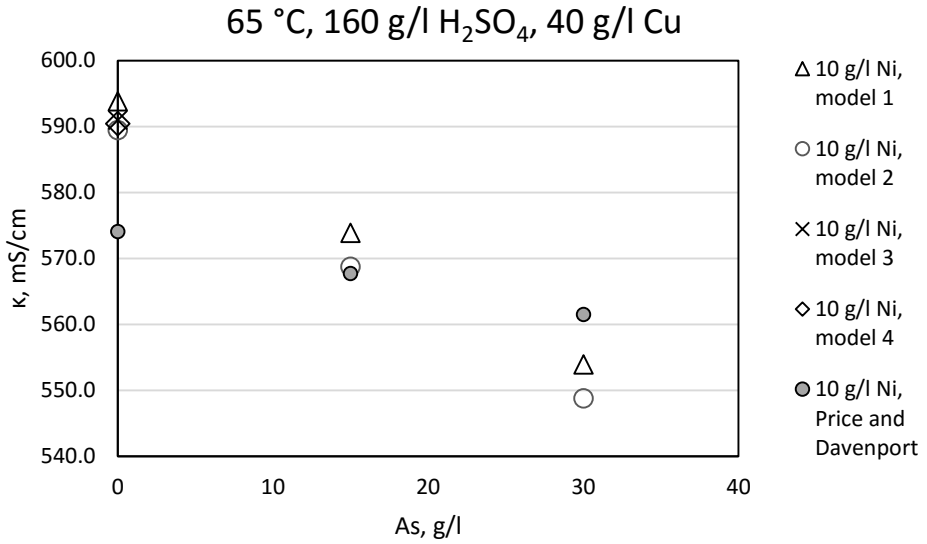

Figure 47. Effects of As defined using models from this work and [7].

As seen in table 15, the values defined using models from this work are in good agreement with Kern and Chang's results [11], which Price and Davenport had reported to be in good agreement with their results [7].

Table 15. Comparison of values defined with models 1–4 to equivalent values from [7] and to measured values from [11].

T, °C	Concentration. g/l				κ, mS/cm					
					Model				Price and Davenport	Kern and Chang
	H_2SO_4	Cu	Ni	As	1	2	3	4		
55	135	35	0	0	538.4	534.0	536.9	528.3	527.3	530.7
55	135	35	30	0	453.4	440.9	472.1	456.1	458.4	444.0
55	135	35	0	30	504.8	498.9			516.7	523.1
55	135	35	0	40	493.6	487.7			513.2	519.4

6.2. Density

The density results were processed prior to analyzing them, as mentioned in section 5.3, since the values obtained using the viscosity and density meter increased during measurement series. That was detected when the readings of the meter were checked with water after some pretest measurements. The processed density values as well as unnormalized and normalized viscosity values are presented in appendix A (table A2).

The histogram of raw data of density values (figure 48) had a tail to the right. However, the histogram did not change better with logarithmic transformation, and the skewness was not substantial. Thus the data was regarded as distributed normally enough, and the model was constructed of it.

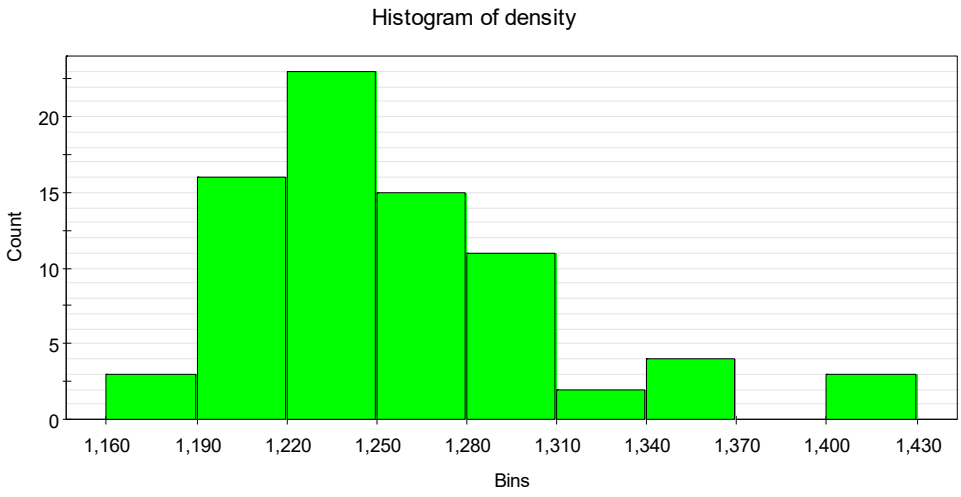

Figure 48. Histogram of density values.

Scatter plots of the factors are shown in figures 49 and 50. According to these plots, Cu, Ni, As and H_2SO_4 increase but temperature decreases density, as described in literature [6, 7, 9]. The temperature does not seem to affect much, partly since the temperature range between 50 and 59 °C is narrow. The effects of temperature would have been determined more reliably if the temperature range had been wider.

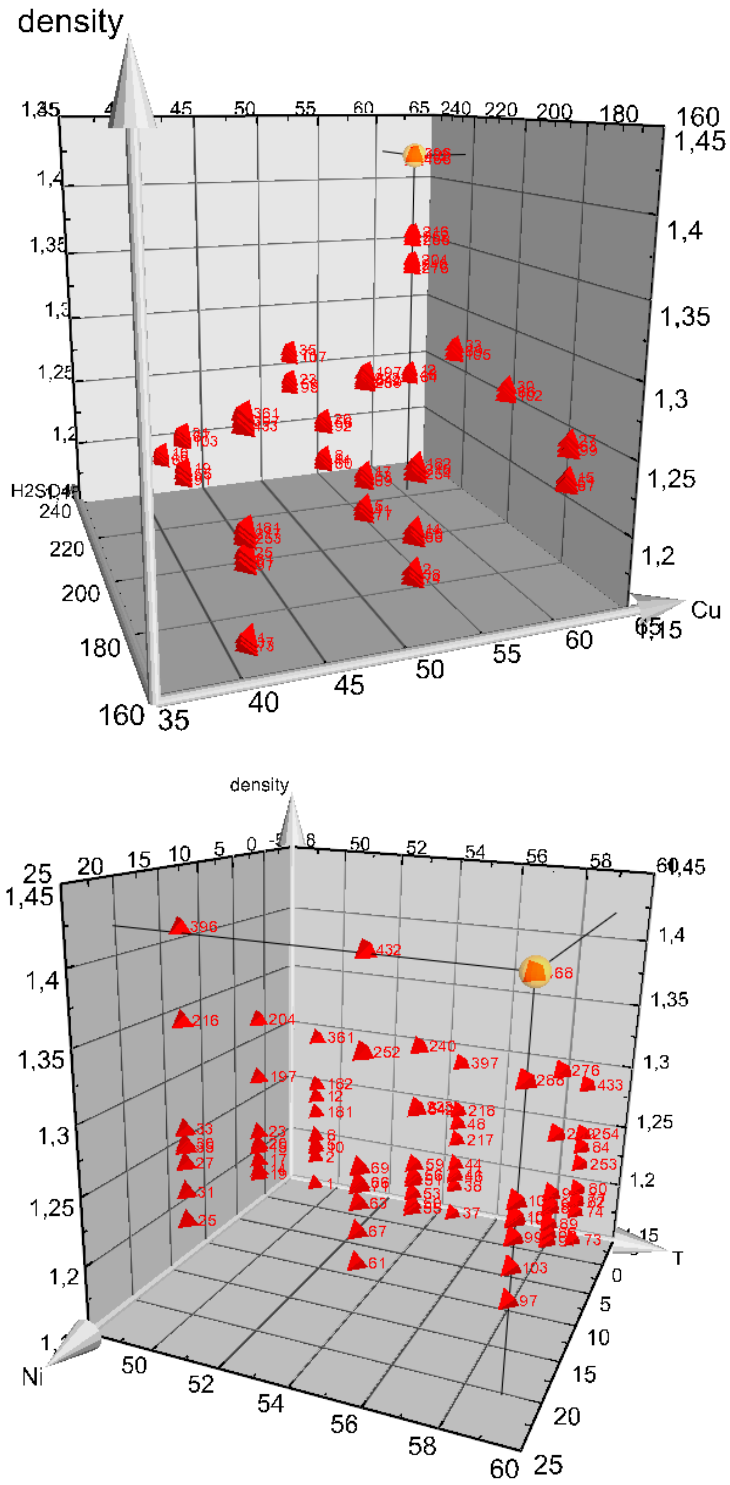

Figure 49. Scatter plots of H_2SO_4 and Cu concentration as well as Ni concentration and temperature for density model.

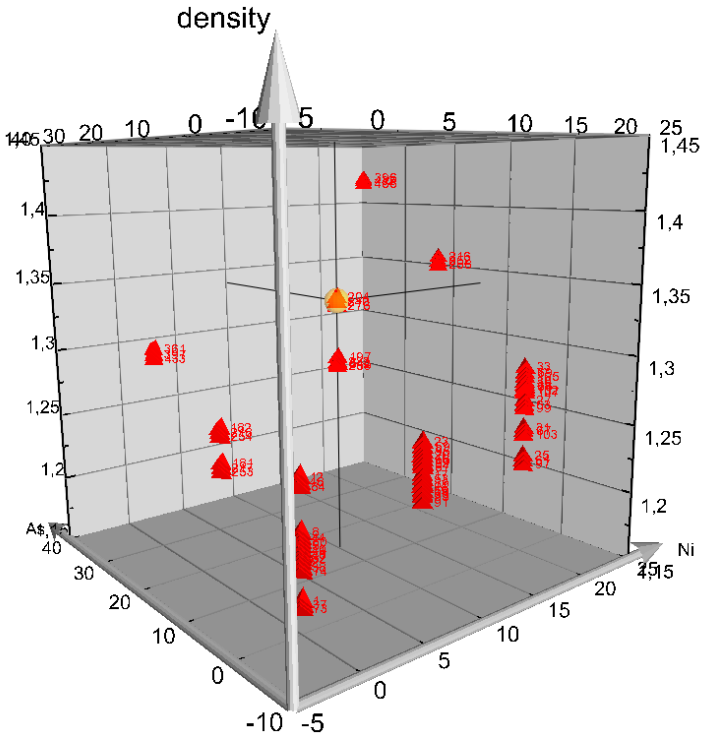

Figure 50. Scatter plot of arsenic and nickel concentration for density model.

The density model of the measured values with evaluations is presented in table 16 and figures 51 and 52. The coefficients of the model are shown in the table and the evaluations in summary of fit as well as ANOVA plots in figures. The tables and figures have terms of concentrations and temperature which are in g/dm^3 and °C respectively. Density is in g/cm^3.

Table 16. Coefficients for density model.

Scaled and centered coefficients		**Std. Err.**	**P**	**Conf. int(±)**	**Coefficients**	
Constant	1.25692	0.000337	0	0.000672	**Constant**	1.0853
Cu	0.0181503	0.000374	0	0.000746	**Cu**	0.00113382
H_2SO_4	0.0124147	0.000376	0	0.00075	**H_2SO_4**	0.000176924
Ni	0.0207931	0.000361	0	0.00072	**Ni**	0.0026134
T	-0.00197095	0.000323	5.20E-08	0.000643	**T**	-0.000538824
As	0.0383452	0.00038	0	0.000759	**As**	0.00423168
Cu*H_2SO_4	0.00122106	0.000371	0.00157	0.00074	**Cu*H_2SO_4**	6.31E-06
Ni*As	-0.00135107	0.000348	0.000231	0.000694	**Ni*As**	-1.73E-05

N = 77	Q^2 = 0.982	Cond. no. =	2.158
DF = 69	R^2 = 0.998	Y-miss =	0
Comp. = 4	R^2 Adj. = 0.997	RSD =	0.002812
		Conf. lev. =	0.95

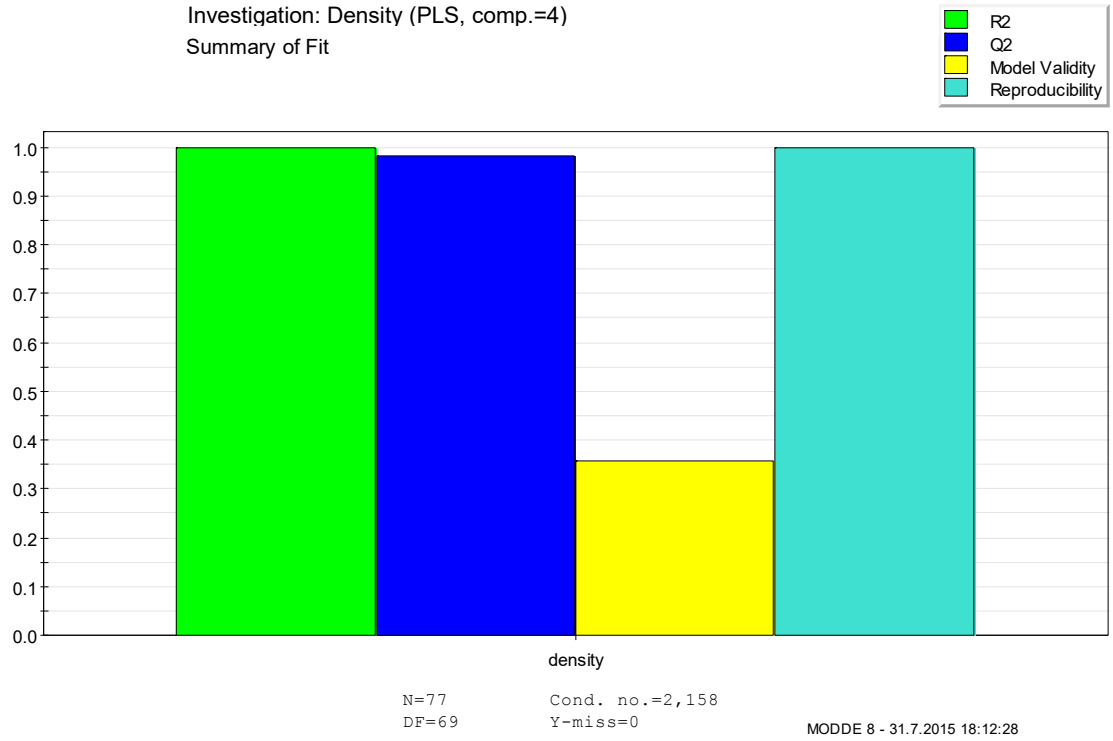

Figure 51. Summary of fit for density model.

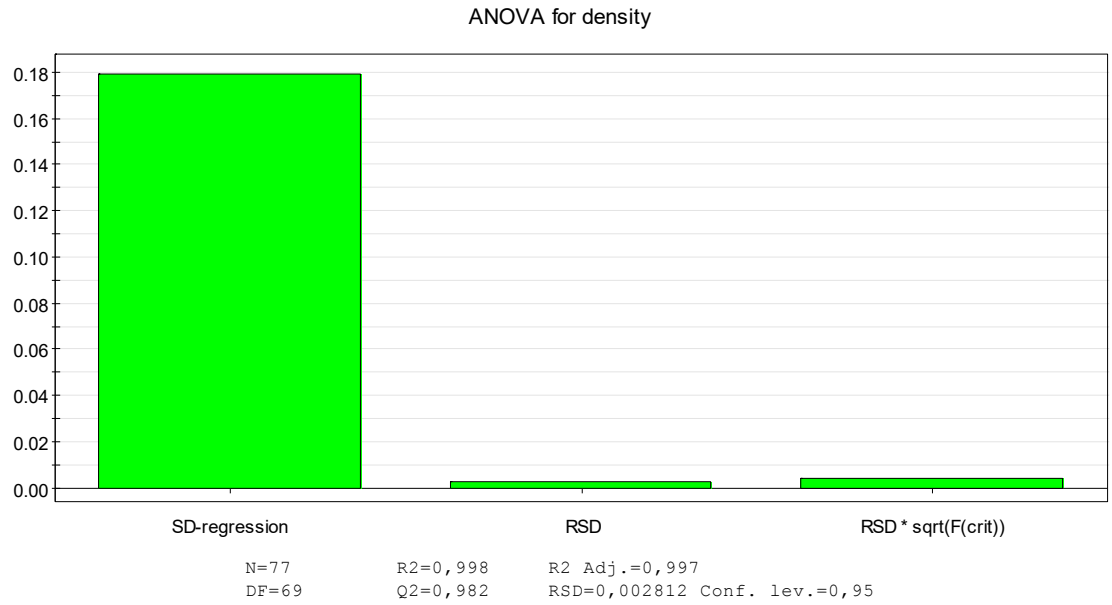

Figure 52. ANOVA plot for density model.

The equation (38) for density was compiled according to unscaled coefficients (table 16). As seen of the P values in table 16 the density model does not have really strong combined effects between the single terms.

$$\rho = 1.0853 + 0.001134\,[\mathrm{Cu}] + 0.002613\,[\mathrm{Ni}] + 0.004232\,[\mathrm{As}] + 0.0001769\,[\mathrm{H_2SO_4}] - 1.732 \cdot 10^{-5}\,[\mathrm{Ni}][\mathrm{As}] + 6.312 \cdot 10^{-6}\,[\mathrm{Cu}][\mathrm{H_2SO_4}] - 0.0005388\,\mathrm{T}, \quad (38)$$

where the concentrations are in g/dm^3 and T is in °C, while ρ is in g/cm^3.

The density model is valid according to summary of fit and ANOVA. In addition, the condition number of the model is good, under 3. However, the narrow temperature range in experiments might have caused some inaccuracy to the model.

The effects of the factors on density can already be seen in the equations, but they are also presented in figures 53–55.

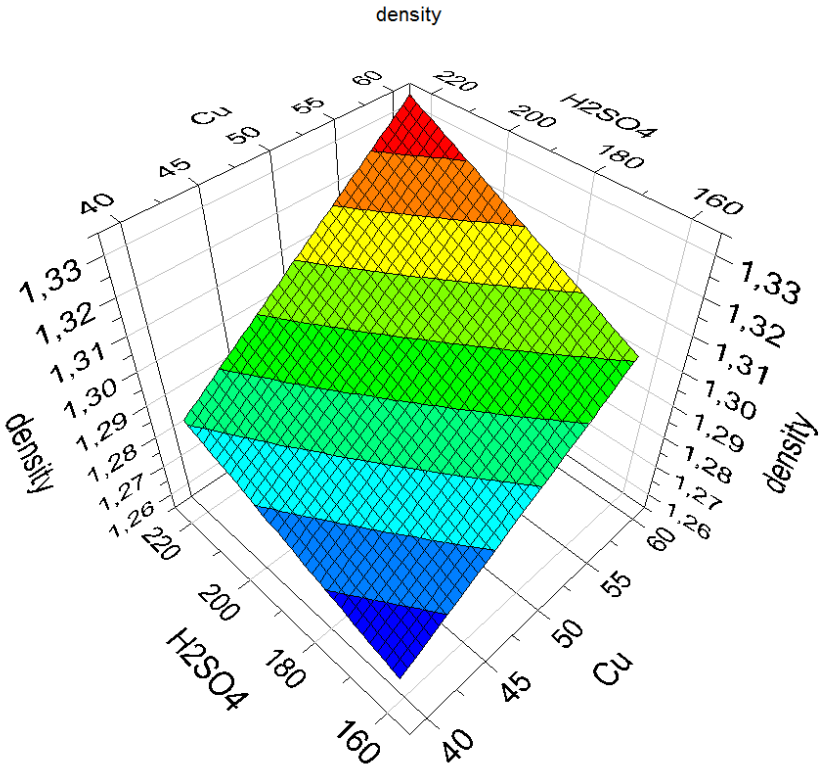

Figure 53. Effects of copper and sulfuric acid on density, while temperature is 59 °C, Ni concentration 10.102 g/l and As concentration 15 g/l.

Density results calculated with equation (38) from this work are in good agreement with previous research work [7, 9], though the narrow temperature range in experiments. However, according to this work As seems to affect the density slightly more than according to [7].

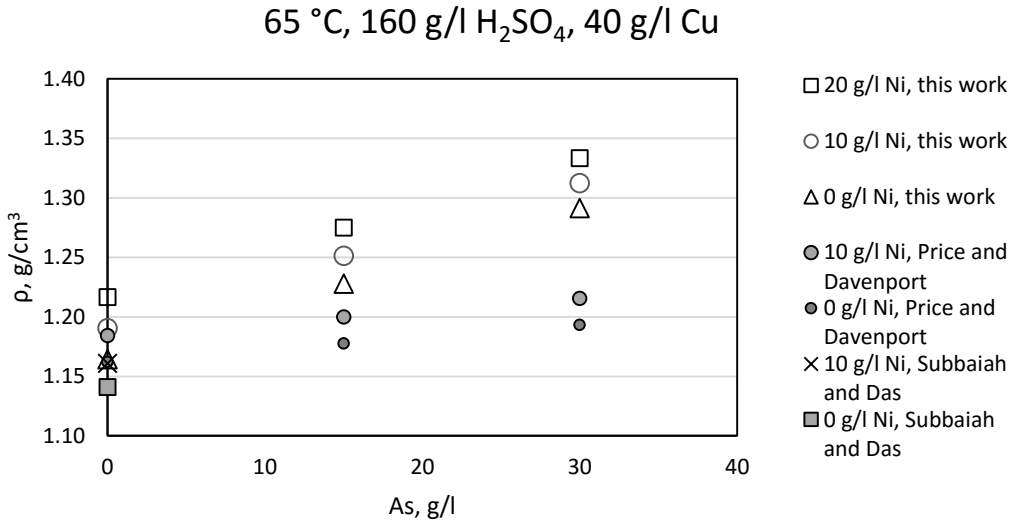

Figure 54. Effects of Ni and As on density according to this work, [7] and [9].

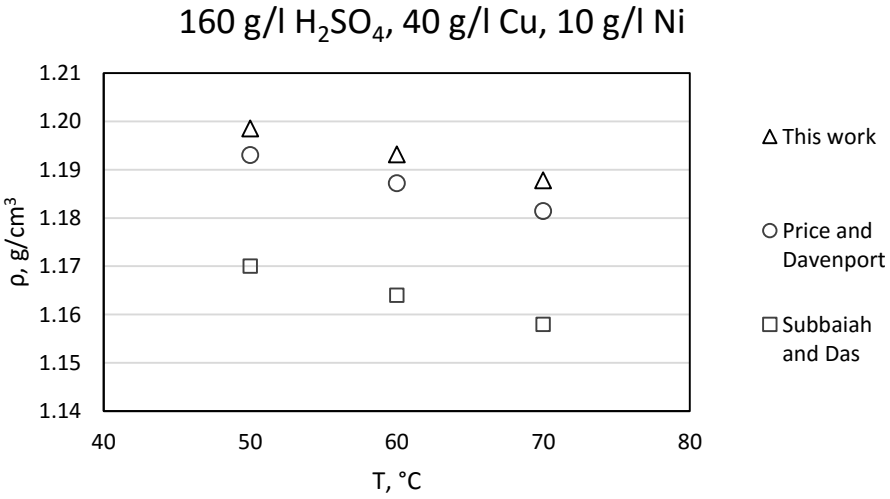

Figure 55. Effect of temperature according to this work, [7] and [9].

6.3. Viscosity

The viscosity models were constructed for kinematic viscosity instead of dynamic viscosity, since kinematic viscosity was needed in defining diffusion coefficients. That simplified the calculation. The viscosity values were not normalized like density values, since the effects of the unstable meter on viscosity were not as evident. The normalization of viscosity values was carried out as described in section 5.3.

The histograms of kinematic viscosity values were not quite normally distributed. The distributions, both of unnormalized and normalized values, had tail to the right (figure 56). On the other hand, the histograms were not completely skew, and the skewness could not be fixed with logarithmic transformation due to the tail. Consequently, the viscosity data was used for constructing the models.

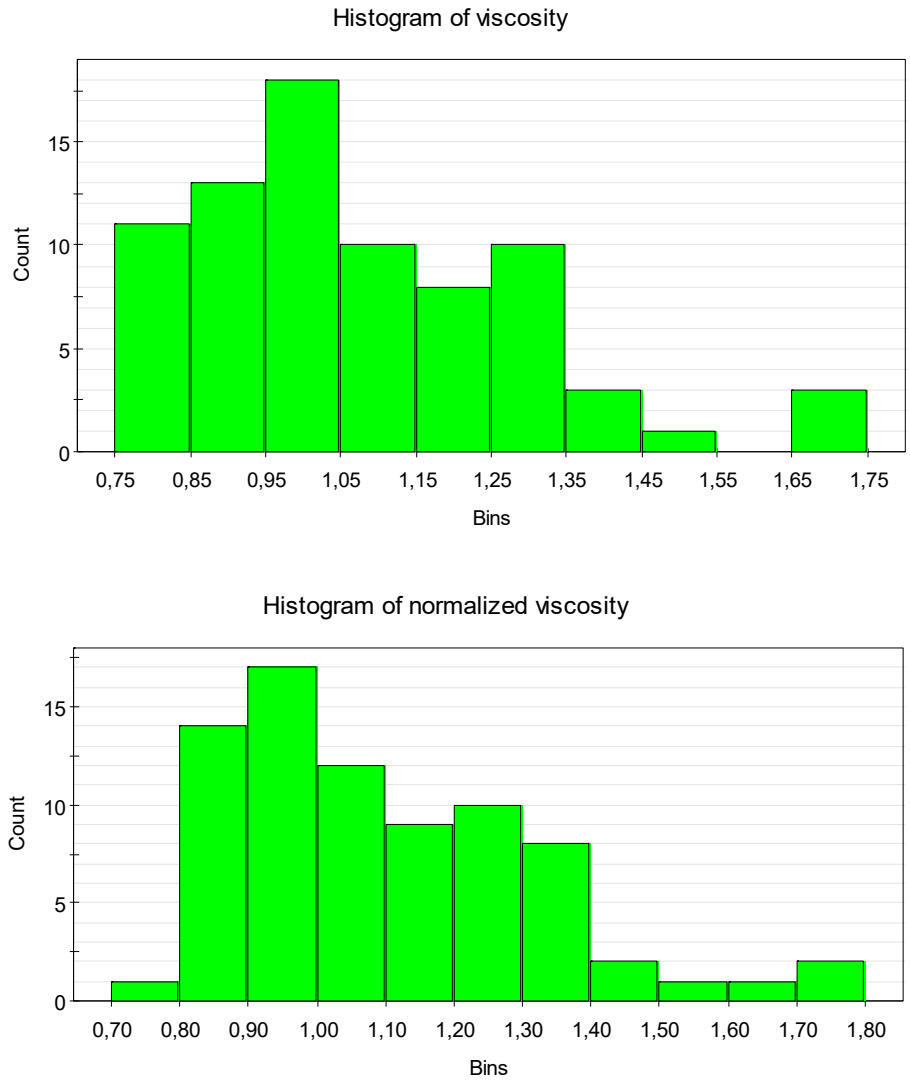

Figure 56. Histograms of unnormalized and normalized kinematic viscosity values.

Scatter plots of the raw normalized viscosity data are shown in figures 57 and 58. The equivalent plots of unnormalized values were practically similar to these and not shown here. According to these plots all the factors except temperature increase viscosity. Temperature decreases viscosity. These effects are in line with literature [6, 7, 10].

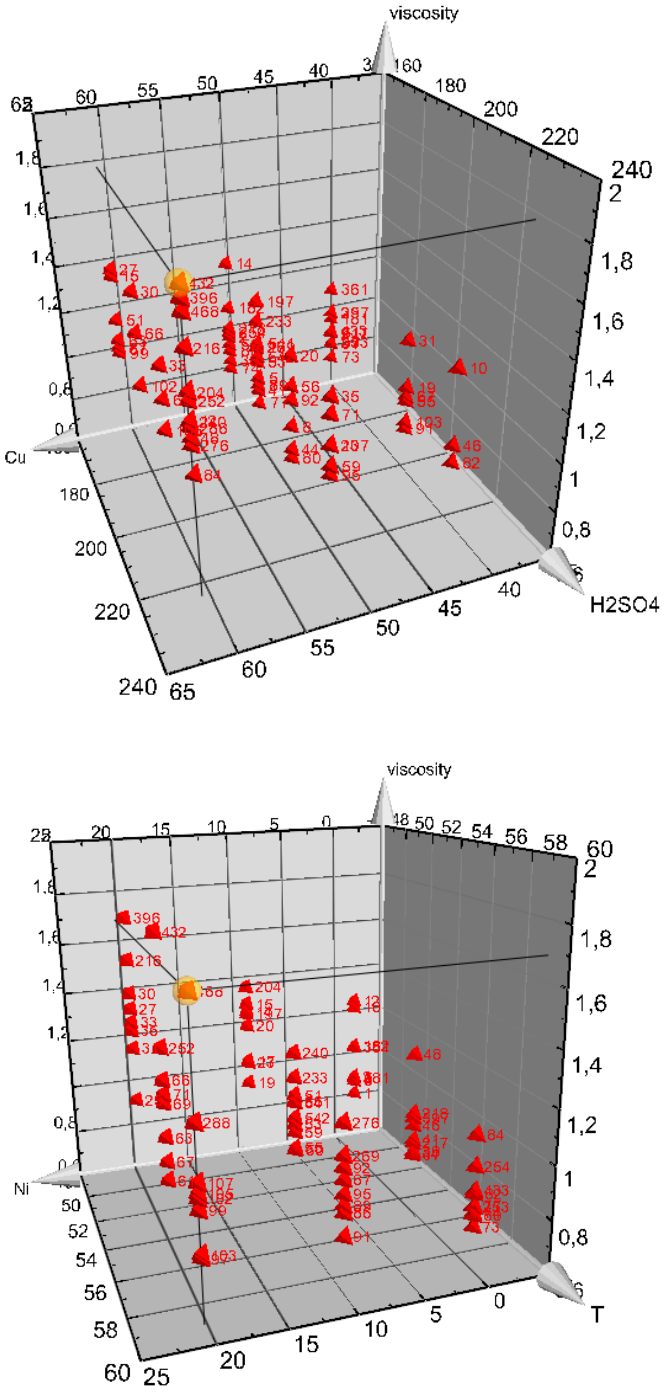

Figure 57. Scatter plots of the H_2SO_4 and Cu concentrations as well as Ni concentration and temperature for normalized viscosity model.

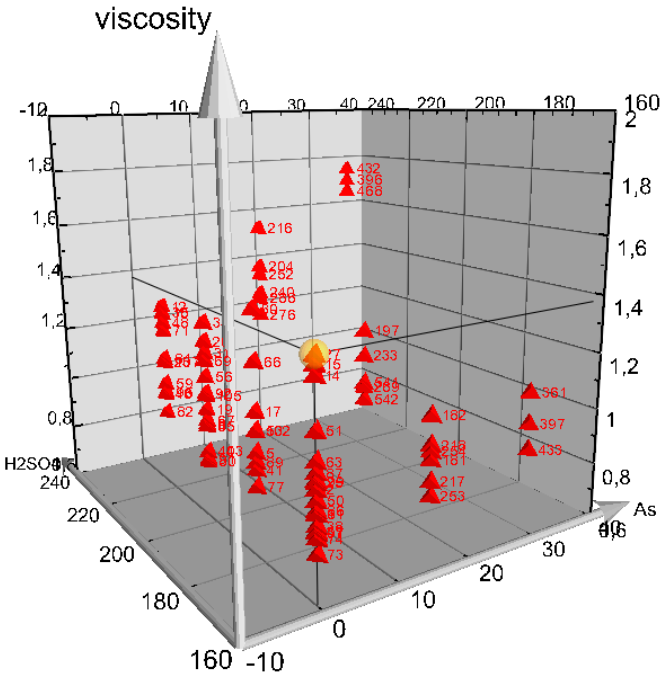

Figure 58. Scatter plot of the H_2SO_4 and As concentration for normalized viscosity model.

The viscosity models of the measured values with evaluations are presented in tables 17 and 18 and figures 59–62. The coefficients of the models are shown in the table and the evaluations in summary of fit as well as ANOVA plots in figures. The tables and figures have terms of concentrations and temperature which are in g/dm^3 and °C respectively. Viscosity is in mm^2/s. The first viscosity model was constructed of unnormalized measured values and the second model of normalized values which were calculated of obtained dynamic viscosity values and normalized density values.

Table 17. Coefficients for viscosity model.

Scaled and centered coefficients		Std. Err.	P	Conf. int(±)	Coefficients	
Constant	1.07624	0.00946	0	0.0189	**Constant**	1.22324
Cu	0.089949	0.01054	1.71E-12	0.0210	**Cu**	0.011586
H_2SO_4	0.057796	0.01005	2.08E-07	0.0200	**H_2SO_4**	0.00232
Ni	0.061799	0.01047	1.11E-07	0.0209	**Ni**	0.007476
T	-0.08726	0.00953	1.19E-13	0.0190	**T**	-0.02385
As	0.087577	0.00956	1.21E-13	0.0191	**As**	0.009281

N = 77	Q^2 = 0.83	Cond. no. =	1.628
DF = 71	R^2 = 0.861	Y-miss =	0
Comp. = 3	R^2 Adj. = 0.851	RSD =	0.08305
		Conf. lev. =	0.95

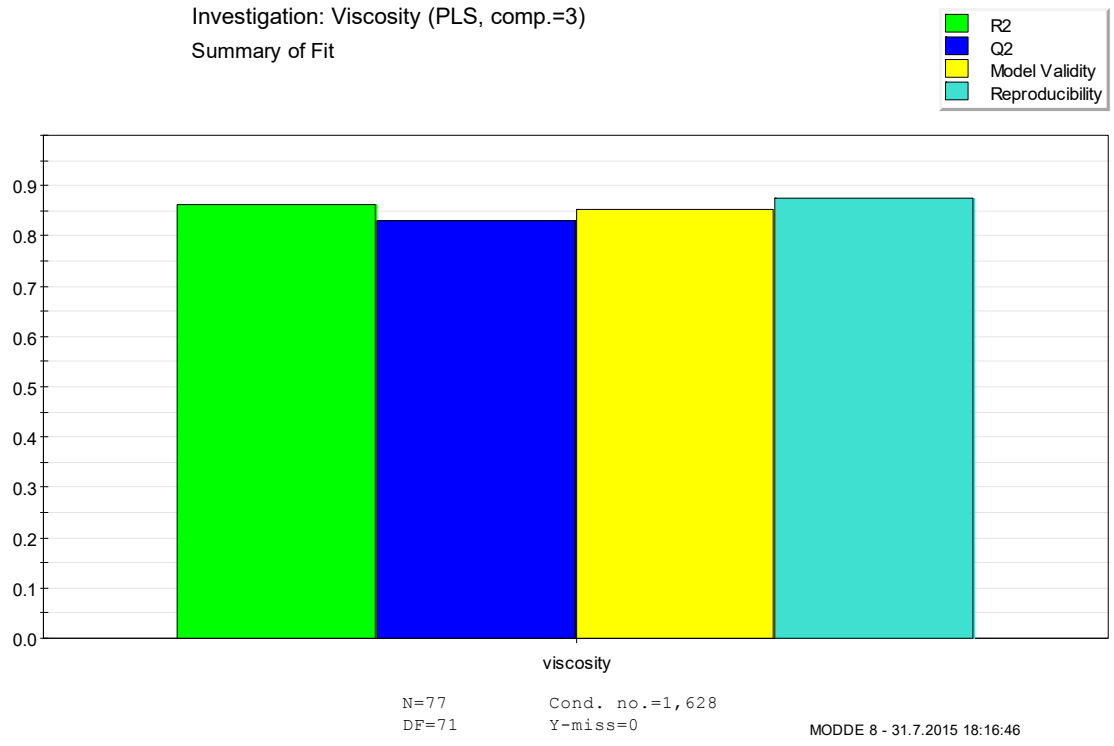

Figure 59. Summary of fit for viscosity model.

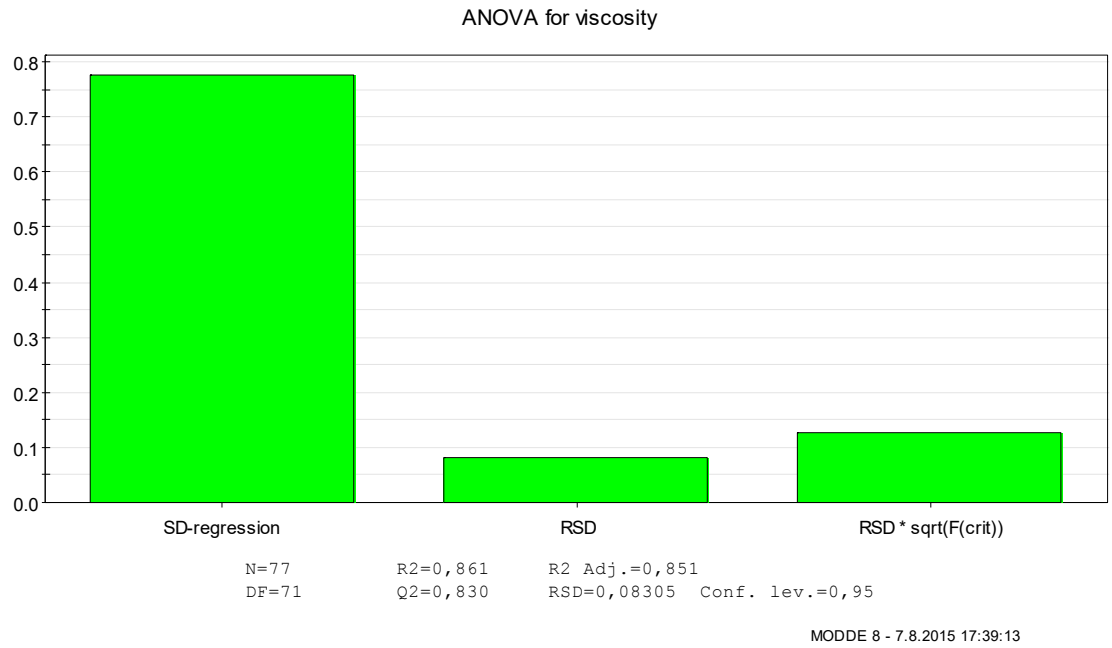

Figure 60. ANOVA plot for viscosity model.

Table 18. Coefficients for normalized viscosity model.

Scaled and centered coefficients		**Std. Err.**	**P**	**Conf. int(±)**	**Coefficients**	
Constant	1.09461	0.00957	0	0.0191	**Constant**	1.23975
Cu	0.091349	0.01066	1.46E-12	0.0213	**Cu**	0.011767
H_2SO_4	0.059139	0.01016	1.58E-07	0.0203	**H_2SO_4**	0.002373
Ni	0.063231	0.01058	8.35E-08	0.0211	**Ni**	0.00765
T	-0.08864	0.00963	9.99E-14	0.0192	**T**	-0.02423
As	0.089825	0.00967	6.93E-14	0.0193	**As**	0.009519

N = 77	Q^2 = 0.833	Cond. no. =	1.628
DF = 71	R^2 = 0.863	Y-miss =	0
Comp. = 3	R^2 Adj. = 0.853	RSD =	0.08398
		Conf. lev. =	0.95

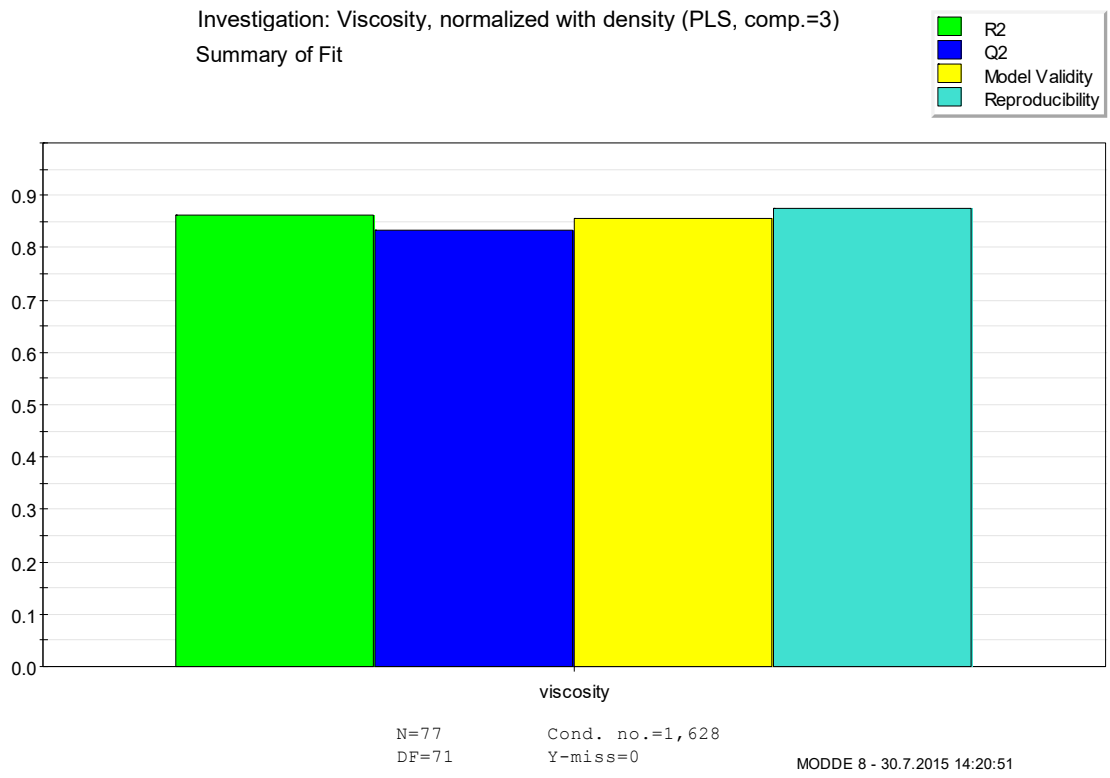

Figure 61. Summary of fit for normalized viscosity model.

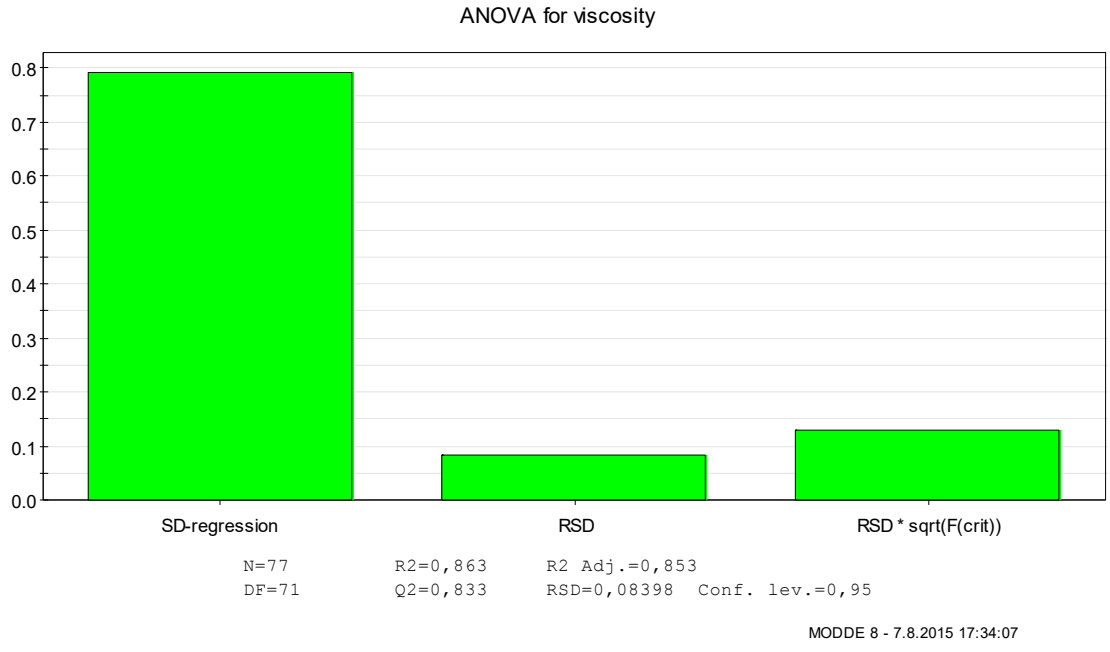

Figure 62. ANOVA plot for normalized viscosity model.

The equation (39) was compiled for unnormalized and (40) for normalized viscosity according to unscaled coefficients (tables 17 and 18).

$$\nu = 1.2232 + 0.011586\,[\mathrm{Cu}] + 0.0074764\,[\mathrm{Ni}] + 0.0092807\,[\mathrm{As}] + 0.0023196\,[\mathrm{H_2SO_4}] - 0.023855\,\mathrm{T}\,, \quad (39)$$

$$\nu = 1.2398 + 0{,}011767\,[\mathrm{Cu}] + 0.0076497\,[\mathrm{Ni}] + 0.0095189\,[\mathrm{As}] + 0.0023735\,[\mathrm{H_2SO_4}] - 0.024232\,\mathrm{T}\,, \quad (40)$$

where the concentrations are in g/dm^3 and T is in °C, while ν is in mm^2/s.

Likewise the density model, the viscosity models are valid according to summary of fit and ANOVA. In addition, the condition numbers of the models are good, under 3. However, the narrow temperature range in experiments caused error at higher temperatures. The viscosity of the electrolyte, which contains minimum amount of the copper and sulfuric acid as well as no nickel and arsenic, was calculated to be 0.388 mm^2/s at 70 °C using equation (39) and 0.394 mm^2/s using equation (40). The both values are less than the equivalent viscosity of water (0.413 mm^2/s) [45]. That cannot be true and suggests that the model should not be used determining viscosities at higher temperatures than 59 °C.

The viscosity models are almost identical, and it is impossible to reliably determine which would be the best, since the viscosity values were not able to be normalized as simply as density values. The result values were normalized since the functioning of the meter was unstable and skewed the result values. That was noticed when the values occasionally increased substantially. The increased values were significantly higher that the literature values, and equally decreased after the probe was rinsed by shaking the beaker or using distilled water, solvent and compressed air. According to that it was suspected that the electrolyte affected the surface of the probe. The probe has vibrating parts which might have been coated by thin layer of deposits or debris which possibly affected the vibration frequency. However that could not be investigated further during this work.

The effects of the factors on viscosity can already be seen in the equations, but they are also presented in figures 63–65.

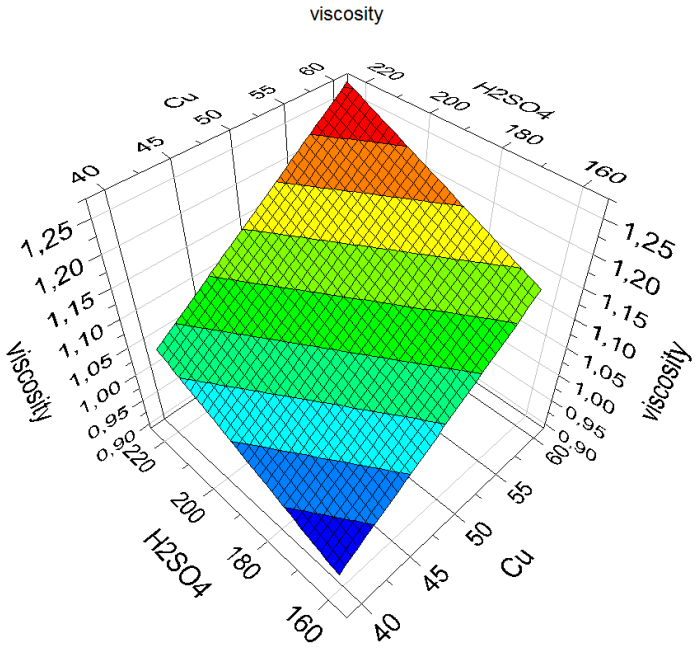

Figure 63. Effects of copper and sulfuric acid on normalized viscosity, while temperature is 59 °C, Ni concentration 10.102 g/l and As concentration 15 g/l according to this work.

The viscosity results are compared to the results of Price and Davenport [7]. The results differ from each other significantly (figures 64 and 65), though the directions of the effects are not completely different. The factors having increasing effect on viscosity according to [7] have found to have increasing effect also according to this work.

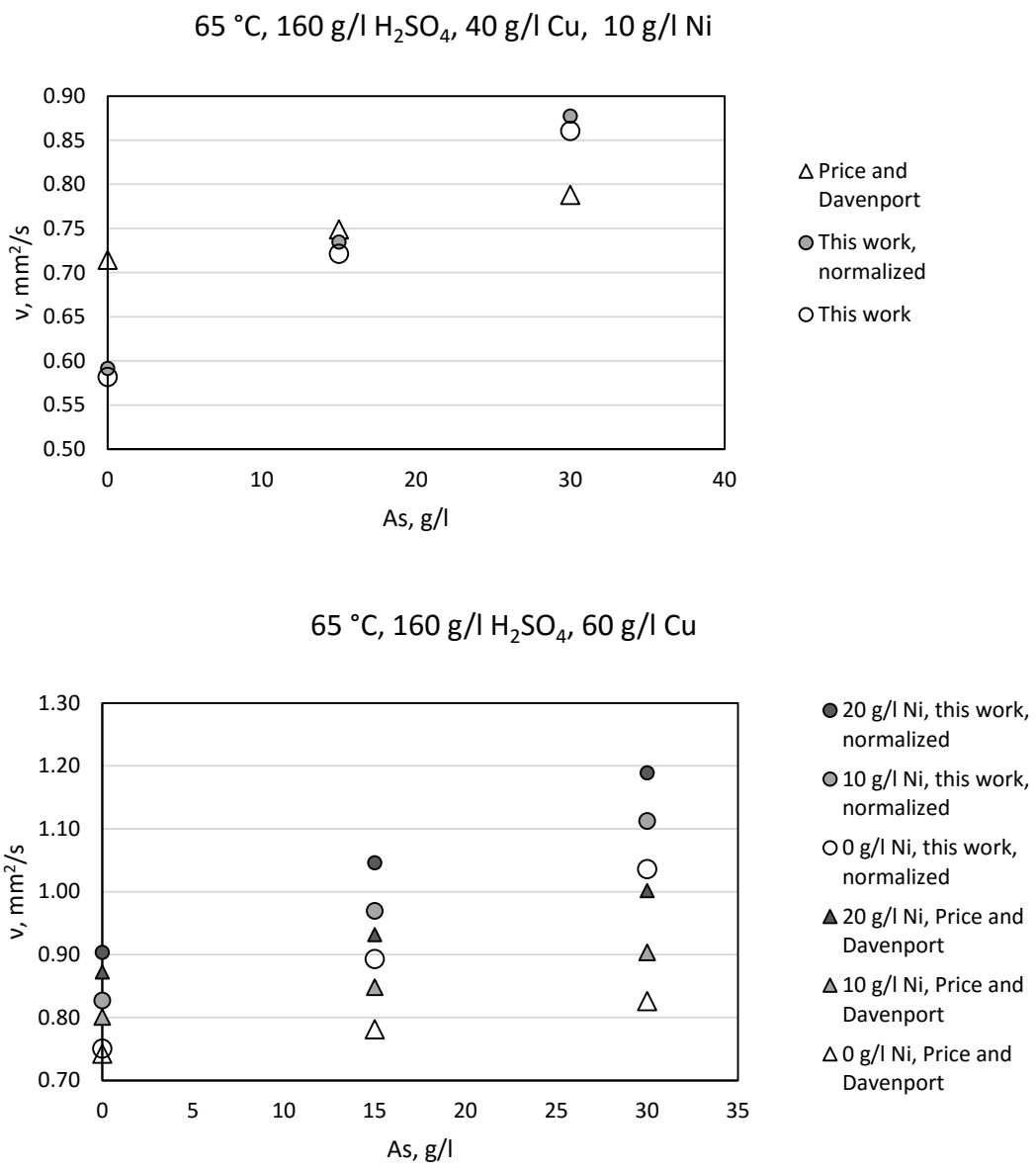

Figure 64. Effect of As and Ni according to this work and [7].

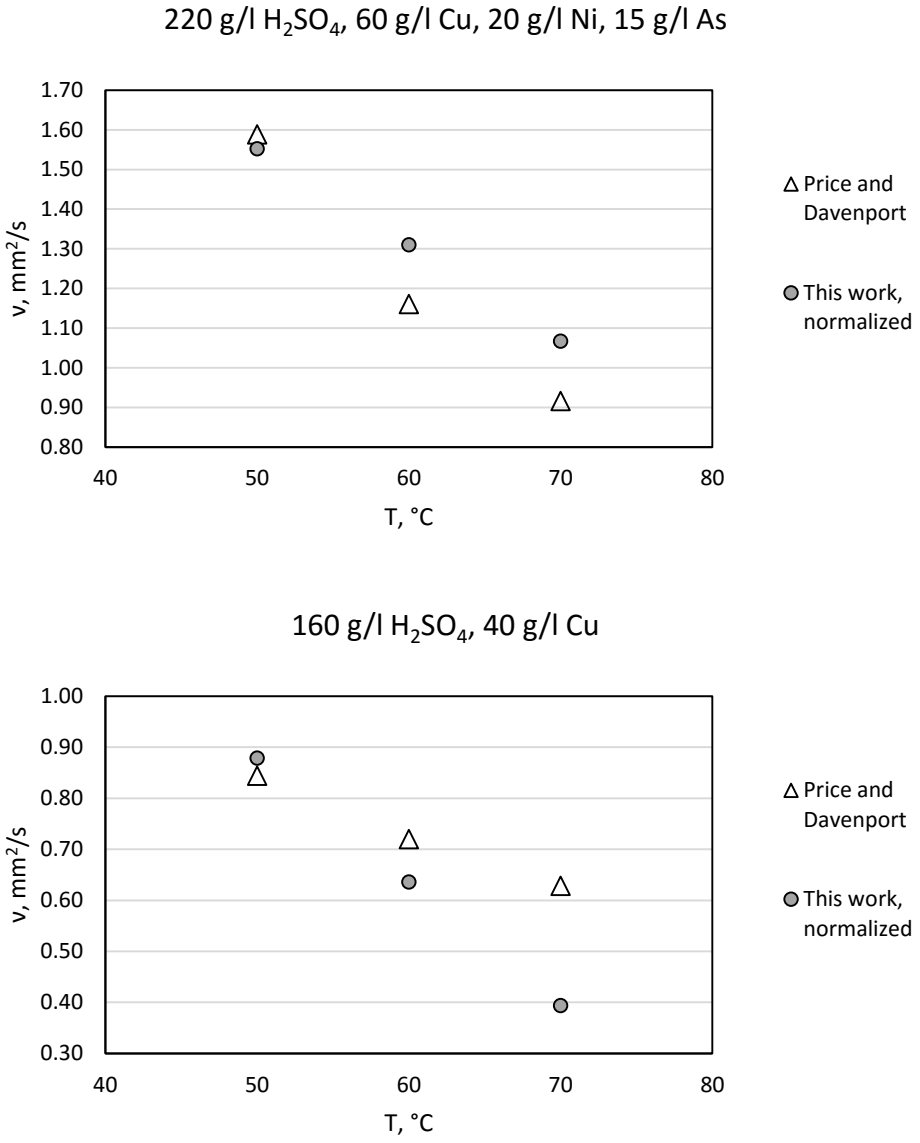

Figure 65. Effect of temperature according to this work and [7].

6.4. Diffusion coefficient of Cu^{2+}

The results of the pretest carried out prior to the actual measurements were noticed to be in line with literature values [13], [9], as their magnitude of the D_{Cu2+} was equivalent. Consequently, that verified the suitability of the procedure and the method.

The diffusion coefficients defined in various ways are presented in Appendix A (table A3) and the models of the measured values with evaluations in tables 19–21 and figures 73–78. The coefficients of the models are shown in the table and the evaluations in summary of fit

as well as ANOVA plots in figures. The models were defined of data calculated using Koutecký-Levich equation (26) due to recommendations [38, 39]. In addition, the fit of the line in Koutecký-Levich plot was better than in Levich plot. In defining model 1 viscosities determined with the equations (13) and (17) were used and in models 2 and 3 viscosity equations of this work.

The i/E curves for defining limiting current densities of one example electrolyte at one temperature are presented in figure 66 and at all temperatures in appendix A (figure A1). The limiting current densities were in this case determined at potentials around -0.5 V. According to these limiting current density values defined Levich and Koutecký-Levich plots are presented in figures 67 and 68, and the slopes of these plots were used in calculating the diffusion coefficients with Levich (25) and Koutecký-Levich (26) equations. The similar definitions were accomplished for each test electrolyte and thus obtained the results in which the correlation of fit was quite like in this example, but the amount of random noise or interference in the i/E curves varied and thus complicated the definitions.

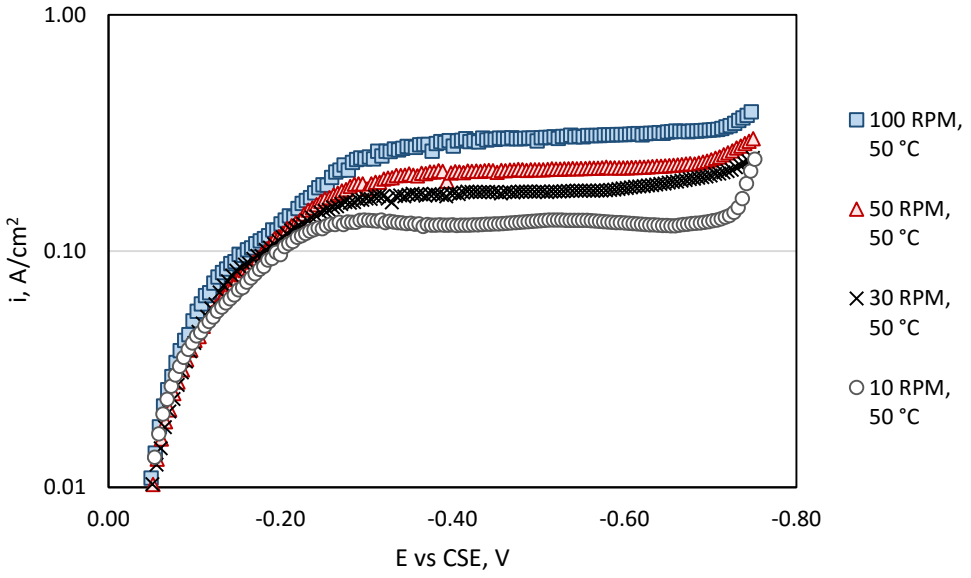

Figure 66. Limiting current density curves of electrolyte sample N5.

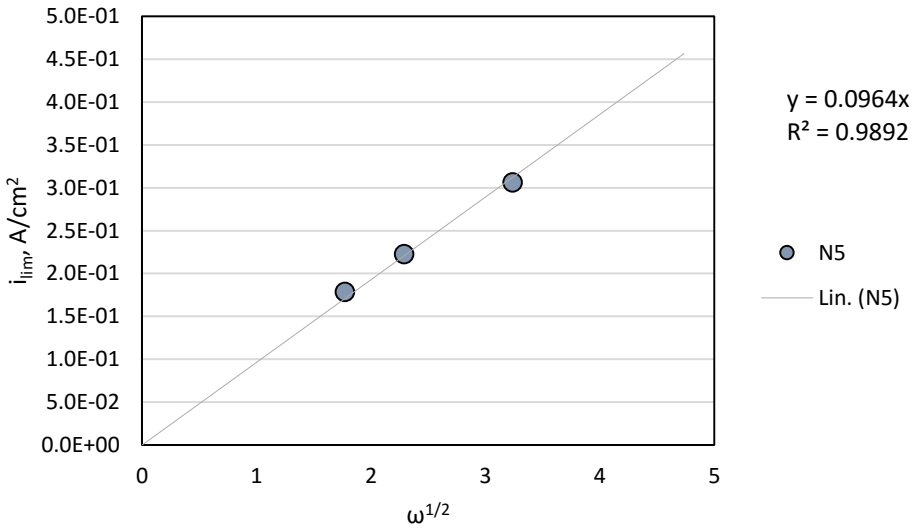

Figure 67. Levich plot of electrolyte N5 at 50 °C.

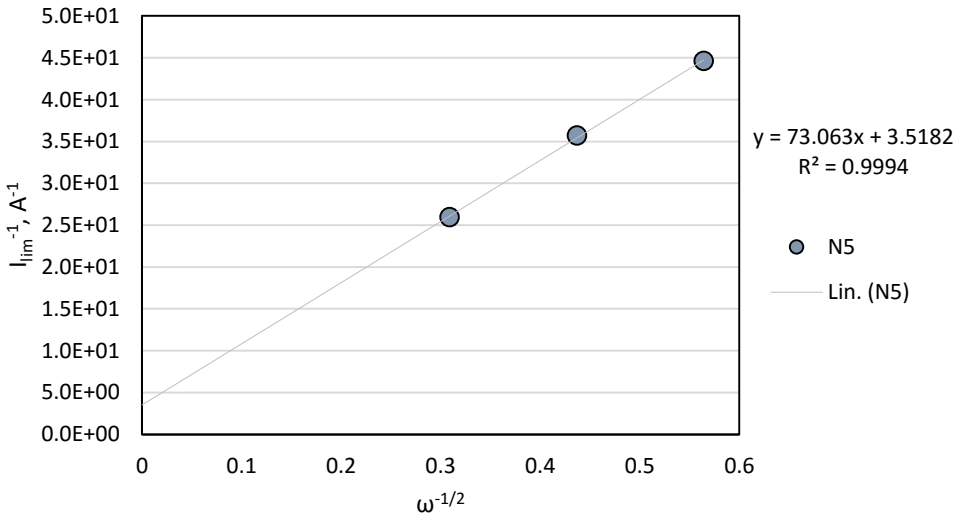

Figure 68. Koutecký-Levich plot of electrolyte N5 at 50 °C.

Histograms of diffusion coefficient data are presented in figure 69. The histograms were not normally distributed. Thus, in addition to the histograms, the descriptive statistics plots (figure 70) were inspected, since the skewness is easier to be observed with it of this kind of data. The distributions were not really skew, but irregular.

1

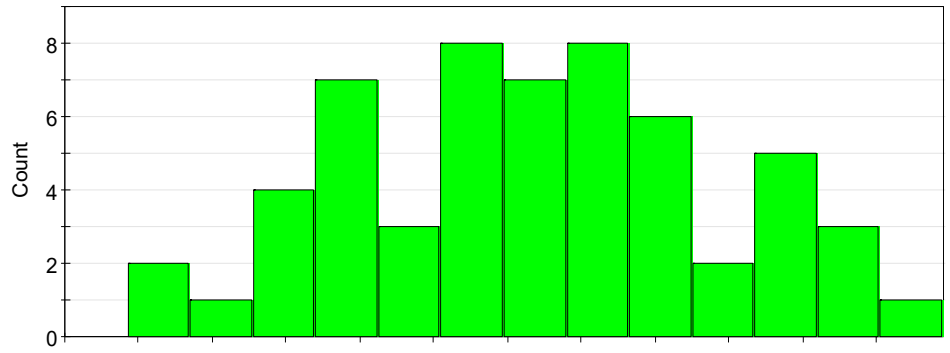

2

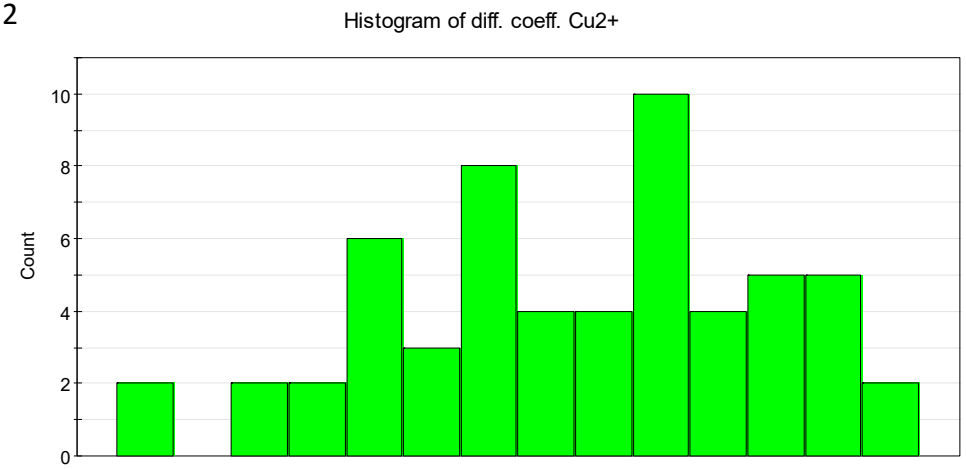

3

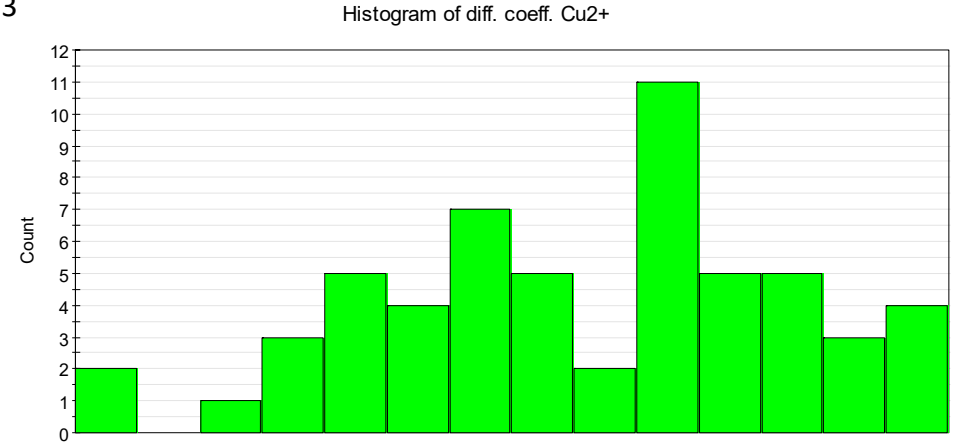

Figure 69. Histograms of $D_{Cu^{2+}}$ data. In 1 the data is calculated using viscosities from [7] as well as in 2 and 3 using unnormalized and normalized viscosities from this work respectively.

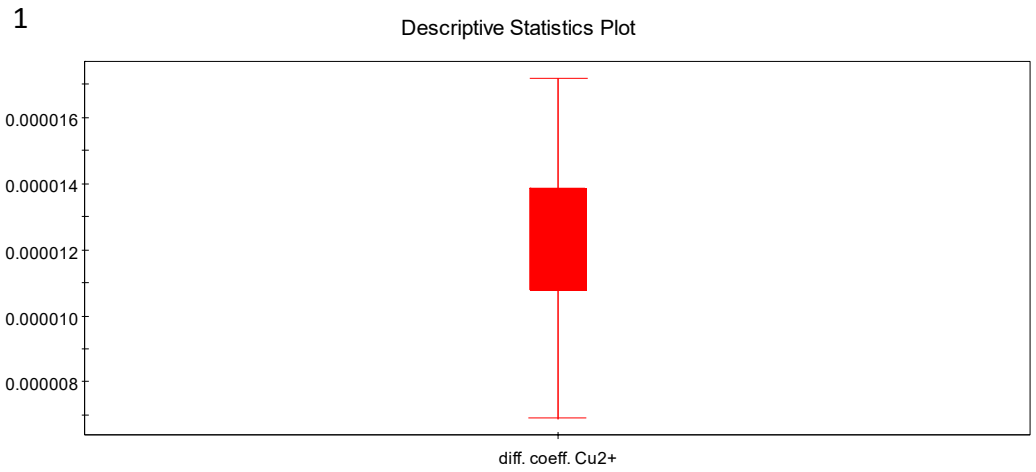

diff. coeff. Cu2+ Min: 6.9107e-006 Max: 1.7186e-005 Median: 1.2344e-005 Mean: 1.23545e-005

MODDE 8 - 30.9.2015 18:06:27

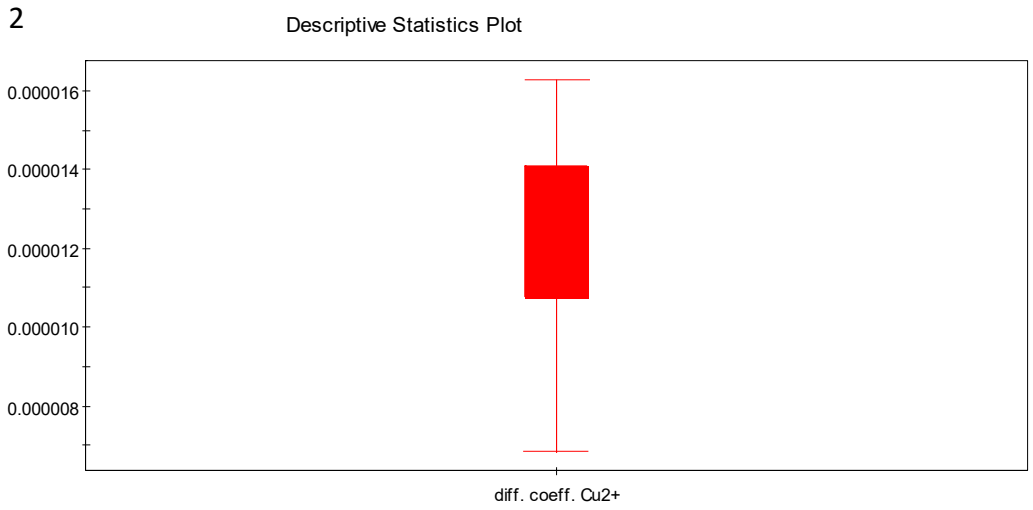

diff. coeff. Cu2+ Min: 6,8405e-006 Max: 1,6289e-005 Median: 1,2806e-005 Mean: 1,24472e-005

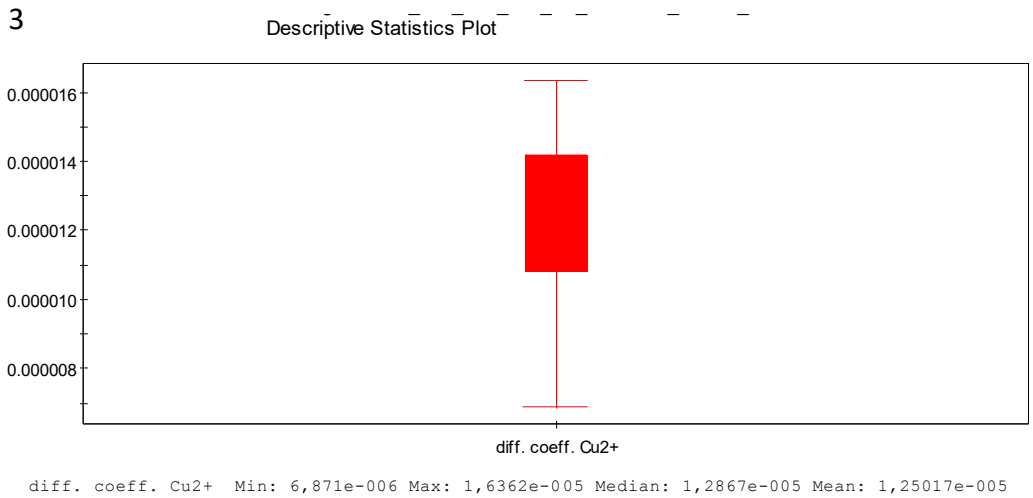

diff. coeff. Cu2+ Min: 6,871e-006 Max: 1,6362e-005 Median: 1,2867e-005 Mean: 1,25017e-005

Figure 70. Descriptive statistics of $D_{Cu^{2+}}$ data. In 1 the data is calculated using viscosities from [7] as well as in 2 and 3 using unnormalized and normalized viscosities from this work respectively.

Scatter plots of raw diffusion coefficient data, in which the values were calculated using viscosities from [7], are shown in figures 71 and 72. The other versions of scatter plots from data calculated using viscosities from this work are basically similar. The viscosity values did not affect the diffusion coefficients that dramatically at temperatures 50–70 °C (appendix A, table 3). However, the three models obtained from these data series were not similar. According to the scatter plots (figures 71 and 72) all the factors except temperature decrease $D_{Cu^{2+}}$. Temperature increases $D_{Cu^{2+}}$. These effects are in line with literature [8–10].

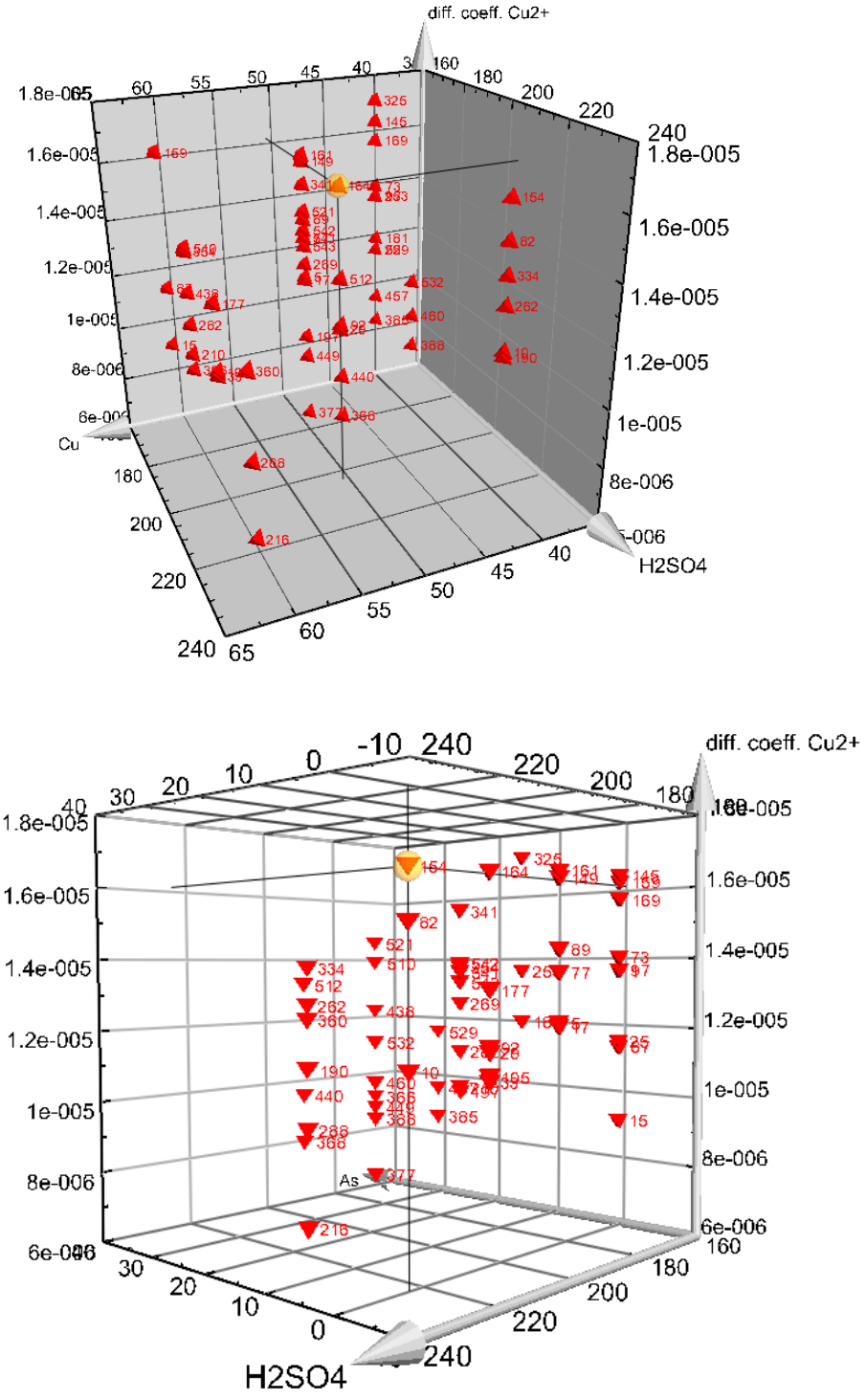

Figure 71. Scatter plots of H_2SO_4 and Cu concentrations as well as H_2SO_4 and As concentrations for diffusion coefficient model in which the values were calculated using viscosities from [7].

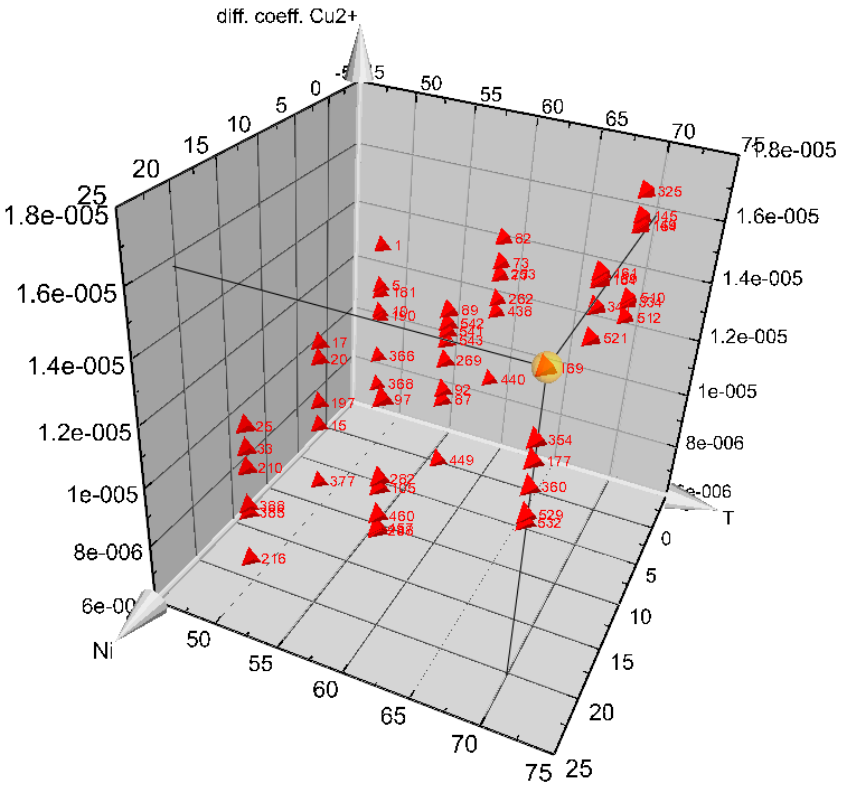

Figure 72. Scatter plot of Ni concentration and temperature for diffusion coefficient model in which the values were calculated using viscosities from [7].

6.4.1. D_{Cu2+} model 1

Diffusion coefficient model 1 was defined of data which was calculated using viscosity values from Price and Davenport [7]. The D_{Cu2+} model of the measured values with evaluations is presented in table 19 and figures 73 and 74.

Table 19. Coefficients for diffusion coefficient model in which the values were calculated using viscosities from [7].

Scaled and centered coefficients		Std. Err.	P	Conf. int(±)	Coefficients	
Constant	1.23816E-05	4.71E-08	0	9.3E-08	**Constant**	-1.70745E-06
Cu	-4.85957E-07	4.92E-08	3.42E-18	9.7E-08	**Cu**	-9.36713E-08
H_2SO_4	-1.93848E-07	4.81E-08	0.000086	9.5E-08	**H_2SO_4**	3.66713E-08
Ni	-5.47418E-07	4.82E-08	3.21E-22	9.5E-08	**Ni**	1.44765E-07
T	1.58151E-06	4.61E-08	0	9.1E-08	**T**	3.65869E-07
As	-1.07842E-06	4.66E-08	0	9.2E-08	**As**	-4.45589E-07
Cu*Ni	-1.49894E-07	4.44E-08	0.000930	8.8E-08	**Cu*Ni**	-2.23522E-09
Cu*As	5.19195E-07	4.62E-08	6.73E-22	9.1E-08	**Cu*As**	5.20807E-09
H_2SO_4*T	-1.24461E-07	4.63E-08	0.00796	9.1E-08	**H_2SO_4*T**	-7.47585E-10
Ni*T	-9.47371E-08	4.60E-08	0.04097	9.1E-08	**Ni*T**	-1.60892E-09
T*As	1.37675E-07	4.62E-08	0.00334	9.1E-08	**T*As**	1.57282E-09

N = 168	Q^2 =	0.782	Cond. no. = 1.573
DF = 157	R^2 =	0.841	Y-miss = 111
Comp. = 3	R^2 Adj. =	0.806	RSD = 5.96E-07
			Conf. lev. = 0.95

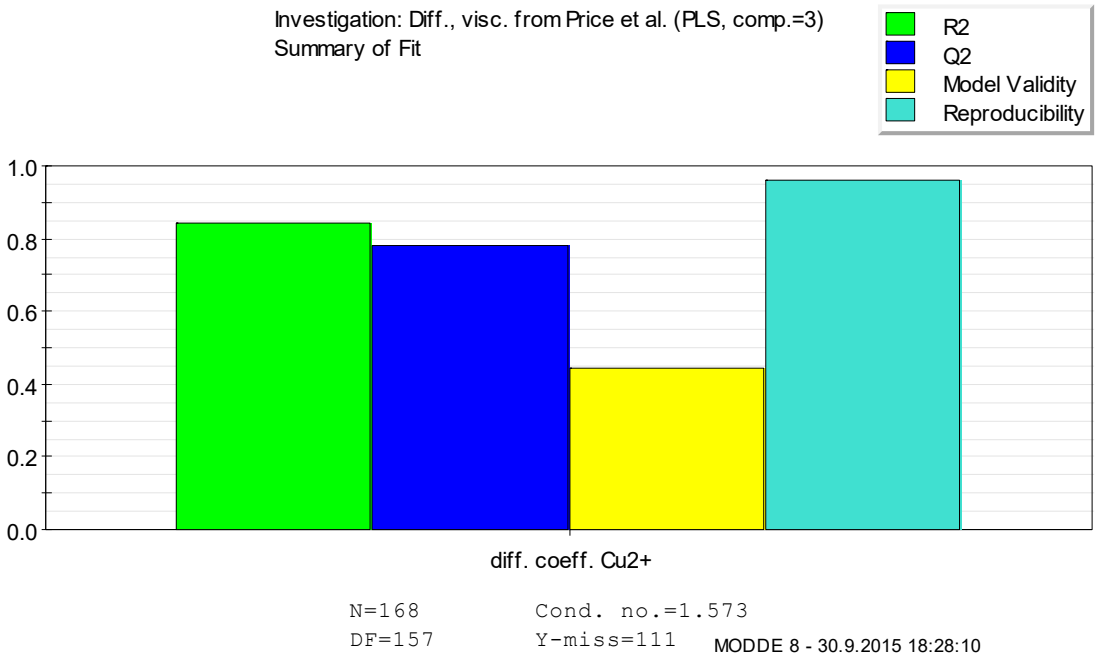

Figure 73. Summary of fit for diffusion coefficient model in which the values were calculated using viscosities from [7].

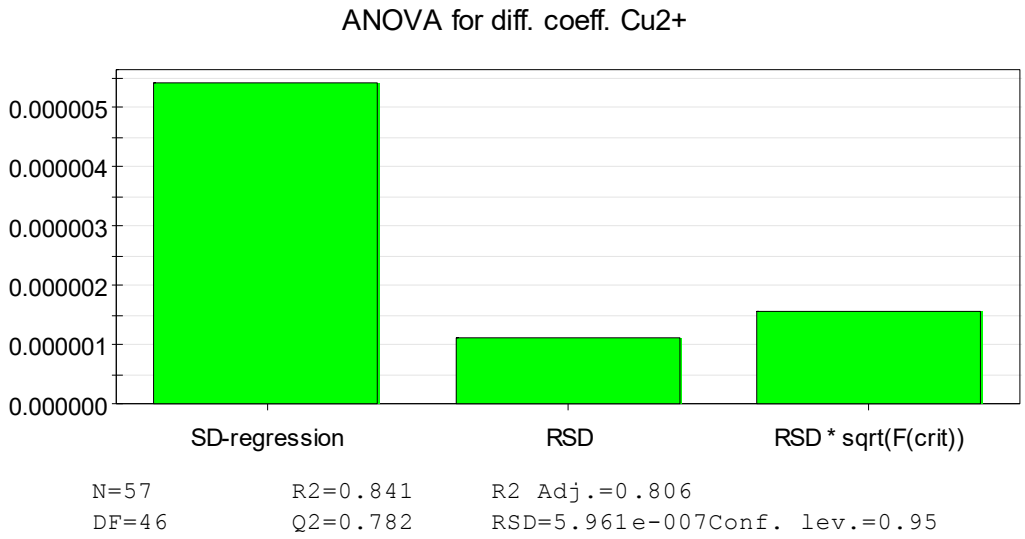

Figure 74. ANOVA plot for diffusion coefficient model in which the values were calculated using viscosities from [7].

The equation (41) for $D_{Cu^{2+}}$ was compiled according to unscaled coefficients (table 19). As seen in table 19, the strongest combined effect according to low P values is with Cu and As. However, the combined effects are minor compared to effects of single terms.

$$D_{Cu^{2+}} = -1.7075 \cdot 10^{-06} - 9.3671 \cdot 10^{-8}\,[Cu] + 1.4477 \cdot 10^{-7}\,[Ni] - 4.4559 \cdot 10^{-7}\,[As] + 3.6671 \cdot 10^{-8}\,[H_2SO_4] - 2.2352 \cdot 10^{-9}\,[Cu][Ni] + 5.2081 \cdot 10^{-9}\,[Cu][As] - 1.6089 \cdot 10^{-9}\,[Ni]\,T + 1.5728 \cdot 10^{-9}\,T\,[As] - 7.4759 \cdot 10^{-10}\,[H_2SO_4]\,T + 3.6587 \cdot 10^{-7}\,T\,, \quad (41)$$

where the concentrations are in g/dm^3, T in °C and $D_{Cu^{2+}}$ in cm^2/s.

According to summary of fit and ANOVA the model is valid. In addition, the condition number of the model is good (under 3). Compared to viscosity evaluations, R^2, Q^2 and especially model validity values are lower, but reproducibility value is higher.

6.4.2. $D_{Cu^{2+}}$ model 2

Diffusion coefficient model 2 was defined of data which was calculated using viscosity values calculated with equation (39) of this work. The $D_{Cu^{2+}}$ model with evaluations is presented in table 20 as well as in figures 75 and 76.

Table 20. Coefficients for diffusion coefficient model in which the values were calculated using viscosities from this work.

Scaled and centered coefficients		Std. Err.	P	Conf. int(±)	Coefficients	
Constant	1.25056E-05	4.71E-08	0	9.3E-08	**Constant**	1.14381E-05
Cu	-3.52980E-07	4.86E-08	1.60E-11	9.6E-08	**Cu**	-1.08814E-07
H_2SO_4	-2.84367E-07	4.75E-08	1.43E-08	9.4E-08	**H_2SO_4**	4.25335E-08
Ni	-4.61214E-07	4.77E-08	1.16E-17	9.4E-08	**Ni**	5.82142E-08
T	1.44278E-06	4.55E-08	0	9.0E-08	**T**	-3.42711E-08
As	-8.64107E-07	4.70E-08	0	9.3E-08	**As**	-5.16374E-07
Cu*H_2SO_4	-2.03517E-07	4.46E-08	1.02E-05	8.8E-08	**Cu*H_2SO_4**	-1.07337E-09
Cu*Ni	-1.49491E-07	4.39E-08	0.000843	8.7E-08	**Cu*Ni**	-2.22921E-09
Cu*T	2.25114E-07	4.52E-08	1.70E-06	8.9E-08	**Cu*T**	4.00118E-09
Cu*As	4.72059E-07	4.60E-08	3.05E-19	9.1E-08	**Cu*As**	4.73525E-09
T*As	3.01098E-07	4.53E-08	4.68E-10	8.9E-08	**T*As**	3.43980E-09

N = 168	Q^2 = 0.746	Cond. no. = 1.59
DF = 157	R^2 = 0.813	Y-miss = 111
Comp. = 3	R^2 Adj. = 0.773	RSD = 5.88E-07
		Conf. lev. = 0.95

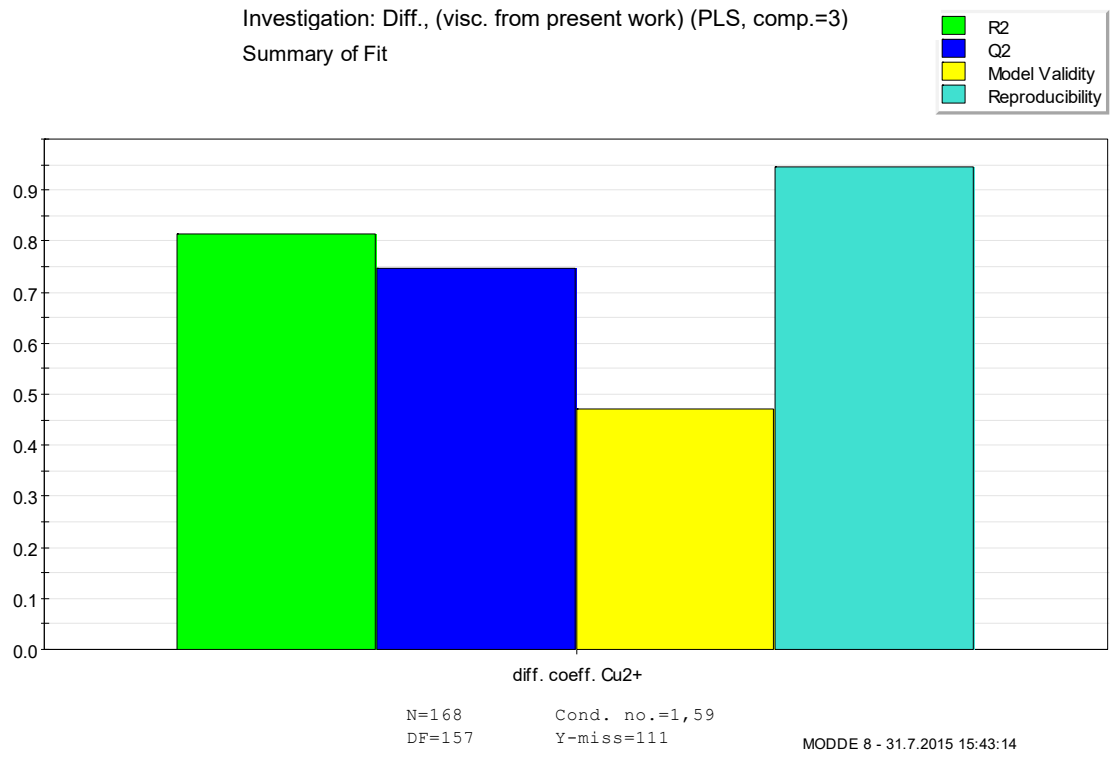

Figure 75. Summary of fit for diffusion coefficient model in which the values were calculated using viscosities from this work.

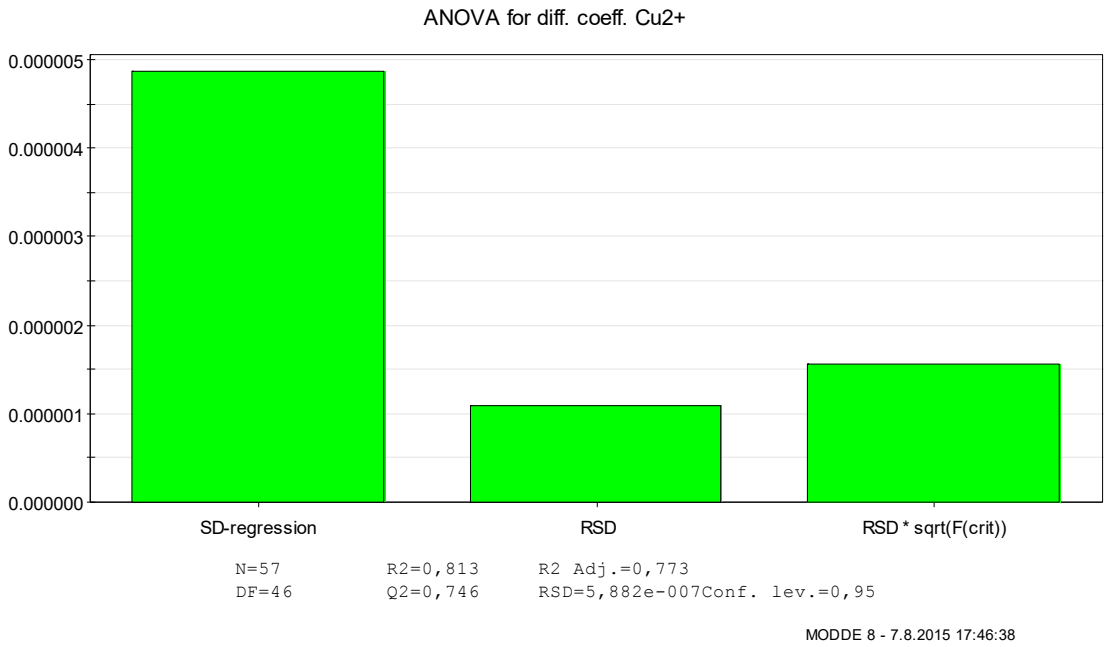

Figure 76. ANOVA plot for diffusion coefficient model in which the values were calculated using viscosities from this work.

The equation (42) for $D_{Cu^{2+}}$ was compiled according to unscaled coefficients (table 20). The coefficients differ from those of model 1, but the strongest combined effect is the same: Cu and As.

$$D_{Cu^{2+}} = 1.1438 \cdot 10^{-5} - 1.0881 \cdot 10^{-7}\,[Cu] + 5.8214 \cdot 10^{-8}\,[Ni] - 5.1637 \cdot 10^{-7}\,[As] + 4.2534 \cdot 10^{-8}\,[H_2SO_4] - 2.2292 \cdot 10^{-9}\,[Cu][Ni] + 4.7353 \cdot 10^{-9}\,[Cu][As] - 1.0734 \cdot 10^{-9}\,[Cu][H_2SO_4] + 4.0012 \cdot 10^{-9}\,[Cu]\,T + 3.4400 \cdot 10^{-9}\,T\,[As] - 3.4271 \cdot 10^{-8}\,T\,, \quad (42)$$

where the concentrations are in g/dm^3, T in °C and $D_{Cu^{2+}}$ in cm^2/s.

According to summary of fit and ANOVA the model is valid. In addition, the condition number of the model is good (under 3). Compared to model 1 evaluations, R^2, Q^2 and reproducibility value are lower, but model validity value is higher.

6.4.3. D_{Cu2+} model 3

Diffusion coefficient model 3 was defined of data which was calculated using viscosity values calculated with equation (40) of this work. The D_{Cu2+} model with evaluations is presented in table 21 and figures 77 and 78.

Table 21. Coefficients for diffusion coefficient model in which the values were calculated using normalized viscosities from this work.

Scaled and centered coefficients		**Std. Err.**	**P**	**Conf. int(±)**	**Coefficients**	
Constant	1.25515E-05	4.92E-08	0	9.71E-08	**Constant**	1.04934E-05
Cu	-3.89037E-07	5.05E-08	1.47E-12	9.98E-08	**Cu**	-1.15150E-07
H_2SO_4	-2.17849E-07	4.99E-08	2.31E-05	9.86E-08	**H_2SO_4**	3.95923E-08
Ni	-5.54092E-07	4.89E-08	4.71E-22	9.66E-08	**Ni**	1.18547E-07
T	1.41774E-06	4.64E-08	0	9.17E-08	**T**	-1.70835E-08
As	-8.46797E-07	4.88E-08	3.86E-38	9.64E-08	**As**	-3.98462E-07
Cu*H_2SO_4	-1.61829E-07	4.71E-08	0.000750	9.30E-08	**Cu*H_2SO_4**	-8.53504E-10
Cu*Ni	-2.23132E-07	4.65E-08	3.81E-06	9.20E-08	**Cu*Ni**	-3.32734E-09
Cu*T	2.00433E-07	4.61E-08	2.52E-05	9.12E-08	**Cu*T**	3.56248E-09
Cu*As	4.46079E-07	4.91E-08	4.62E-16	9.70E-08	**Cu*As**	4.47464E-09
H_2SO_4*As	-1.51817E-07	5.65E-08	0.00800	1.12E-07	**H_2SO_4*As**	-5.14646E-10
Ni*As	-1.54705E-07	4.73E-08	0.00132	9.34E-08	**Ni*As**	-1.48280E-09
T*As	3.13898E-07	4.62E-08	2.20E-10	9.13E-08	**T*As**	3.58602E-09

N = 168	Q^2 = 0.75	Cond. no. =	2.034
DF = 155	R^2 = 0.81	Y-miss =	111
Comp. = 3	R^2 Adj. = 0.758	RSD =	6.00E-07
		Conf. lev. =	0.95

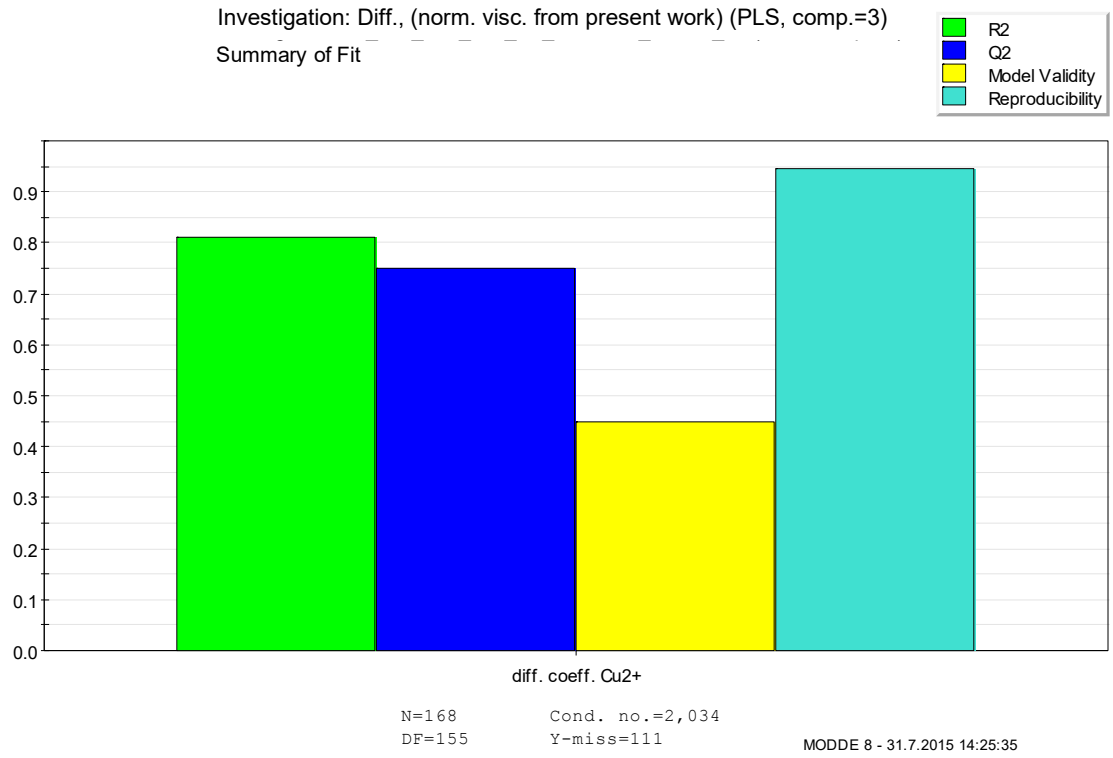

Figure 77. Summary of fit for diffusion coefficient model in which the values were calculated using normalized viscosities from this work.

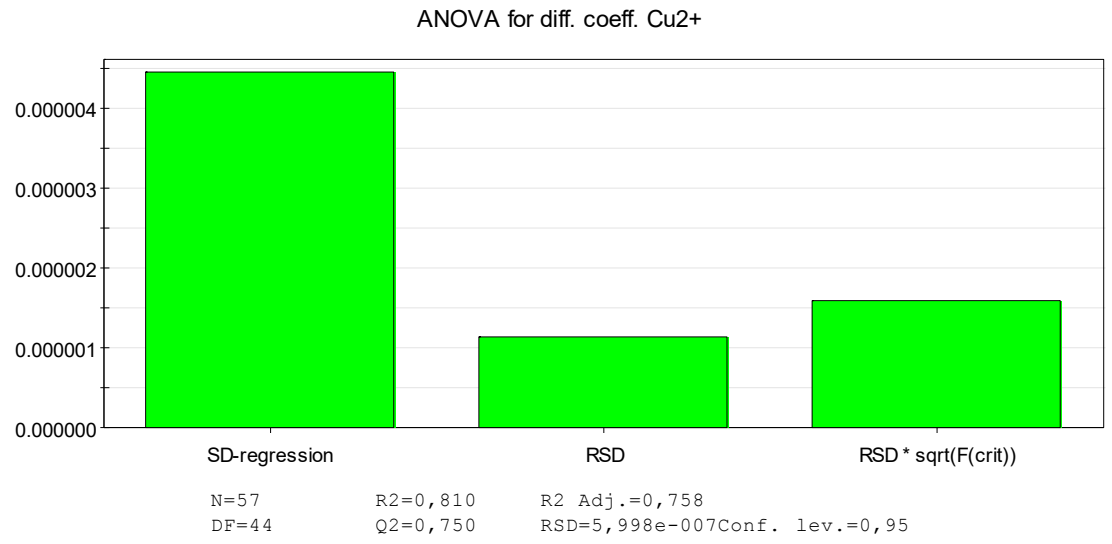

Figure 78. ANOVA plot for diffusion coefficient model in which the values were calculated using normalized viscosities from this work.

The equation (43) for $D_{Cu^{2+}}$ was compiled according to unscaled coefficients (table 21). Like in model 1 and 2, the strongest combined effect in model 3 is the same: Cu and As.

$$D_{Cu^{2+}} = 1.0493 \cdot 10^{-5} - 1.1515 \cdot 10^{-7}\,[Cu] + 1.1855 \cdot 10^{-7}\,[Ni] - 3.9846 \cdot 10^{-7}\,[As] + 3.9592 \cdot 10^{-8}\,[H_2SO_4] - 3.3273 \cdot 10^{-9}\,[Cu][Ni] + 4.4746 \cdot 10^{-9}\,[Cu][As] - 1.4830 \cdot 10^{-9}[Ni][As] - 5.1465 \cdot 10^{-10}\,[H_2SO_4][As] - 8.5350 \cdot 10^{-10}\,[Cu][H_2SO_4] + 3.5625 \cdot 10^{-9}\,[Cu]\,T + 3.5860 \cdot 10^{-9}\,T\,[As] - 1.7084 \cdot 10^{-8}\,T\,, \quad (43)$$

where the concentrations are in g/dm^3, T in °C and D_{Cu2+} in cm^2/s.

According to summary of fit and ANOVA the model 3 is valid. In addition, the condition number of the model is good (under 3). Compared to model 1 evaluations, R^2, Q^2 and reproducibility values are lower than in model 1, but model validity higher. Compared to model 2, R^2 value is lower, Q^2 value higher, model validity lower and reproducibility value approximately equal.

6.4.4. Comparisons

The D_{Cu2+} equations defined are quite complicated due to the interactions of the factors, and the effects of the factors are impossible to be directly seen in the equations. The effects of As and Ni are determined with model 1, which was regarded as the best of these D_{Cu2+} models, in figure 79 at 65 °C. In figure 80 the effects of As are defined with models 1–3 at 60 °C. At that temperature, the difference between the models was moderate. More difference was detected at 50 and 70 C°. According to these determinations, As and Ni decrease the diffusion coefficient. The effect of Ni was already known [10] but the effect of As was not, though the hypothesis was that As lowers D_{Cu2+} values.

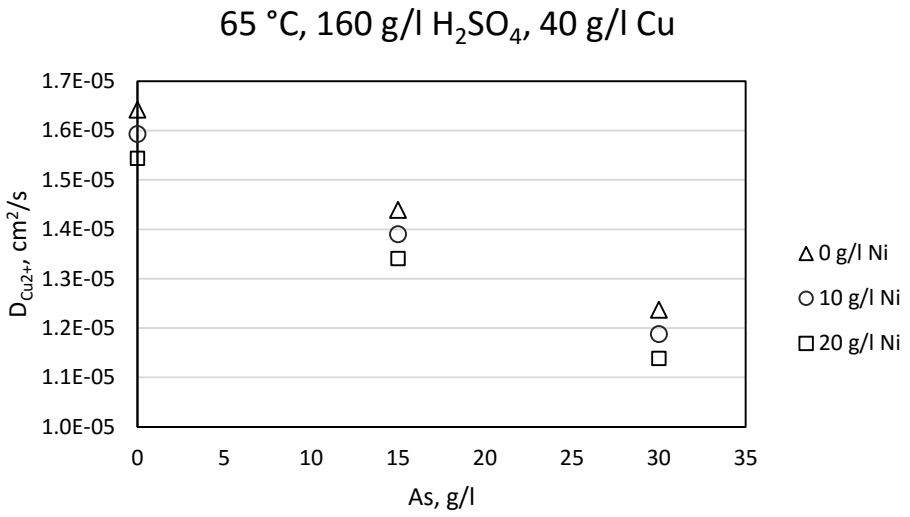

Figure 79. Effects of As and Ni on D_{Cu2+} defined with model 1.

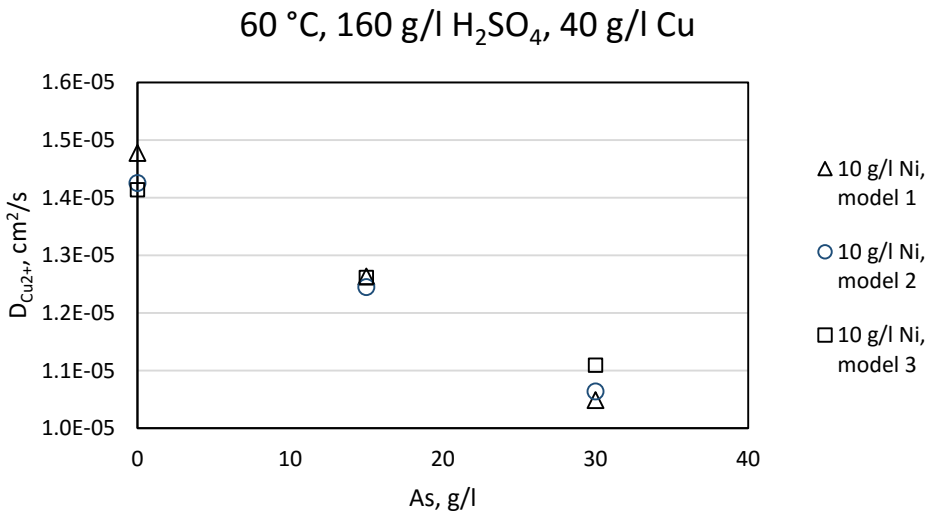

Figure 80. Effects of As on D_{Cu2+} defined with models 1–3.

The effects of Cu and H_2SO_4 on D_{Cu2+} are presented in figures 81 and 82 with comparisons to results from [8]. Figure 83 shows the effects of temperature with comparison to previous results from, [8], [9] and [10]. The results defined with model 1 from this work are in good agreement with previous research work when taken into account the fact that the diffusion coefficients commonly vary quite significantly depending on the measurer [38, 39]. Moats et al. [5] used Levich equation (25) defining their diffusion coefficient equation. As seen in figure 83, the values measured and calculated with Levich equation were closer to those values than the equivalent values defined with Koutecký-Levich equation (26). The values

obtained using Levich equation were lower than those obtained using Koutecký-Levich equation, as Quickenden and Xu [39] stated.

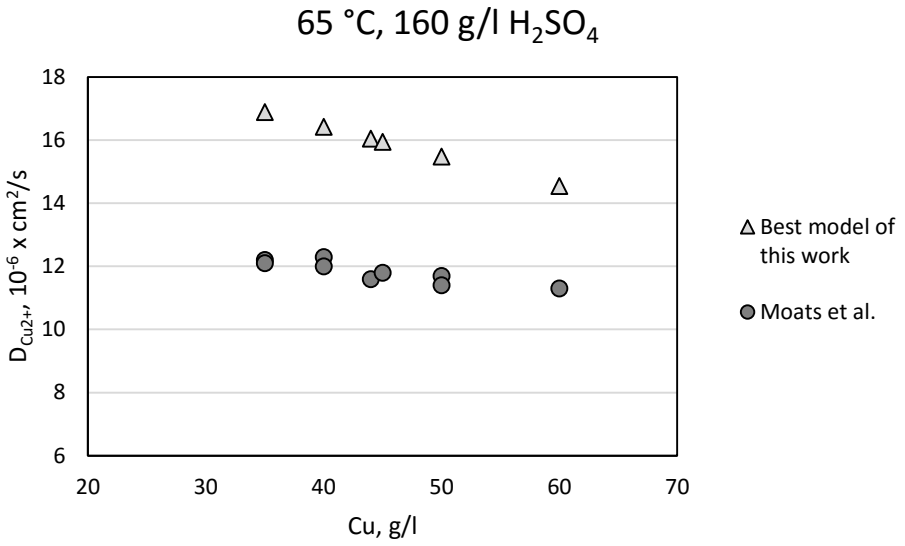

Figure 81. Effect of copper concentration at 65 °C according to this work and [8].

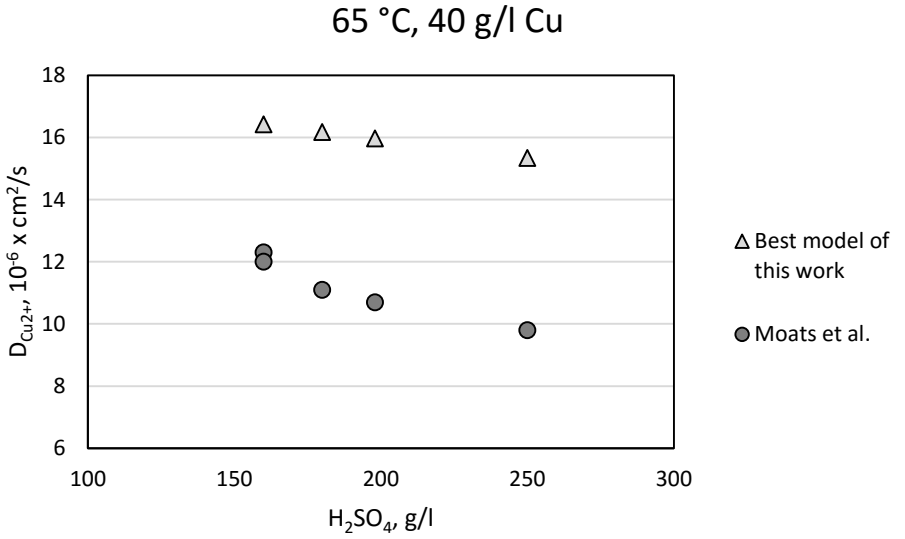

Figure 82. Effect of sulfuric acid concentration at 65 °C according to this work and [8].

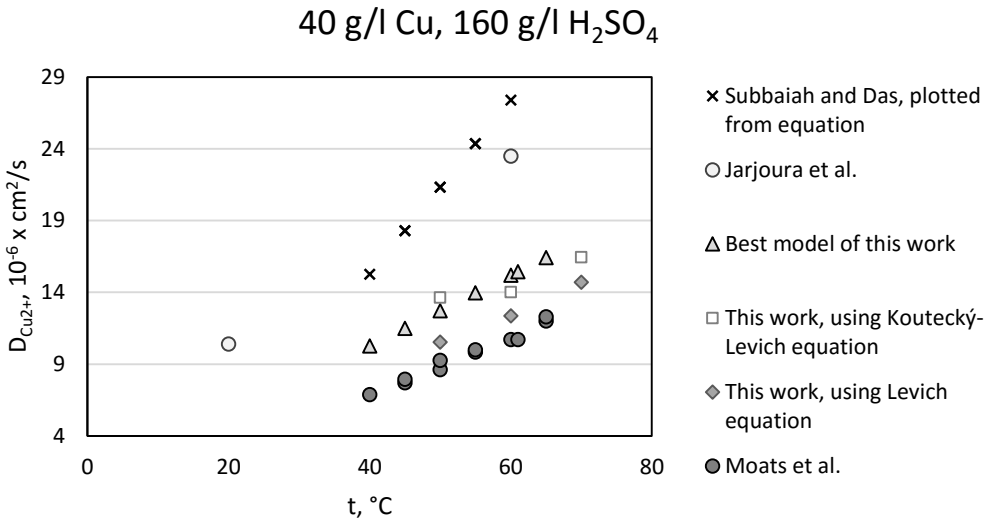

Figure 83. Effect of temperature according to this work as well as [8], [9] and [10].

6.5. Accuracy

The measurements were carried out as accurately as possible. Some inaccuracies, however, occurred in electrolyte concentrations, measurements and other determinations. The inaccuracies of electrolyte concentrations were mostly due to evaporation during measurements, slightly too high temperature in preparing the electrolytes and tolerances for the concentrations of elements in the chemicals. However, the impurities in the technical grade chemicals used not only caused inaccuracy but also made the electrolytes more like the real industrial electrolytes.

Some minor error was caused by inaccuracies in volumes of the pipettes and accuracy limitations of the weighting scale. The error due to too high temperature was ignored since it was regarded as insignificant, and calculating the correct volumes would have taken too much time. The room temperature was generally 24 °C, while the pipettes and measuring bottles were calibrated at 20 °C.

The effects of evaporation or the amount of water loss during the measurements could not be calculated, but they were assumed to be slight, since the test cells were kept covered as tightly as possible, and the holes in lids plugged. Basically, the measurements were carried out inserting a sensor through a hole of the lid to the electrolyte. Thus some evaporation occurred through the holes during the measurements, especially at 70 °C, if the hole around

the sensor could not be sealed. Nevertheless, the effects of evaporation were taken into account by MODDE as it calculated the error limits, because at least one of the reproduced measurements was carries out using once or twice measured and thus heated electrolytes.

The inaccuracies in measurements were lowest in conductivity measurements, according to high R^2 values, since the meter and its sensor, also the integrated temperature sensor, functioned well. The functioning of viscosity and density meter was not that good. The meter seemed to function unstably, which caused error. In addition, the temperature sensor in the probe was slow, which also interfered the measurements. Temperature affected significantly the measured values. The inaccuracies in viscosity and density measurements could be seen in the R^2 values of viscosity models compared to the equivalent values of conductivity. Nevertheless, the accuracy of density values was good, partly due to normalization and partly due to less fluctuation during measurements in density values than in viscosity values.

The models of the diffusion coefficients of Cu^{2+} had the lowest R^2 values of the models constructed in this work, which indicates that either in rotating disc electrode measurements, limiting current density defining or calculating diffusion coefficient is inaccuracies. Moreover, it is possible that in all these phases occurred inaccuracies, which together caused lower R^2 values compared to other models. Though these worst R^2 values were still over 0.8, which is quite good.

If the potentiostat and RDE apparat are assumed to have functioned accurately, the most probable causes of these moderate inaccuracies in D_{Cu2+} defining were variation of surface quality of the rotating disc electrode as well as difficulties in defining the limiting current densities from the current density potential curves. In some cases it was difficult to define the most horizontal and linear part of the curve due to random noise or interference in the curves. The surface of the rotating disc electrode was finished manually and only with emery paper. If the surfaces were polished and using for example turning machine to make the surface straight, the measurements might have been slightly more accurate. Polishing of the rotating disc surface is a usual procedure, which is used for example in [39] and [10], before the measurement to obtain smooth surface to be able to accurately define the area of it.

In RDE measurements, the temperature was measured using a thermometer, which was not as accurate as, for instance, the temperature sensor in the conductivity meter. That might also have had a minor effect on accuracy.

The calculating of D_{Cu2+} could be assumed to have been quite accurate, especially when using Koutecký-Levich equation (26) as well as density and viscosity equations from Price and Davenport [7]. Moats et al. [8] as well as Quickenden and Xu [39] had also used Price and Davenport's density and viscosity equations in their D_{Cu2+} definitions, but they used for some reason equivalent equations from the former research [6]. Although Quickenden and Xu [39] recommended to use mixed-control Newman equation (31) in calculating D_{Cu2+} the simplier Koutecký-Levich equation (26) was chosen to be used in this research. Levich equation (25) was used in calculating D_{Cu2+} only for comparisons, not for constructing D_{Cu2+} models. Moats et al. [8] used Levich equation which is according to [39] and [38] significantly less accurate than Koutecký-Levich equation.

7 Conclusions

Conductivity, density, viscosity and the diffusion coefficient of cupric ion were measured, and the results were in line with previous research, except for viscosity. Conductivity and limiting current densities were able to be measured reliably, and thus the models from the conductivity results were constructed directly. The best model of the diffusion coefficient of Cu^{2+} was constructed from values calculated of limiting current density results using Koutecký-Levich equation and viscosity values from [7]. Furthermore, density results containing error were able to be corrected rather well by normalization, and used in modelling. Thus, the previously reported effects [7–11] of composition and temperature on conductivity, density and the diffusion coefficient of Cu^{2+} were mainly verified, except for the accurate effects of arsenic. According to this work, it seems to decrease conductivity more and increase density more than according to literature. In addition, the effect of arsenic on the diffusion coefficient of Cu^{2+}, which was not known was detected to be decreasing it as expected.

Viscosity values obtained were noticed to contain error, since the functioning of the meter or its probe was unstable, and one viscosity value at high temperature calculated with the viscosity model constructed was lower than that of water [45]. The reason for unstable functioning remained unclear, but the surface of the probe was suspected to be covered with thin layer of deposit or debris. Nevertheless, the density values could be corrected. The suitable normalization procedure for viscosity values was, however, not found, and the normalization calculated using dynamic viscosity and normalized density values was not efficient enough to correct the viscosity values. The probe could work better at higher temperatures when the possible precipitation of solid matter of the electrolyte on the surfaces might be lower.

The suitability of the viscosity and density meter for measuring copper electrolytes in electrorefining conditions still remained uncertain. At least at temperatures 50–59 °C the meter functioned unstably, and the temperature sensor of the probe was slow for these kind of measurements. However, the temperatures of the real electrolytes are commonly higher than 59 °C [15], thus, further research is needed to survey the suitability.

The models constructed were all valid and had high correlation coefficients, even the viscosity models. In addition, the reproducibility was good, and the models did not have lack

of fit. Combined effects were also detected, except in the viscosity model, but the effects were minor. However, a valid model does not necessarily guarantee the suitability of the models for defining accurate values for these physico-chemical properties. As can be noticed comparing the conductivity models 1 and 2, the models can vary even, when the same data is used in modelling. Thus, it is probable that even more accurate models could be compiled from the test results of this work using different kind of modelling, since the modelling used in this work was quite simple. Nevertheless, the models for conductivity, the diffusion coefficient of Cu^{2+} and density are regarded as fairly good, except for the diffusion coefficient models constructed using viscosity values from this work in calculations.

The best models determined for conductivity, density and the diffusion coefficient of cupric ion in this work were respectively

$$\log_{10}(\kappa) = 2.17388 - 0.0023479\,[\mathrm{Cu}] - 0.0027733\,[\mathrm{Ni}] - 0.00073729\,[\mathrm{As}] + 0.0037764\,[\mathrm{H_2SO_4}] - 1.0649 \cdot 10^{-5}\,[\mathrm{H_2SO_4}][\mathrm{As}] + 2.1627 \cdot 10^{-5}\,\mathrm{T}\,[\mathrm{As}] + 8.8019 \cdot 10^{-6}\,[\mathrm{H_2SO_4}]\,\mathrm{T} + 0.0051846\,\mathrm{T} - 6.9222 \cdot 10^{-6}\,[\mathrm{H_2SO_4}]^2 - 3.2506 \cdot 10^{-5}\,\mathrm{T}^2\,,$$

$$\rho = 1.0853 + 0.001134\,[\mathrm{Cu}] + 0.002613\,[\mathrm{Ni}] + 0.004232\,[\mathrm{As}] + 0.0001769\,[\mathrm{H_2SO_4}] - 1.732 \cdot 10^{-5}\,[\mathrm{Ni}][\mathrm{As}] + 6.312 \cdot 10^{-6}\,[\mathrm{Cu}][\mathrm{H_2SO_4}] - 0.0005388\,\mathrm{T} \quad \text{and}$$

$$D_{Cu^{2+}} = -1.7075 \cdot 10^{-06} - 9.3671 \cdot 10^{-8}\,[\mathrm{Cu}] + 1.4477 \cdot 10^{-7}\,[\mathrm{Ni}] - 4.4559 \cdot 10^{-7}\,[\mathrm{As}] + 3.6671 \cdot 10^{-8}\,[\mathrm{H_2SO_4}] - 2.2352 \cdot 10^{-9}\,[\mathrm{Cu}][\mathrm{Ni}] + 5.2081 \cdot 10^{-9}\,[\mathrm{Cu}][\mathrm{As}] - 1.6089 \cdot 10^{-9}\,[\mathrm{Ni}]\,\mathrm{T} + 1.5728 \cdot 10^{-9}\,\mathrm{T}\,[\mathrm{As}] - 7.4759 \cdot 10^{-10}\,[\mathrm{H_2SO_4}]\,\mathrm{T} + 3.6587 \cdot 10^{-7}\,\mathrm{T}\,,$$

where the concentrations are in g/dm^3, T is in °C, κ in mS/cm, ρ in g/cm^3, and D_{Cu2+} in cm^2/s.

The viscosity models were not as accurate and reliable as the other models due to the unstable functioning of the meter and too narrow temperature range during the measurements. The viscosity models were presented and evaluated in section 6.3.

8 Summary

The physico-chemical properties of the copper electrolyte affect significantly the electrorefining process and thus the yield of cathodic copper [6, 7] as well as the quality of the deposit on cathodes [30]. The best yield of copper can be obtained keeping the viscosity low and electrical conductivity [6] as well as the diffusion coefficient high [8]. Four typical physico-chemical properties are conductivity, density, viscosity and the diffusion coefficient of cupric ion (Cu^{2+}) [6–12]. These properties of the copper electrolyte are influenced by composition and temperature.

The physico-chemical properties of copper electrolytes were measured, and the results were in line with previous research, except for viscosity and the accurate effects of arsenic. According to this work, arsenic seems to decrease conductivity more and increase density more than according to literature [7, 9]. The best equations for conductivity, density and diffusion coefficient obtained in this work are respectively

$$\log_{10}(\kappa) = 2.17388 - 0.0023479\,[\mathrm{Cu}] - 0.0027733\,[\mathrm{Ni}] - 0.00073729\,[\mathrm{As}] + 0.0037764\,[\mathrm{H_2SO_4}] - 1.0649 \cdot 10^{-5}\,[\mathrm{H_2SO_4}][\mathrm{As}] + 2.1627 \cdot 10^{-5}\,\mathrm{T}\,[\mathrm{As}] + 8.8019 \cdot 10^{-6}\,[\mathrm{H_2SO_4}]\,\mathrm{T} + 0.0051846\,\mathrm{T} - 6.9222 \cdot 10^{-6}\,[\mathrm{H_2SO_4}]^2 - 3.2506 \cdot 10^{-5}\,\mathrm{T}^2\,,$$

$$\rho = 1.0853 + 0.001134\,[\mathrm{Cu}] + 0.002613\,[\mathrm{Ni}] + 0.004232\,[\mathrm{As}] + 0.0001769\,[\mathrm{H_2SO_4}] - 1.732 \cdot 10^{-5}\,[\mathrm{Ni}][\mathrm{As}] + 6.312 \cdot 10^{-6}\,[\mathrm{Cu}][\mathrm{H_2SO_4}] - 0.0005388\,\mathrm{T}$$ and

$$\mathrm{D_{Cu^{2+}}} = -1.7075 \cdot 10^{-06} - 9.3671 \cdot 10^{-8}\,[\mathrm{Cu}] + 1.4477 \cdot 10^{-7}\,[\mathrm{Ni}] - 4.4559 \cdot 10^{-7}\,[\mathrm{As}] + 3.6671 \cdot 10^{-8}\,[\mathrm{H_2SO_4}] - 2.2352 \cdot 10^{-9}\,[\mathrm{Cu}][\mathrm{Ni}] + 5.2081 \cdot 10^{-9}\,[\mathrm{Cu}][\mathrm{As}] - 1.6089 \cdot 10^{-9}\,[\mathrm{Ni}]\,\mathrm{T} + 1.5728 \cdot 10^{-9}\,\mathrm{T}\,[\mathrm{As}] - 7.4759 \cdot 10^{-10}\,[\mathrm{H_2SO_4}]\,\mathrm{T} + 3.6587 \cdot 10^{-7}\,\mathrm{T}\,.$$

Neither of the viscosity equations was quite reliable though the models were valid. The suitable normalization procedure for viscosity values was not found, and normalization calculated using dynamic viscosity and normalized density values was not efficient enough to correct the viscosity values.

Viscosities and densities were not measured at higher temperatures 60, 65 and 70 °C. These measurements should be conducted after the meter recalibration, since the viscosity model defined in this work was not reliable, especially not at higher temperatures, though densities were able to be defined rather reliably due to normalization. Thus, the suitability or the meter on measuring copper electrolytes in electrorefining conditions and the reason for unstable functioning of the probe remained unclear. Therefore, more tests are required to find out, whether the meter would be suitable for measuring density and viscosity of copper electrolytes at higher temperatures.

The modeling in this work was carried out with quite simple modeling tools. Thus, the data acquired in this work could be used in making more accurate models with further data analysis.

References

[1] Davenport, W.G., King, M., Schlesinger, M. and Biswas A.K., "Overview," in *Extractive Metallurgy of Copper*, 4th Edition, ISBN: 0-08-044029-0, Elsevier Science Ltd., 2002.

[2] Wraith, A.E., Mackey, P.J., Jones, R.P., "Origins of Electrorefining: Birth of The Technology and The World's First Commercial Electrofinery," Proceedings of Copper 2013, Santiago, Chile, 2013.

[3] Moats, M.S. and Hiskey, J. B., "How Anodes Passivate in Copper Electrorefining," in *The Copper 2010-Proceedings, Volume 4, Electrowinning and -refining*, ed. GDMB, ISBN 978-3-940276-28-5, 2010.

[4] Davenport, W.G., King, M., Schlesinger, M., Biswas, A.K. and Robinson, T., "Electrolytic Refining," in *Extractive Metallurgy of Copper*, 4th Edition, ISBN: 0-08-044029-0, Elsevier Science Ltd., pp. 265–288, 2002.

[5] Moats, M., Davenport, W., Demetrio, S., Robinson, T. and Karcas, G., "Electrolytic Copper Refining – 2007 World Tankhouse Operating Data," in *Copper Electrorefining and Electrowinning*, Copper 2007 – Cobre 2007 Conference, ed. Houlachi, G.E., Edwards, J.D. and Robinson, T.G., ISBN: 1-894475-75-5, Canadian Institute of Mining, Metallurgy and Petroleum, pp. 202–241 , 2007.

[6] Price, D.C. and Davenport, W.G., "Densities, Electrical Conductivities and Viscosities of $CuSO_4/H_2SO_4$ Solutions in the Range of Modern Electrorefining and Electrowinning Electrolytes," *Metallurgical Transactions B*, vol. 11B, pp. 159–163, March 1980.

[7] Price, D.C. and Davenport, W.G., "Physico-Chemical Properties of Copper Electrorefining and Electrowinning Electrolytes," *Metallurgical Transactions B*, vol. 12B, pp. 639–643, December 1981.

[8] Moats, M.S., Hiskey, J.B. and Collins, D.W., "The effect of copper, acid, and temperature on the diffusion coefficient of cupric ions in simulated electrorefining electrolytes," *Hydrometallurgy*, vol. 56, pp. 255–268, 2000.

[9] Subbaiah, T. and Das, S.C., "Physico-Chemical Properties of Copper Electrolytes," *Metallurgical Transactions B*, vol. 20B, pp. 375–380, June 1989.

[10] Jarjoura, G., Muinonen, M. and Kipouros, G.J., "Physicochemical properties of nickel copper sulfate solutions," *Canadian Metallurgical Quarterly*, vol 42, No 3 pp. 281–288, 2003.

[11] Kern, E.F. and Chang, M.Y., "Conductivity of Copper Refining Electrolytes," Meeting of the American Electrochemical Society, held in Baltimore, April 28, 1922.

[12] Skowronski, S. and Reinoso E.A., "The specific Resistivity of Copper Refining Electrolytes and Method of Calculation," Meeting of the American Electrochemical Society, held in Philadelphia, Pa., April 30, 1927.

[13] Hinatsu, T. and Foulkes, F.R., "Diffusion Coefficients of Copper (II) in Aqueous Cupric Sulfate-Sulfuric Acid Solutions," *Journal of Electrochemical Society*, vol. 136, No 1, pp. 125–132, January 1989.

[14] Davenport, W. G., King, M., Schlesinger, M. and Sole, K.C. *Extractive Metallurgy of Copper*. 5th Edition, ISBN 0-08-096789-9, Oxford: Pergamon. 2011.

[15] Aromaa, J., "Electrochemical Engineering," in *Encyclopedia of Electrochemistry*, Wiley-VHC Verlag GmbH & Co. KGaA, 2007, pp. 161–196.

[16] Laitinen, I., "Modelling, Simulation and Optimization of a Copper Electrolysis Cell Group," PhD thesis, Tampere University of Technology, publication 828, ISSN 1459-2045. 2009.

[17] Ilkhchi, M.O., Yoozbashizadeh, H., Safarzadeh, M.S., "The effect of additives on anode passivation in electrorefining of copper," *Chemical Engineering and Processing*, vol. 46, pp. 757–763, Elsevier B.V., 2007.

[18] Gu, Z.H., Chen, J., Fahidy, T.Z., "A study of anodic slime behaviour in the electrorefining of copper" *Hydrometallurgy*, vol 37, pp. 149–167, Elsevier Science B.V., 1995.

[19] Wang, X., Chen, Q., Yin, Z., Wang, M., Xiao, B. and Zhang, F., "Homogeneous precipitation of As, Sb and Bi impurities in copper electrolyte during electrorefining," *Hydrometallurgy,* vol. 105, pp. 355–358. ISSN: 0304-386X, 2011.

[20] Atkins, P., De Paula, J., *Physical chemistry*, 8th edition, Oxford University Press, ISBN-10: 0198700725, ISBN-13: 978-0198700722, 2006.

[21] Gupta, C.G., *Chemical Metallurgy: Principles and Practice*, WILEY-VCH Verlag GmbH & Co. KGaA, Weinheim, ISBN: 3-527-30376-6, 2003

[22] Schab, D. and Hein, K., "Problems of Anodic and Cathodic Mass Transfer in Copper Refining Electrolysis with Increased Current Density," *Canadian Institute of Mining and Metallurgy*, Vol. 31, No. 3. pp. 173–179, 1992.

[23] Bard, A.J. and Faulkner, L.R., "Methods Involving Forced Convection – Hydrodynamic Methods," in *Electrochemical Methods: Fundamentals and Applications*, 2nd edition, ISBN: 0-471-04372-9, John Wiley & Sons, INC, pp. 331–367, 2001.

[24] Dini, J.W. and Snyder, D.D., "Electrodeposition of copper," in *Modern Electroplating*, Fifth Edition, Ed. Schlesinger, M. and Paunovic, M., John Wiley & Sons, Inc., 2010.

[25] Aromaa, J., *Materiaalien sähkökemia*, Helsinki University of Technology Publications in Materials Science and Metallurgy, Teknillisen korkeakoulun materiaalitekniikan ja metallurgian julkaisuja, TKK-MK-102, Espoo, 2000.

[26] Milchev, A., Zapryanova, T., "Nucleation and growth of copper under combined charge transfer and diffusion limitations: Part I," *Electrochimica Acta*, vol 51, pp. 2926–2933, Elsevier Ltd., 2006.

[27] Plieth, W., "Electrocrystallization—factors influencing structure," *Journal of Solid State Electrochemistry*, vol. 15, pp. 1417–1423, 2011.

[28] Winand, R., "Contribution to the study of copper electrocrystallization in view of industrial applications – submicroscopic and macroscopic considerations," *Electrochimica Acta*, vol 43, Nos 19–20, pp. 2925–2932, Elsevier Science Ltd., 1998.

[29] Aromaa, J., Kekki, A., Stefanova, A. and Forsén, O., "Copper nucleation and growth patterns on stainless steel cathode blanks in copper electrorefining," *Journal of Solid State Electrochem*, vol. 16, pp. 3529–3537, Springer-Verlag Berlin Heidelberg, 2012.

[30] Winand, R. 1992, "Electrocrystallization-theory and applications," *Hydrometallurgy,* vol. 29, no. 1, pp. 567–598.

[31] Fischer, H., "Elektrolytische Abscheidung und Elektrokristallisation von Metallen," Berlin, Springer, 1954.

[32] Winand, R., "Electrodeposition of metals and alloys—new results and perspectives," *Electrochimica Acta*, vol. 39, Issues 8–9, pp. 1091–1105, ISSN: 00134686, June 1994.

[33] Winand, R., Van Ham, P., Colin, R. and Milojevic, D., "An Attempt to Quantify Electrodeposit Metallographic Growth Structures," *Journal of The Electrochemical Society*, vol. 144, No.2, February 1997, pp. 428–436, 1997.

[34] Zhang, X., Hu, Y., Peng, X., Yue, W., "Conductivities of Several Ternary Electrolyte Solutions and Their Binary Subsystems at 293.15, 298.15, and 303.15 K," *Journal of Solution Chemistry*, vol. 38, Issue 10, pp. 1295–1306, 2009.

[35] Hu, Y., Zhang, X., Li, J. and Liang, Q., "Semi-ideal Solution Theory. Extension to Conductivity of Mixed Electrolyte Solutions," *Journal of Physical Chemistry B*, Vol. 112, No 48, pp. 15376–15381, 2008.

[36] Claessens, P., Ph.D. Thesis, Université de Louvain, 1967.

[37] Bard, A.J. and Faulkner, L.R., *Electrochemical Methods: Fundamentals and Applications*, 1st edition, ISBN 0-471-05542-5, John Wiley & Sons, pp. 281–298, 1980.

[38] Quickenden, T.I. and Jiang, X., "The Diffusion Coefficient of Copper Sulfate in Aqueous Solution," *Electrochimica Acta*, vol. 29, No. 6, pp. 693–700, 1984.

[39] Quickenden, T.I. and Xu, Q., "Toward a Reliable Value for the Diffusion Coefficient of Cupric Ion in Aqueous Solution," *Journal of Electrochemical Society*, vol. 143, No. 4, pp. 1248–1253, April 1996.

[40] Claessens, P., Feneau, Cl., Breckpot, R., "Étude viscosimétrique de solutions électrolytiques a base de sulfate de cuivre," *Bulletin des Sociétés Chimiques Belges*, 77 (1968) 213–226, 1968.

[41] Hinatsu, T. and Foulkes, F.R., "Electrochemical Kinetic Parameters for the Cathodic Deposition of Copper from Dilute Aqueous Acid Sulfate Solutions," *The Canadian Journal of Chemical Engineering*, vol. 69, April, 1991.

[42] Eriksson, L., Johansson, E., Kettaneh-Wold, N., Wikström, C., and Wold, S., *Design of Experiments: Principles and Applications*, MKS Umetrics AB, ISBN-10: 91-973730-4-4, ISBN-13: 978-91-973730-4-3, 2008

[43] MODDE 8, software's info wizard Analysis Advisor, MKS Umetrics AB.

[44] Seisko, S., "Autoclave leaching of copper electrorefining anode slimes," master's thesis, Aalto University, 2015.

[45] Lobo, V.M.M., Quaresma, J.L., *Physical sciences data 41, Handbook of electrolyte solutions, Part B*, p. 2232–2235, Elsevier, ISBN 0-444-98847-5 (Vol. 41), 1989.

Table A1. Conductivity results.

Sample		N1	N2	N5	N8	N10	N12	N14	N15	N17	N19	N20
Cu	g/l	40	50	50	50	40	60	50	60	50	40	50
H_2SO_4		160	160	180	200	220	220	160	160	180	200	200
As		0	0	0	0	0	0	0	0	0	0	0
Ni		0	0	0	0	0	0	10	10	10	10	10
50 °C	κ, mS/cm	575.20	540.20	593.60	639.60	714.20	648.33	515.38	480.60	554.80	631.40	598.00
55 °C		595.80	560.67	616.80	664.20	743.25	675.15	534.14	499.25	576.00	654.40	622.20
60 °C		613.60	580.00	639.60	689.80	772.00	699.84	551.14	515.80	596.00	680.60	647.00
65 °C		631.80	596.80	658.60	712.40	800.00	725.95	568.23	530.60	615.20	703.00	667.75
70 °C		648.40	613.67	676.40	732.80	824.00	749.41	582.28	543.60	632.40	723.80	688.60

Sample		N23	N25	N27	N30	N31	N33x	N35	N17/37	N17/38	N17/39	N37
Cu	g/l	50	40	60	60	40	60	50	50	50	50	40
H_2SO_4		220	160	160	180	200	200	220	180	180	180	160
As		0	0	0	0	0	0	0	0	0	0	15
Ni		10	20	20	20	20	20	20	10	10	10	0
50 °C	κ, mS/cm	631.20	507.40	453.00	490.00	592.20	529.00	589.00				553.60
55 °C		656.80	524.60	470.00	510.80	615.00	552.20	617.20				572.60
60 °C		682.60	542.20	487.00	530.40	638.60	574.60	642.20	596.40	593.80	597.40	595.00
65 °C		708.20	557.00	501.60	548.80	660.00	594.40	665.75				612.20
70 °C		730.40	570.60	515.00	565.00	679.80	615.40	688.40				630.60

Sample		N38x	N46	N53	N60	N66	N72	N73	N78	N80	N87	N89
Cu	g/l	50	40	50	60	60	60	40	60	50	60	50
H_2SO_4		160	220	180	220	180	220	160	180	200	160	180
As		15	15	15	15	15	15	30	30	30	30	30
Ni		0	0	10	10	20	20	0	0	0	10	10
50 °C	κ, mS/cm	524.25	673.40	530.50	559.00	464.40	517.00	526.00	501.60	561.80	435.20	499.20
55 °C		544.60	701.20	552.50	584.80	485.40	543.20	548.60	524.80	588.20	455.60	522.00
60 °C		564.60	731.00	576.00	611.40	506.00	567.00	569.20	548.60	613.00	474.40	544.80
65 °C		584.20	758.40	595.60	635.60	525.20	592.40	590.00	570.60	637.60	493.20	566.40
70 °C		601.75	785.60	613.50	658.40	542.80	614.20	609.00	591.00	659.60	510.60	586.40

Sample		N97	N100	N108x	N53/109	N53/110	N53/111
Cu	g/l	40	40	60	50	50	50
H_2SO_4		160	180	220	180	180	180
As		30	30	30	15	15	15
Ni		20	20	20	10	10	10
50 °C	κ, mS/cm	457.80	490.80	480.20			
55 °C		478.40	513.80	502.20			
60 °C		497.20	535.20	528.40	574.00	573.20	576.00
65 °C		515.80	556.80	552.60			
70 °C		533.40	577.00	575.80			

Table A2. Density and kinematic viscosity results.

			N1	N2	N5	N8	N10	N12x	N14	N15	N17	N19	N20	N23x
Sample	Cu	g/l	40	50	50	50	40	60	50	60	50	40	50	50
	H_2SO_4		160	160	180	200	220	220	160	160	180	200	200	220
	As		0	0	0	0	0	0	0	0	0	0	0	0
	Ni		0	0	0	0	0	0	10	10	10	10	10	10
Normalized values	50 °C	ρ, g/cm^3	1.1733	1.1982	1.2091	1.2174	1.2064	1.2525	1.2236	1.2422	1.2317	1.2202	1.2449	1.2544
	55 °C		1.1705	1.1950	1.2058	1.2142	1.2034	1.2491	1.2204	1.2389	1.2288	1.2165	1.2422	1.2509
	59 °C		1.1681	1.1923	1.2027	1.2116	1.2009	1.2465	1.2181	1.2369	1.2253	1.2123	1.2396	1.2478
	50 °C	ν, mm^2/s	0.896	0.972	0.964	0.951	1.279	1.307	1.311	1.342	1.100	1.005	1.250	1.092
	55 °C		0.842	0.857	0.906	0.849	0.964	1.244	0.937	1.147	1.036	0.945	1.124	1.007
	59 °C		0.769	0.819	0.847	0.812	0.892	1.105	0.905	1.022	0.932	0.821	1.065	0.972
Original values	50 °C	ν, mm^2/s	0.882	0.959	0.951	0.938	1.261	1.282	1.295	1.322	1.083	0.989	1.228	1.071
	55 °C		0.829	0.846	0.894	0.837	0.950	1.220	0.925	1.130	1.020	0.929	1.104	0.988
	59 °C		0.757	0.808	0.836	0.800	0.879	1.084	0.894	1.007	0.917	0.807	1.046	0.953

			N25	N27	N30	N31	N33	N35	N37	N38x	N53	N60	N72	N73
Sample	Cu	g/l	40	60	60	40	60	50	40	50	50	60	60	40
	H_2SO_4		160	160	180	200	200	220	160	160	180	220	220	160
	As		0	0	0	0	0	0	15	15	15	15	15	30
	Ni		20	20	20	20	20	20	0	0	10	10	20	0
Normalized values	50 °C	ρ, g/cm^3	1.2242	1.2660	1.2797	1.2454	1.2901	1.2775	1.2386	1.2632	1.2979	1.3417	1.3637	1.3035
	55 °C		1.2205	1.2622	1.2757	1.2426	1.2860	1.2738	1.2353	1.2600	1.2941	1.3382	1.3600	1.2993
	59 °C		1.2171	1.2595	1.2732	1.2398	1.2831	1.2716	1.2325	1.2572	1.2910	1.3353	1.3571	1.2963
	50 °C	ν, mm^2/s	0.992	1.370	1.432	1.209	1.316	1.282	0.964	1.108	1.300	1.412	1.564	1.103
	55 °C		0.895	1.056	1.264	0.965	1.182	1.213	0.891	1.012	1.214	1.306	1.380	0.994
	59 °C		0.836	0.999	1.038	0.849	1.056	1.090	0.843	0.991	1.105	1.217	1.284	0.902
Original values	50 °C	ν, mm^2/s	0.974	1.347	1.409	1.187	1.292	1.260	0.946	1.088	1.277	1.388	1.537	1.083
	55 °C		0.878	1.038	1.243	0.948	1.161	1.192	0.874	0.994	1.192	1.283	1.356	0.976
	59 °C		0.821	0.982	1.021	0.834	1.037	1.072	0.827	0.973	1.085	1.195	1.261	0.886

			N108x	N53/109	N53/110
Sample	Cu	g/l	60	50	50
	H_2SO_4		220	180	180
	As		30	15	15
	Ni		20	10	10
Normalized values	50 °C	ρ, g/cm^3	1.4231	1.2931	1.2925
	55 °C		1.4212		
	59 °C		1.4190		
	50 °C	ν, mm^2/s	1.727	1.120	1.062
	55 °C		1.773		
	59 °C		1.683		
Original values	50 °C	ν, mm^2/s	1.698	1.100	1.042
	55 °C		1.743		
	59 °C		1.655		

Appendix A Results

Table A3. Diffusion coefficients of Cu^{2+}.

	g/l	T, °C	Diffusion coefficient, cm^2/s Calculated using Levich equation+	Koutecký-Levich equation +	Levich equation*	Koutecký-Levich equation *	Levich equation**	Koutecký-Levich equation **
Cu	40	50	1.053E-05	1.363E-05	1.060E-05	1.372E-05	1.064E-05	1.377E-05
H_2SO_4	160	60	1.236E-05	1.402E-05	1.193E-05	1.354E-05	1.198E-05	1.359E-05
Ni	0	70	1.470E-05	1.643E-05	1.303E-05	1.456E-05	1.308E-05	1.462E-05
As	0							
Cu	50	50	1.017E-05	1.220E-05	1.043E-05	1.252E-05	1.047E-05	1.257E-05
H_2SO_4	180	60	1.172E-05	1.360E-05	1.177E-05	1.366E-05	1.182E-05	1.371E-05
Ni	0	70	1.426E-05	1.619E-05	1.359E-05	1.543E-05	1.365E-05	1.549E-05
As	0							
Cu	40	50	9.390E-06	1.127E-05	9.633E-06	1.156E-05	9.672E-06	1.160E-05
H_2SO_4	220	60	1.150E-05	1.482E-05	1.152E-05	1.484E-05	1.156E-05	1.490E-05
Ni	0	70	1.386E-05	1.613E-05	1.312E-05	1.526E-05	1.317E-05	1.533E-05
As	0							
Cu	60	50	9.829E-06	9.168E-06	1.002E-05	9.351E-06	1.006E-05	9.388E-06
H_2SO_4	160	60	1.199E-05	1.137E-05	1.218E-05	1.155E-05	1.222E-05	1.159E-05
Ni	10	70	1.402E-05	1.624E-05	1.382E-05	1.600E-05	1.387E-05	1.606E-05
As	0							
Cu	50	50	9.653E-06	1.209E-05	9.835E-06	1.232E-05	9.875E-06	1.237E-05
H_2SO_4	180	60	1.169E-05	1.424E-05	1.178E-05	1.434E-05	1.183E-05	1.440E-05
Ni	10	70	1.409E-05	1.639E-05	1.364E-05	1.587E-05	1.370E-05	1.593E-05
As	0							
Cu	50	50	9.241E-06	1.155E-05	9.437E-06	1.179E-05	9.476E-06	1.184E-05
H_2SO_4	200	60	1.081E-05	1.169E-05	1.097E-05	1.186E-05	1.101E-05	1.191E-05
Ni	10	70	1.285E-05	1.618E-05	1.261E-05	1.587E-05	1.266E-05	1.594E-05
As	0							
Cu	40	50	9.184E-06	1.154E-05	9.187E-06	1.154E-05	9.226E-06	1.159E-05
H_2SO_4	160	60	1.092E-05	1.365E-05	1.072E-05	1.340E-05	1.077E-05	1.346E-05
Ni	20	70	1.308E-05	1.573E-05	1.221E-05	1.468E-05	1.226E-05	1.474E-05
As	0							
Cu	60	50	8.363E-06	1.079E-05	8.362E-06	1.078E-05	8.397E-06	1.083E-05
H_2SO_4	200	60	1.033E-05	1.093E-05	1.051E-05	1.112E-05	1.055E-05	1.117E-05
Ni	20	70	1.128E-05	1.317E-05	1.136E-05	1.327E-05	1.141E-05	1.333E-05
As	0							
Cu	40	50	9.204E-06	1.199E-05	9.476E-06	1.234E-05	9.515E-06	1.239E-05
H_2SO_4	160	60	1.086E-05	1.362E-05	1.090E-05	1.367E-05	1.095E-05	1.373E-05
Ni	0	70	1.252E-05	1.719E-05	1.186E-05	1.629E-05	1.192E-05	1.636E-05
As	15							
Cu	40	50	8.028E-06	1.109E-05	8.369E-06	1.156E-05	8.406E-06	1.162E-05
H_2SO_4	220	60	9.747E-06	1.277E-05	1.004E-05	1.316E-05	1.009E-05	1.322E-05
Ni	0	70	1.101E-05	1.374E-05	1.093E-05	1.364E-05	1.098E-05	1.371E-05
As	15							
Cu	50	50	7.854E-06	1.001E-05	8.084E-06	1.030E-05	8.119E-06	1.034E-05
H_2SO_4	180	60	9.340E-06	1.266E-05	9.621E-06	1.304E-05	9.664E-06	1.310E-05
Ni	10	70	1.109E-05	1.542E-05	1.116E-05	1.551E-05	1.121E-05	1.558E-05
As	15							
Cu	60	50	7.680E-06	1.015E-05	7.689E-06	1.016E-05	7.722E-06	1.020E-05
H_2SO_4	180	60	8.408E-06	1.122E-05	8.627E-06	1.151E-05	8.666E-06	1.156E-05
Ni	20	70	1.033E-05	1.376E-05	1.058E-05	1.410E-05	1.063E-05	1.416E-05
As	15							

Appendix A Results

	g/l	T, °C	Diffusion coefficient, cm^2/s Calculated using Levich equation[+]	Koutecký-Levich equation [+]	Levich equation*	Koutecký-Levich equation *	Levich equation**	Koutecký-Levich equation **
Cu	60	50	6.603E-06	6.911E-06	6.536E-06	6.840E-06	6.565E-06	6.871E-06
H_2SO_4	220	60	7.791E-06	9.516E-06	7.994E-06	9.763E-06	8.030E-06	9.808E-06
Ni	20	70	9.351E-06	1.239E-05	9.669E-06	1.281E-05	9.714E-06	1.287E-05
As	15							
Cu	60	50	7.234E-06	9.582E-06	7.585E-06	1.005E-05	7.618E-06	1.009E-05
H_2SO_4	180	60	8.570E-06	1.234E-05	9.094E-06	1.310E-05	9.135E-06	1.316E-05
Ni	0	70	9.939E-06	1.388E-05	1.044E-05	1.458E-05	1.049E-05	1.465E-05
As	30							
Cu	50	50	7.158E-06	8.458E-06	7.531E-06	8.898E-06	7.565E-06	8.938E-06
H_2SO_4	200	60	8.010E-06	9.876E-06	8.474E-06	1.045E-05	8.514E-06	1.050E-05
Ni	0	70	9.748E-06	1.323E-05	1.015E-05	1.378E-05	1.020E-05	1.384E-05
As	30							
Cu	50	50	6.378E-06	7.014E-06	6.596E-06	7.255E-06	6.626E-06	7.288E-06
H_2SO_4	180	60	7.913E-06	9.238E-06	8.282E-06	9.668E-06	8.320E-06	9.713E-06
Ni	10	70	9.220E-06	1.450E-05	9.543E-06	1.501E-05	9.589E-06	1.508E-05
As	30							
Cu	40	50	6.519E-06	8.613E-06	6.655E-06	8.793E-06	6.686E-06	8.834E-06
H_2SO_4	160	60	7.631E-06	9.601E-06	7.846E-06	9.871E-06	7.884E-06	9.919E-06
Ni	20	70	9.088E-06	1.154E-05	9.183E-06	1.166E-05	9.229E-06	1.172E-05
As	30							
Cu	40	50	6.317E-06	8.841E-06	6.442E-06	9.016E-06	6.472E-06	9.058E-06
H_2SO_4	180	60	7.363E-06	1.002E-05	7.596E-06	1.033E-05	7.633E-06	1.038E-05
Ni	20	70	8.550E-06	1.132E-05	8.710E-06	1.153E-05	8.754E-06	1.159E-05
As	30							
Cu	50	60	9.570E-06	1.360E-05	9.858E-06	1.401E-05	9.902E-06	1.407E-05
H_2SO_4	180	60	9.356E-06	1.385E-05	9.637E-06	1.427E-05	9.680E-06	1.433E-05
Ni	10	60	9.849E-06	1.330E-05	1.015E-05	1.370E-05	1.019E-05	1.376E-05
As	15							

[+] Viscosity from Price et al.

* Viscosity from present work

** Normalized viscosity from present work

Appendix A Results

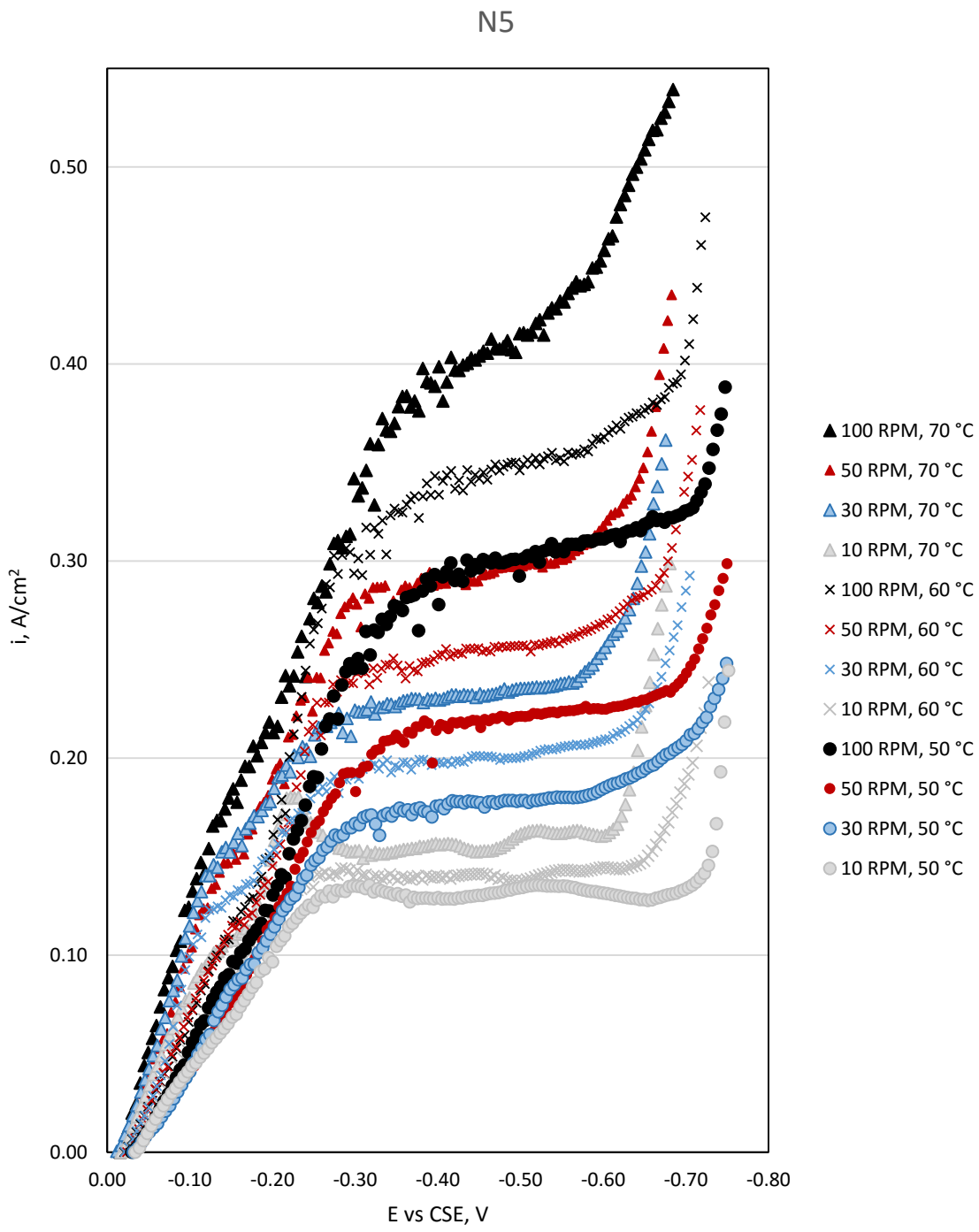

Figure A1. Limiting current density measurement curves of electrolyte N5.